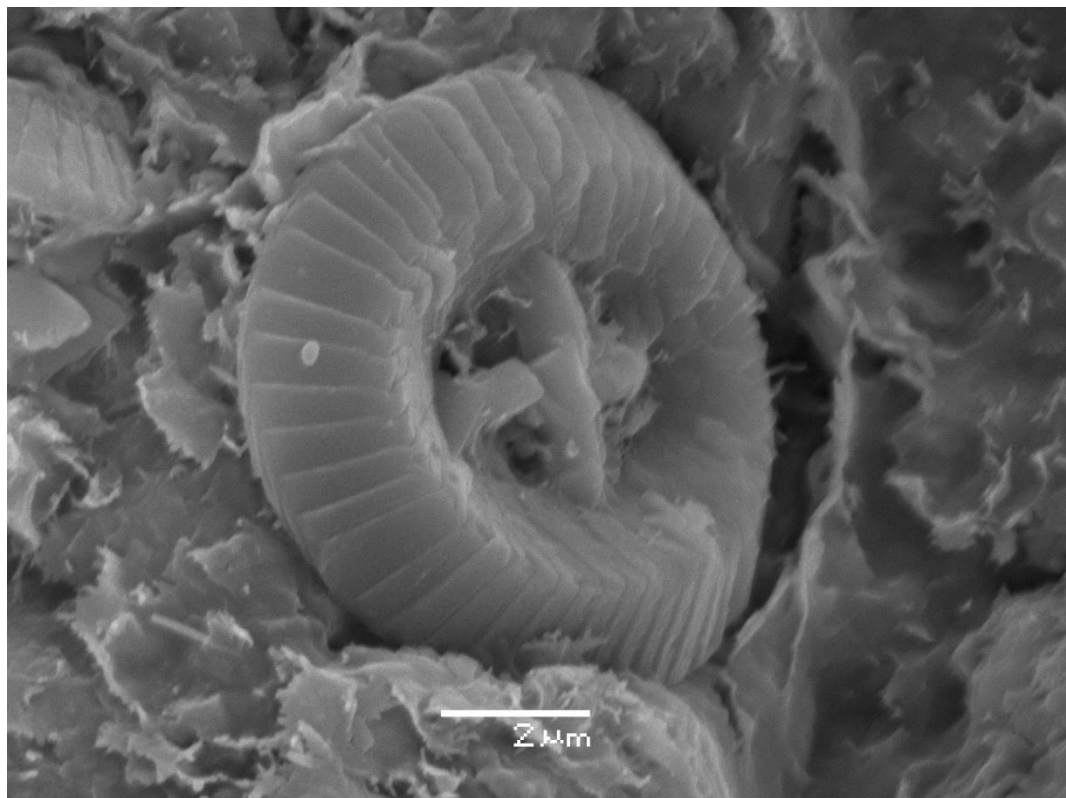


Master Thesis, Department of Geosciences

Distribution of chalk in the Lower Palaeocene reservoir sandstones of the Maureen Formation

Consequences for reservoir quality

Tera Elizabeth Lyons



UNIVERSITY OF OSLO

FACULTY OF MATHEMATICS AND NATURAL SCIENCES

Front page: Wagonwheel Coccolith. Picture taken in SEM-microscope.

Distribution of chalk in the Lower Palaeocene reservoir sandstones of the Maureen Formation

Consequences for reservoir quality

Tera Elizabeth Lyons



Master Thesis in Geosciences

Discipline: Petroleum Geology and Petroleum Geophysics

Department of Geosciences

Faculty of Mathematics and Natural Sciences

University of Oslo

09.03.2015

© **Tera Elizabeth Lyons, 2014**

Tutor (s): **Professor Jens Jahren (UiO), Dr. Fawad Chuhan (Statoil) and Professor emeritus Knut Bjørlykke (UiO)**

This work is published digitally through DUO – Digitale Utgivelser ved UiO

<http://www.duo.uio.no>

It is also catalogued in BIBSYS (<http://www.bibsys.no/english>)

All rights reserved. No part of this publication may be reproduced or transmitted, in any form or by any means, without permission.

“Carbonates are born not made”

- Noel James

Abstract

Maureen reservoir quality can be explained by several factors, such as the depositional environment, shallow burial and early hydrocarbon emplacement. The reservoir consists of homogeneous oil-stained sand interfingering with carbonate beds of various thickness, frequency and properties. The understanding of the lateral and vertical distribution of chalk within the upper reservoir unit, the diagenetic processes and how this chalk affects the overall reservoir quality is of great importance with regards to production of the Maureen heavy oil province.

The reservoir unit in this study are cored from well 9/11b-11 within a depth of 1900 m and have been examined by sedimentological, mineralogical, petrographical and petrophysical analyses to determine the diagenetic history, origin, and distribution of the chalk deposits. In addition, a well correlation of wells 9/11a-10, 9/11a-10Z, 9/11-3, 9/11-4, 9/11a-9, 9/11a-8, 9/11-2, 9/11a-5, 9/11a-7, 9/11-1 and 9/11a-6 in the area has been implemented to better estimate the distribution of chalk.

The study reveals that the Maureen carbonate facies were deposited in a time of interplay between tectonic activities, sea level rise and hinterland characteristics. The deposition took place in a closed to semi-closed system away from ground water infiltration and has been little effected by diagenetic modification. Additionally, little precipitation of authigenic minerals has left the majority of the primary composition intact. Even though chalk compacts tightly it is chemical stable unless it reaches the CCD (carbonate condensation depth). This has resulted in good porosity average value of 28,6% in the well of this study. However, impermeable layers can prevent vertical fluid flow, trapping hydrocarbon beneath carbonate-cemented intervals. Prediction of how these chalk intervals have interact with the reservoir sandstone can help improve further understanding of the chalks origin, behavior and distribution future explorations.

Acknowledgements

First I would like to give a great thanks to my encouraging supervisor Professor Jens Jahren and to my Co-supervisors Dr. Fawad Chuhan and Professor emeritus Knut Bjørlykke for helpful guidance through my thesis. Greater thanks to Johan Petter Nystuen for sheering his knowledge and patience.

Of the technical staff I would like to express my appreciation to Berit Løken Berg, for her assistance in the Sem-lab, Maarten Artz, for being available during my lab work and XRD analysis, and Salahallidin Akhavan for making thin- sections. I would also like to acknowledge Michael Heeremans for his assistance with Petrel.

Thanks to my fellow students in room 217, for helpful feedback, an extraordinary study environment and joyful lunch breaks. Special thanks to Are Reiakvam, for keeping me company at nights, with fjorland meals and lots of licorice. You have been a great fellow student and a friend through my study at UiO.

I would also like to give a huge thanks to Sanne Lorentzen for helping me through my thesis, with good academic discussions, valuable feedback and an overall exceptional good friend to have. I will miss our spicy noodle dates and our fun times at ZEB.

Finally, to Martin Sandbakken, I value your encouragement and extraordinary patience through this last year. Thank you for helping me with figures in Illustrator, and for your positive energy. You always put a smile on my face. At last I would like to thank my loving mom and dad for always motivating me, believing in me and always being supportive of my choices.

Oslo, March 9th 2015

Tera Elizabeth Lyons

Table of content

Chapter 1: Introduction

1.1 Introduction	4
1.2 Purpose and methods	4
1.3 The study area	5

Chapter 2: Geological background

2.1 Introduction	7
2.2 Structural setting	9
2.2.1 Structural setting of the Paleogene sediments	10
2.3 Stratigraphic setting	11
2.3.1 Characterization of the Maureen Formation	13
2.3.2 Distribution of the Maureen Formation	15
2.4 Depositional system of the Cenozoic	16
2.5 Paleogeography and Paleoclimate in Paleogene	16

Chapter 3: Theoretical background

3.1 Introduction	18
3.2 Shallow burial diagenesis	18
3.3 Intermediate and deep burial diagenesis	19
3.4 Carbonates	21
3.4.1 Chalk	22
3.4.2 Reservoir- preserving mechanisms in chalk	22

Chapter 4: Methods and Data

4.1 Introduction	24
4.2 Sedimentological Core study	24
4.2.1 Core description	24
4.2.2 Digitalization of core logs	25

4.3 Petrographical and Mineralogical analysis	25
4.3.1 Thin sections analysis	25
4.3.2 X-ray Diffractometry (XRD)	27
4.3.3 Scanning Electron Microscopy (SEM)	30
4.4 Strontium isotope analysis	31
4.5 Well correlation and Petrophysical evaluation	31
4.5.1 Well correlation	31
4.5.2 Petrophysical analysis	32
Chapter 5: Core description	
5.1 Introduction	34
5.2 Characterization of facies	34
5.3 Characterization and interpretation of the core log	36
Chapter 6: Petrographical and Mineralogical Results	
6.1 Introduction	44
6.2 Composition and texture	46
6.3 Textural parameters and porosity	46
6.4 Optical mineralogy and SEM	49
6.4.1 Framework	49
6.4.2 Clays	53
6.4.3 Matrix	54
6.4.4 Cement	56
6.4.5 Fossils	57
6.5 X-Ray Diffraction (XRD) analysis	62
6.5.1 XRD Bulk	62
6.5.2 XRD Clay fraction	66
Chapter 7: Strontium isotope analysis	70

Chapter 8: Well correlation and petrophysical results

8.1 Introduction	73
8.2 Well correlation	73
8.3 Characterization of the carbonate intervals: combining well correlations and wire line logs from Mariner east.	76
8.4 Petrophysical analysis	78

Chapter 9: Discussion

9.1 Depositional environment	82
9.1.1 Facies distribution	82
9.2 Origin of carbonate beds and Maureen sands	85
9.3 Distribution and dimension of carbonate intervals	87
9.4 Diagenetic modification of carbonate intervals	89
9.4.1 Mechanical compaction	89
9.4.2 Chemical compaction	90
9.5 Origin and source of clay minerals	92
9.6 Other minerals	94
9.7 Consequences for reservoir quality within the Maureen Formation	94

Chapter 10: Conclusion 99

Chapter 11: References 100

Appendix – A: Log template 106

Appendix – B: Sedimentary core logs 107

Appendix – C: Stacked logs 124

Appendix – D: Thin sections 128

Appendix – E : Quantification of XRD bulk samples	129
Appendix – F : Flow diagram for XRD clay fraction identification	130
Appendix – G : Well data and information for all correlated wells	131
Appendix – H : Well sections from Mariner East	133

Chapter 1: Introduction

1.1 Introduction

This thesis is part of a collaboration project with Statoil on reservoir quality in respect to diagenesis linked to facies and provenance, and physical properties in relation to carbonate-cemented intervals. The research project is in the Mariner East area, of well 9/11b-11 located on the UK sector of Quadrant 9, within the Maureen Formation. The goal is to understand the unevenly distribution of the carbonate beds and their dimension with the Maureen reservoir. It is essentially important to acknowledge the upper part of the carbonate intervals and their diagenetic modification, in respect to the underlying Maureen reservoirs, which can influence the production of heavy oil and trap hydrocarbon-filled sands between impermeable carbonate layers. How the carbonates have behaved during deposition is also of importance, because if the chalk deposits were of low density, they may have floated raft-like in the sand and dispersed over a large area. Their origin, composition and how they behave laterally and vertically within the Maureen Formation, is of great interest when in production for hydrocarbons.

1.2 Purpose and methods

This study emphasizes on the sedimentology and the diagenetic processes related to the carbonate beds interbedded with Maureen sand deposits of well 9/11b-11. Several investigations have been implemented to provide an understanding of the depositional environment, the chalks mineralogical framework and its diagenetic instabilities within the good reservoir sands. When referring to carbonate intervals, this applies to deposits composed mainly of chalk, unless otherwise stated. Methods used in this thesis are as follows:

- Sedimentological core description of facies analysis and the depositional environment.
- Mineralogical and petrographical analysis of core samples and thin section through optical microscopy, scanning Electron Microscopy (SEM) and X-ray Diffractometry (XRD).
- Strontium isotope analysis of selected chalk rich samples.
- Petrophysical evaluation of well correlation and interpretation of well and wire line logs, together with porosity and permeability relations.

1.3 The study area

Mariner field is a heavy oil field situated in the UK North Sea, located 320 km north east of Aberdeen (Berg et al., 2013). The discovery was made in 1981 on the eastern flank of the Eastern Shetland Platform block UK- 9/11 (Figure 1.1). The Mariner Field consists of two areas Mariner and Mariner East, where Mariner was discovered within Block 9/11 while Mariner east was discovered within block 9/11b. The latter lies about 5 km to the southeast and is smaller in size. (Offshore-Tecnology, 2014). Today Statoil operates the Mariner field with 65.11% equity of Mariner and 92% equity of Mariner East. The project is expected to commence in 2017, with an expected field production for at least 30 years, with an average plateau production of around 55,00 barrels of oil per day (Statoil, 2014). The Mariner Field reservoir lies within the Maureen Formation and is buried at a shallow depth approximately 1500 m with a water depth ranging between 97m and 112m (Offshore-Tecnology, 2014).

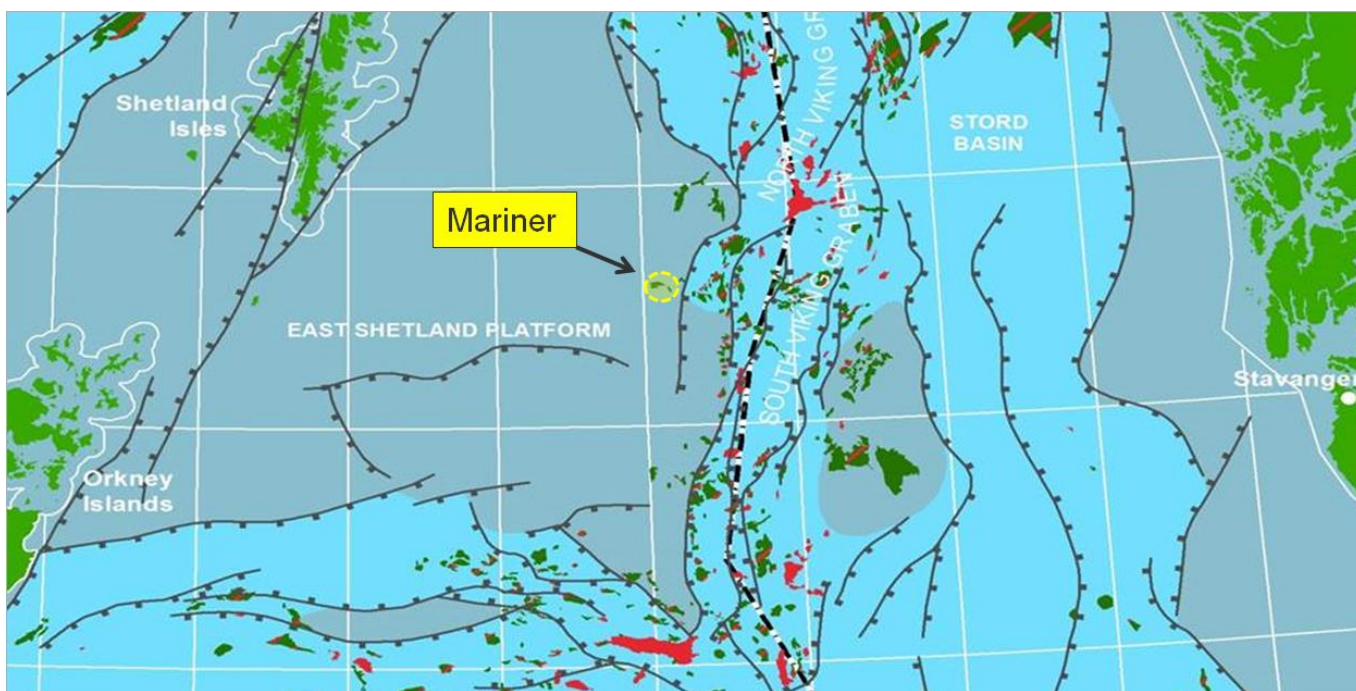


Figure 1.1: Map of the study area marked with a yellow circle. The area is located in quadrant 9, offshore UK.

Chapter 2: Geological background

2.1 Introduction

This chapter will focus on the East Shetland Platform. In addition, a short introduction of the structural setting followed by a description of the stratigraphic framework in Central and Northern North Sea will be presented.

The East Shetland Platform is located in the UK sector of the North Sea, creating a near-flat-topped platform extending from approximately 61°N to about 250 km south. It is part of the Northern North Sea rift system forms the western margin of the Viking Graben (Roberts and Yielding, 1991).

The development of the North Sea began in middle Paleozoic during the Caledonian orogeny (Lyngsie et al., 2006). The area was dominated by several rift stages, which caused extensive stretching and thinning of the continental plate followed by periods with thermal cooling (Faleide et al., 2010). Due to this prolonged extensional history combined with complex structural regimes of the North Sea, numerous papers have been published on this subject.

Due to the low number of wells and seismic lines acquired on the East Shetland Platform, the lithostratigraphic framework and stratigraphic correlation of the different sedimentary facies is poor (Underhill, 2001). However, closely spaced seismic lines and new 3D seismic surveys in the Bressay area was provided to give a better understanding of the proximal sedimentary systems of the Eastern Shetland Flank (Underhill, 2001). Consequently, published literature concerning related areas such as Moray Firth, Central and Viking Graben will be used to describe the geological framework of the Maureen Formation (Figure 2.1).

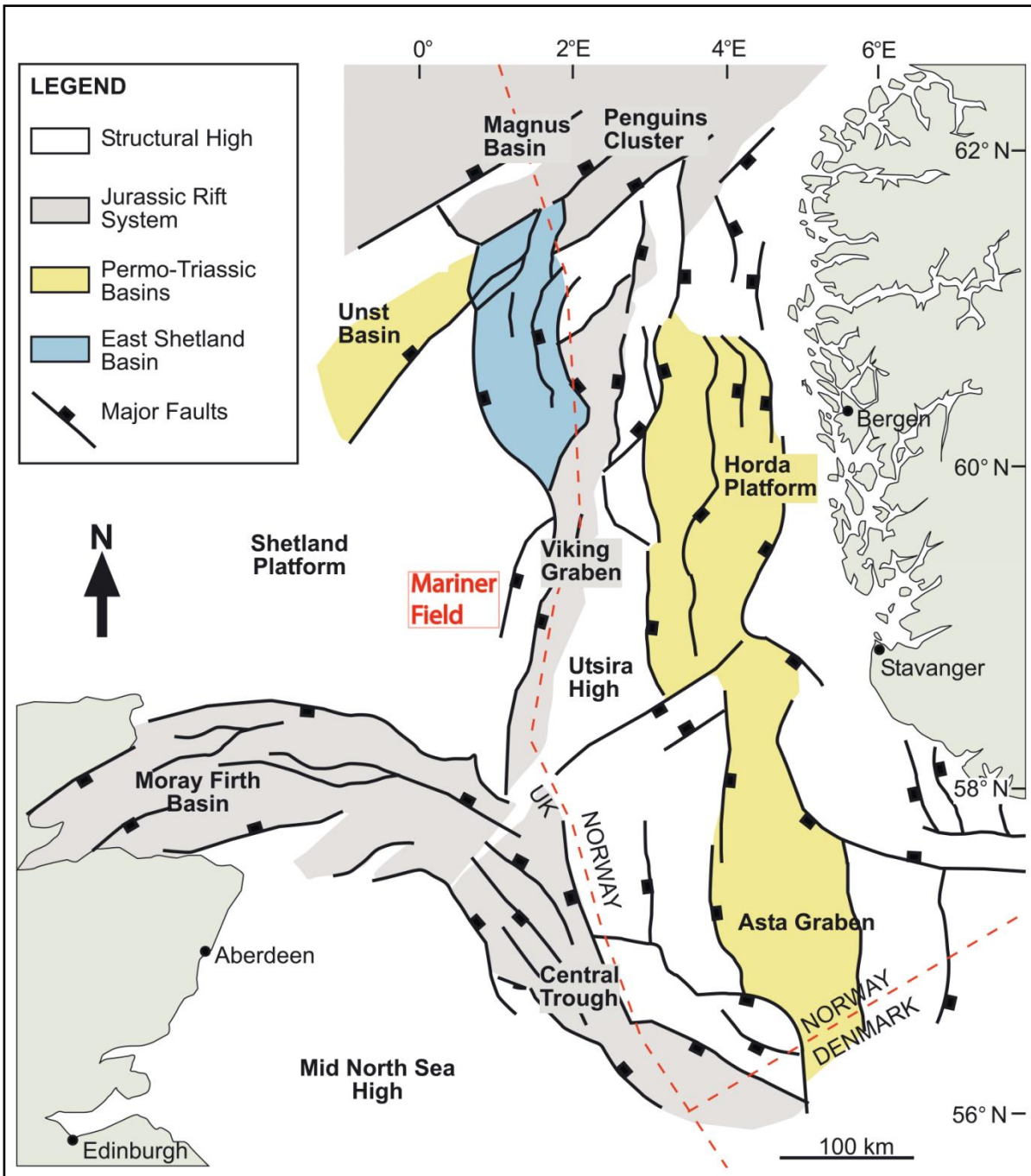


Figure 2.1: Simplified map of the North Sea illustrating the structural framework. Staped red lines represents the border between the Norwegian, Denmark and UK sector. The study area (Mariner Filed) is highlighted in red within the UK sector. Modified after Dominguez (2007).

2.2 Structural setting

The North Sea has one of the largest offshore oil- and gas fields in the world and has undergone major structural tectonic events, which created migration paths for the hydrocarbons and structural hydrocarbon traps. The structural evolution has been accepted to result in two main rift events, and subdivided into different stages; pre-rifting, active crustal stretching and thermal subsidence (Gabrielsen et al., 1990).

The first major extensional event occurred in Permian – Early Triassic (Christiansson et al., 2000). This was a continental rift phase resulting in crustal stretching (Ravnås et al., 2000) in E-W direction (Nøttvedt and Johannessen, 2008) expressed by block tilting, lowering of the surface consisting of half-grabens and thermal subsidence with non-marine syn-rift infill (Ravnås et al., 2000). Several of these Permian-Triassic faults were later reactivated during the second Middle Jurassic - Early Cretaceous extensional event (Christiansson et al., 2000). From Middle Triassic – Middle Jurassic minor extensional event occurred, gradually forming non-marine- to marine syn-rift infill (Ravnås et al., 2000). During Middle Jurassic - Early Cretaceous, the second major rift phase located in the present Viking Graben evolved (Christiansson et al., 2000). A new crustal stretching took place, this time in NE-SW direction, with major rotational block tilting and subsequent cooling (Badley, 1988). The rifting climaxed in Upper Jurassic, concentrating the fault activity on faults along the margins of the Viking Graben. This activity gave rise to a more pronounced graben relief, including the development of platforms and platform marginal heights (Gabrielsen et al., 1990), such as Beryl Embayment and East Shetland Basin. The prime source rocks formed in the northern North Sea reflect a shallow marine environment where the clay stones of Kimmeridge Clay and Draupne Fm. were deposited (Ravnås et al., 2000).

In the Early Paleocene the rifting of the Greenland-European plate caused a thermal uplift of Scotland and the East Shetland Platform, along with rejuvenation of the older Mesozoic hinterlands and basin margins. This resulted in a larger amount of coarse siliciclastic input into the basin during the Paleogene. As a consequence, the earlier sediment-starved, relatively deep marine basin turned into major clastic depocentres of deltaic and submarine fan systems. The tectonic of the Paleogene are distinguished by five key events;

- Danian/Thatian: elastic updoming around a mantle hotspot located beneath East Greenland resulted in hinterland rejuvenation.

- Early Paleocene: during the east-west extension, volcanic activity formed the British and Faeroe-Greenland igneous province, which also had an impact in the North Sea represented by the Andrew Tuff in the Witch Graben.
- Late Paleocene: the onset of seafloor spreading in the Norway-Greenland Sea caused volcanic activity and the deposition of widespread tuff beds, as the Balder Tuff of the Northern North Sea.
- Late Paleocene and early Eocene: thermal doming created a restricted basinal environment in the North Sea, which lead to an anoxic basin.
- Early Eocene: because of the final rupture of the North Atlantic, a minor inversion occurred. Thus resulted in subsidence, marking a clear marine connection between the North Sea and North Atlantic (Bowman, 1998).

2.2.1 Structural setting of the Paleogene sediments

Paleogene sediments was deposited above the Jurassic triple junction structure within a regional syn- and post-rift depocentre (Underhill, 2001). Studies show (Underhill, 2001; Mudge and Bujak, 1996; Mudge and Copestake 1992; Mudge and Bliss, 1983) that the sediments influx was controlled by an earlier rift phase from Mesozoic times. Reactivation of these old Mesozoic faults during the Danian - Middle Paleocene tensional period increased the offset of the pre-existing tectonic framework. This gave rise to new depositional fairways for the sediments, which more or less followed the old ocean bathymetry (Mudge and Bliss, 1983).

The fault-controlled setting along the East Shetland margin during Danian - Middle Paleocene gave rise to an easterly- directed drainage system (Mudge and Bliss, 1983). This was associated to the uplift and tilting of the Scotland - Shetland region and generated a high relief of the hinterland. This relief contributed to large quantities of siliciclastic input to the basinal depocentre in the Viking Graben and Central Graben (Mudge and Copestake, 1992; Mudge and Bliss, 1983).

2.3 Stratigraphic setting

The Early Cenozoic (Palaeocene to Eocene) sediments were originally divided into two depositional packages, the Montrose Group and the Moray Group (Underhill, 2001), which are separated by a change in dip and acoustic impedance (Deegan and Scull, 1977). Deegan and Scull (1977) further divided the Paleocene to Holocene sediments into five different lithostratigraphic groups developed for the UK sector (Bowman, 1998). The groups were later subdivided into formations and members, which with minor modifications are still in use (Underhill, 2001). The first package, Montrose Group, took place during the early stages of deposition. The package shows an aggradation signature, dominated by deep marine fans consisting of sand and mudstone. The shelfal and deltaic systems at this time functioned as a bypass zone with siliclastic sediments. Only thin units and erosional remnants are preserved due to reworking and redistribution. The second depositional package (Moray Group) includes a predominantly progradational deltaic setting, where shelfal and coastal depositional systems are dominant (Bowman, 1998).

The Maureen Formation, located on the eastern flank of the East Shetland Platform, is one of the reservoirs in the Mariner field area (Berg et al., 2013). The formation range from Late Danian to Early Thanetian age, and overlies the Cretaceous to Early Danian Chalk Group (Hod, Tor and Ekofisk formation) (Cutts, 1991). The Maureen formation makes up the lower part of the Montrose Group and is bonded by the overlying Lista Formation.

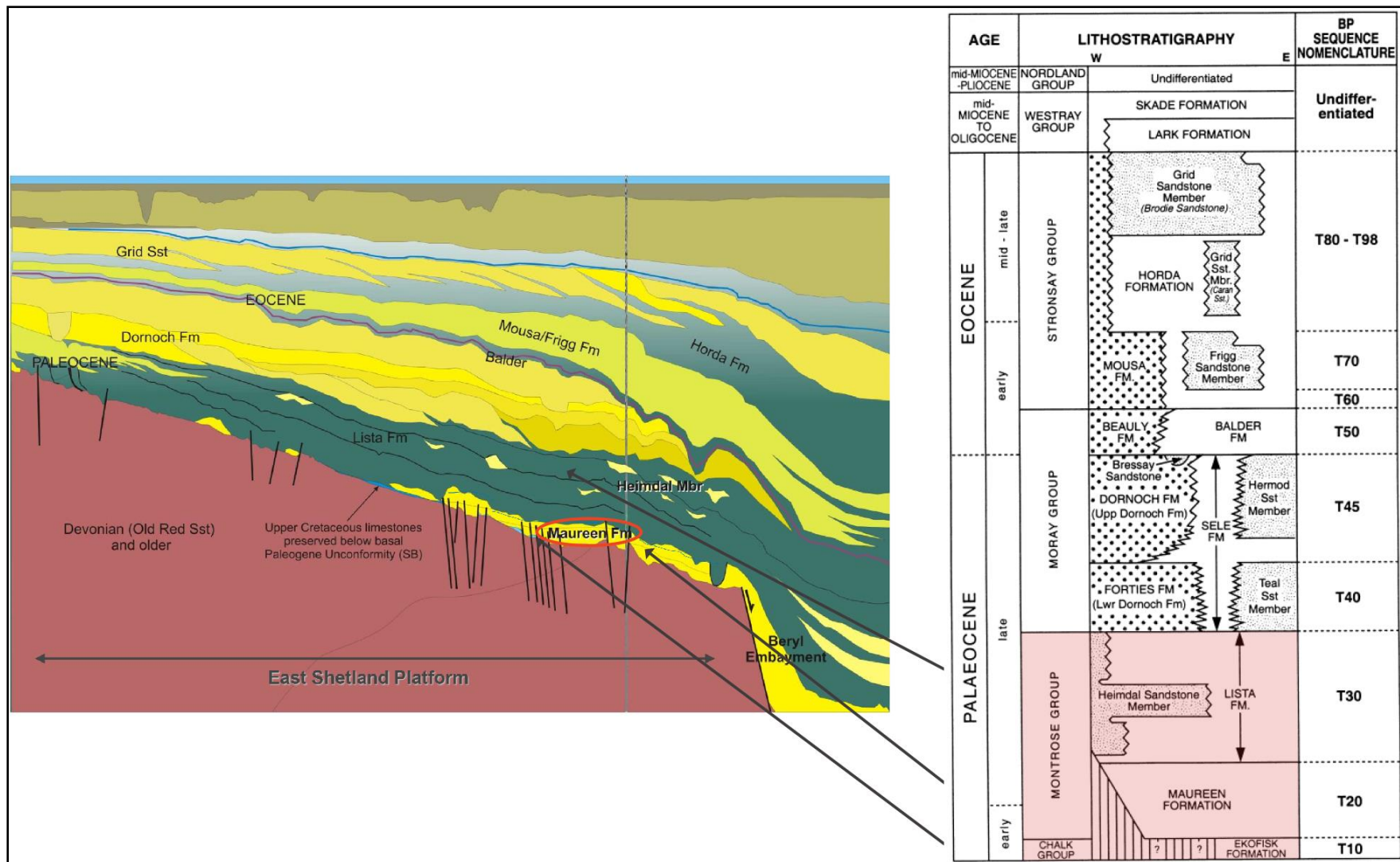


Figure 2.2: Stratigraphy of the Early Cenozoic sediments on the East Shetland Platform. Arrows pointing to the distribution of the Chalk Group, Maureen- and Lista Formation. Maureen Formation is highlighted with a red circle. Modified from Underhill (2001) and Statoil (2013).

2.3.1 Characterization of the Maureen Formation

The upper boundary of the Maureen Formation is defined by a downward change from waxy claystone with greenish or reddish tints belonging to the overlying Lista Formation, to dark grey, silty mudstone, defining the top Maureen Formation. This change in lithology corresponds to the base of a high-gamma peak, characterizing the boundary between Lista- and Maureen Formation. However, in the more distal parts, the upward-fining profile from Maureen- to Lista Formation is not strongly marked in the gamma and sonic logs. This boundary will thus be more difficult to distinguish in the central and northern part of the Viking Graben (Knox and Holloway, 1992).

The base of the Maureen Formation is characterized by a rapid change in lithology from marl to limestone of the underlying Ekofisk Formation. This boundary is presented as low gamma-ray readings and high velocity in the sonic logs from the Ekofisk Formation, and shifting to higher gamma-ray readings and lower velocity in the Maureen Formation. In areas where these logs do not correspond in such a way, the shift in gamma ray is used to define the boundary. Where the sandstone or reworked limestone is present and the basal marl is absent, the boundary is set by a downward change from variable to more consistent gamma and sonic readings. In areas where the Ekofisk Formation is absent, the Maureen Formation lies directly on older cretaceous chalk or older formations. Such settings are common in the marginal zones (Knox and Holloway, 1992), and on the East Shetland Platform of the Mariner Field. In this specific area (Mariner Field) where the Maureen Formation lies directly on top of the Tor Formation, it gradually decreases in thickness westwards and onlaps onto the Devonian basemen (Ahmadi, et al., 2003).

The Maureen Formation primarily consists of a heterogeneous mix of sandstone, limestone (marl) and reworked chalk. Some of these sequences in the North Sea are also interbedded with mudstone (Mudge & Bujak, 1996). From the interpretations made by Knox and Holloway (1992), the unit can be recognized as a liming downward sequence with more input of reworked chalk taking place at the base of the Maureen formation. In the Northern North Sea, Base Maureen lies on top of the Chalk Group. This group consists of a calcareous content composed of chalk and clay-sized particles (Deegan and Scull, 1977).

The Maureen Formation has recently been re-evaluated in the Central parts of the North Sea by Kilhams et al. (2014), using modern semi- regional 3D-seismic megasurvey data, extensive

well database and cored intervals. From the core facies analysis, four distinctive chalks related facies within the Maureen interval was recognized:

- (i) **Pelagic Chalks and Calcareous Mudstones:** from the base of Maureen Formation and upward, a gradual transition from chalk to calcareous mudstone to non-calcareous mudstone is usually displayed. This indicates that the chalk-rich pelagic deposition did not end suddenly after the deposition of the Chalk Group, but was gradually replaced by non-calcareous sedimentation.
- (ii) **Chalk Debris Flows in Mudstones:** appear as thin sections (cm to tens of cm), angular to sub-rounded chalk clasts within a mudstone matrix, usually calcareous. This indicates that locally reworked chalk and chalk-rich material from bathymetric highs can be mistaken for sand-rich units in a mudstone in log signatures.
- (iii) **Chalk Clasts within Sandstones:** sub-angular to sub-rounded chalk clasts within a sandstone matrix, consistent with a turbidity unit, can also include similar sized mud clasts. This demonstrated that turbidity flows generated from the shelf eroded the seafloor, mostly consisting of pelagic chalk, creating rip-up clasts of semi-consolidated chalk. The amount of chalk clasts is upward decreasing, indicating that the seafloor becomes less calcareous through time. This facies can be displayed by lower gamma-ray readings and sonic values than usual, whereas the neutron/density logs show a small positive separation.
- (iv) **Calcite Cementation Bands:** sandstones within the Maureen Formation often show localized calcitisation. 1-3 ft thick units of this calcitisation commonly occur at the boundary between chalks/calcareous mudstone and sandstones. However, the precise developments of these bands are unclear and can influence the well logs in a similar manner to chalk clasts within sandstones (Kilhams et al., 2014).

If these chalk facies are recognized together with the proportion of sandstone mudstone interval in the Maureen Formation, a four-fold facies scheme might be possible to utilized according to Kilhams et al. (2014).

2.3.2 Distribution of the Maureen Formation

In the Northern North Sea, including Viking Graben, Beryl Embayment and East Shetland Basin were important accommodation space for sediment infill during deposition of Early Paleogene (Paleocene- Early Eocene) sediments. The time of deposition represents a period of basin margin uplift and fall in relative sea level, resulting in episodic submarine fans containing sands separated by pelagic mud. Depocentre of the East Shetland Platform hanging walls, Beryl Embayment and western part of East Shetland Basin, were filled in by 1400 m thick package of clastic sediments (Mudge and Copestake, 1992). The thickest section of the Maureen Formation is found in the Beryl Embayment located close to the East Shetland platform margin fault zone. This section displays a thickness reaching 600 m. However, the Maureen sandstones are drastically thinning westward on to the East Shetland Platform and eastward into the Viking Graben. These deposits represent sand sheets of 100-150 m in thickness (Mudge and Bujak, 1996). In the East Shetland Basin, the thickness of Maureen Formation is still questionable due to lack of biostratigraphic data. Thus making it difficult to distinguish the two formations in the Montrose Group. Mudge and Copestake (1992) have assigned the Maureen Formation with a questionable thickness of 640 m to the east of the platform margin fault zone.

For the Central North Sea, the Maureen sequence, which closely corresponds to the Maureen Formation, can be traced over a large part of the area. However, the Maureen Formation is not recognized across the Halibut Horst and on the southern part of the East Shetland Platform. There are two sand-rich depositional packages, separated by a thin reworked chalk deposits over the Fladen Ground Spur. One of the depositional packages was spreading southeastward through the Morey Firth Basin, whilst the other occupies the South Viking Graben. During the Mesozoic tectonic activity, a series of depocentres along the Witch Ground Graben, Buchan Graben and South Viking Graben were formed. The Maureen sequence reaches a thickness up to 240 m in the Witch Ground Graben, thinning northward to zero over the East Shetland Platform. In the South Viking Graben it reaches 150 m in depocentres close to the East Shetland Platform fault margin (Mudge and Bujak, 1996). Maureen sands in the Central Graben can be traced as far out as Quadrant 30, and in the distal parts it gradually passes into mudstones, approximately 30-50 m thick (Mudge and Bujak, 1996).

2.4 Depositional system of the Cenozoic

Factors controlling the sediment input consists of a complex system of tectonic activity, eustasy and characteristics of the hinterland. This led to a complex depositional pattern across the basin, with a peak of volume and grain size of the clastic input in the late Paleocene (mid-Thanian). The increase of coarser clastic input was deposited as major submarine-fans into the North Sea and Faeroe-Shetland Basin. Through the Eocene and Oligocene the rate of clastic input was reduced due to the continuous erosion of the hinterland causing a change in the lithology. Later on, the relative sea-level changes were the main factor controlling the sedimentation patterns (Bowman, 1998).

2.5 Paleogeography and Paleoclimate in Paleogene

During the Paleogene and Neogene, the proto-Eurasian continental plates merged in a northward direction. In this period, the continents changed their location and shape, similar to the present appearance. Between the North Sea and the North Atlantic, the Norwegian Sea functioned as a barrier, at this time. However, in Paleogene the continental movements between Greenland and Norway occurred and created an open system environment, from anoxic to oxic, with new circulations between the North Sea and North Atlantic (Martinsen and Nøttvedt, 2008).

The climate was still warm and humid during the Paleogene, as it had been throughout most of the Cretaceous and Jurassic time. The volcanic activity described in the structural setting, is believed to have supplied high amounts of greenhouse gasses into the atmosphere, resulting in a global warming. However in the Neogene, the climate was drastically changed from warm and humid to a colder dryer climate (Martinsen and Nøttvedt, 2008).

Chapter 3: Theoretical background

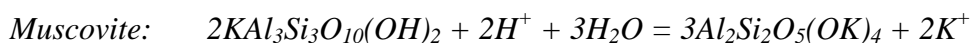
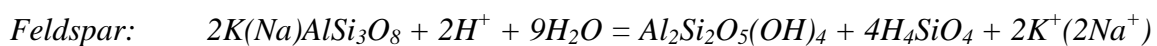
3.1 Introduction

Diagenesis is the processes influencing the rock from the time of deposition to deeper burial (Chilingar and Larsen, 1983). The main diagenetic processes leading to reduced/destruction of porosity in sandstone is mechanical and chemical compaction and precipitation of quartz cement (Houseknecht, 1987). However, as the Maureen reservoir consist of both sand and chalk and is buried at approximate 1500 m below sea floor, this chapter will focus on the diagenetic processes occurring at a shallow burial stage. The main emphasis will be directed to the carbonate rock, specifically chalk. Knowledge of how the different diagenetic processes affect the reservoir is important when trying to predict reservoir properties, such as porosity and permeability.

3.2 Shallow burial diagenesis

At the upper 1-10m of shallow burial depths the primary sediment composition can strongly be influenced both by marine and meteoric conditions. During reactions at the subsurface with groundwater flow, dissolved solids are transported by fluid flow or by diffusion (Bjørlykke, 1994). The initial rock framework may then be subjected to mineralogical changes such as early carbonate cementation. Early carbonate cementation is a result of dissolution of unstable minerals such as high- Mg calcite and aragonite, and precipitation calcite cement. (Mapstone, 1975). Other unstable minerals are feldspar and mica. Leaching of these minerals is depended on the influx of groundwater supply, which will lead to precipitate of kaolinite.

The reaction for such transition is given as:



After (Bjørlykke, 1994)

From the given reaction precipitation of kaolinite is therefore depended on a low K^+/H^+ ratio, and requires that Na, K and silica be constantly removed from the system by meteoric flushing. This in turn varies according to the depositional environment and climate (Bjørlykke and Aagaard, 1992)

As burial progresses, the stress of the overburden will increase the effective stress on the grains, representing the realm of the mechanical compaction. The processes controlling mechanical compaction includes; breakage, crushing, reorientation and repacking of the grains in response to increasing effective stress during burial (Houseknecht, 1987). At depth of 2-3 km corresponding to temperatures below 80 degrees, depending on grain strength and size, these processes will have reduced the initial porosity in clastic sediments (Bjørlykke, et al., 2009). However, due to early calcite cementation in carbonates the cement may strengthen the rocks framework and counteract mechanical compaction. This will cause the area of grain contact to increase and further reduced the overburden stress (Bjørlykke, 2013).

For chalk deposits, the grain size is relatively small ($<10\mu\text{m}$), which will cause a distribution of the overburden stress over a larger area, hence reducing the effective stress at grain contact (Hillis, 2001). The coccoliths are also rather chemical stable due to little aragonite, however during settling the coccoliths are subjected to dissolution. Dissolution appears within the species that are the least solution-competent. However, the chemically stable low- Mg coccoliths in chalk deposits are less dependent on precipitation of early cement, compared to other coarser carbonates (Feazel, et al., 1992).

3.3 Intermediate and deep burial diagenesis

At 70-80 C°, the change from shallow to intermediate burial is marked by the transition from mechanical- to chemical compaction. This temperature range corresponds to depths less than 2 km, given a normal geothermal gradient. At this depth, framework is no longer controlled by effective stress. Conversely, the dominating factor of porosity and permeability loss is quartz cementation and chemical compaction. Chemical compaction involves re-precipitation of dissolved minerals on available grains surfaces and pressure solution, both at grain- to grain contact and at stylolite interfaces (Heald, 1956).

Another important factor at this stage is illitization of smectite, which is initiated at 60 – 80 °C (Peltonen et al., 2008). With increasing burial depth and a subsequent increase in temperature, dissolution of smectite and precipitation of a more stable mineral will occur given the right conditions.

The reaction for smectite – illite transition can be written as:



(Boles & Franks, 1979; modified by Peltonen et al., 2008).

Given from the reaction above, this type of a diagenetic transition requires dissolved potassium (K^+), which is usually stripped of from detrital feldspar grains (Bjørlykke, 1998).

Below 3.5 – 4 km of burial depth (temperatures above 130 C°), quartz cementation and illitization reduces the reservoir properties in sandstones (Bjørlykke et al, 1995).

3.4 Carbonates

The general compositional unit for all carbonate minerals consists of CO_3^{2-} . The type of carbonate mineral is determined based on the amount and type of cations that are linked together with the ion-group. The most common minerals in rock-forming carbonate sediments can be structurally grouped either as calcite (rhombohedral) or as aragonite (orthorhombic), which forms in normal marine environments (Morse & Mackenzie, 1990). The common names of carbonate minerals are listed in Table 3.1.

Table 3.1: Common carbonate minerals formed in marine environments, with the three most prevalent minerals marked in a red box. Modified after Hanken et al., (2010).

Low-Mg calcite CaCO_3 (<4% MgCO_3) (hexagonal)
High-Mg calcite $(\text{Ca},\text{Mg})\text{CO}_3$ (>4% MgCO_3) (hexagonal)
Aragonite (CaCO_3) (orthorhombic)

Other common carbonate minerals are:

Siderite FeCO_3
Magnesite MgCO_3
Strontianite SrCO_3
Rhodochrosite MnCO_3
Smithsonite ZnCO_3
Ankerite $\text{Ca}(\text{Mg},\text{Fe})(\text{CO}_3)_2$
Dolomite $\text{CaMg}(\text{CO}_3)_2$

3.4.1 Chalk

Chalks are made up of pelagic sediments, commonly formed from coccolithophores. These organisms are primarily made of low-Mg calcite, but may contain small amounts of aragonite. Due to their chemically stable nature, coccolithophores are mineralogically stable during early diagenesis (Hillis, 2001).

Coccolithophores

Coccolithophores are single-celled plants consisting of free-floating algae. They are composed of thin calcareous plates (coccoliths) and vary in size (few μm) and shape (round to oval). The coccoliths consist of thin and flat rhombic crystals (0.25-1 μm) and are made from low-Mg calcite, which are stacked together in a spiral pattern. The skeleton (coccosphere) is shaped in a spheroidal or ovoidal structure, ranging in size from 5-20 μm , and is composed of numerous coccoliths attached together (Scoffin, 1987). However, when the

coccolithophores has perished, the skeleton is usually dissembled to a single cell coccoliths (Hanken et, al., 2010).

Habitat of chalks

The ecology of coccolithophores is predominantly in open marine basins within the photic zone, but they may also occur in near shore lagoons. Coccolithophores are plants belonging to the golden brown algae, and are vital contributors to the distal shelf and deep marine deposits (Hanken et, al., 2010). Throughout Cretaceous and Lower Tertiary, the coccoliths have shown to be prevalent in the marine depositional system forming thick extensive chalk beds (Surlyk, 2003). They are important indicators of the marine paleoecology, seeing how they commonly occur in the uppermost part of the ocean in temperate zones. Today coccolithophores comprise around 25% of all calcareous planktonic deposits. Nevertheless, in Cretaceous and Tertiary the coccolithophores contributed with approximately 90% of the planktonic deposits, where the majority was deposited as chalk (Hanken et, al., 2010).

3.4.2 Reservoir- preserving mechanisms in chalk

Chalks that are composed of coccoliths can be extremely porous, forming high porosity in chalk reservoir even at deep burial depths. The porosity preserved may be as high as 40-50%, due to the primary shape of the interparticle micropores. However, the diameters of the pore-throat are small, less than 1 μ m, and reduce the permeability drastically (only a few millidarcys preserved). A relatively high permeability is important for hydrocarbon to infiltrate the pores. In a reservoir quality point of view, the coccoliths are therefore reliant on combinations of other mechanisms, such as fracturing, which will improve the permeability. In the North Sea, fractured chalk is essential for production of major hydrocarbon reservoirs, formed during Cretaceous to Early Tertiary time (Hanken et, al., 2010).

Chapter 4: Methods and Data

4.1 Introduction

The main emphasis is to interpret the sedimentological features and the diagenetic modifications related to carbonate intervals within the Maureen Formation. This was carried out using various methods and data, such as core logging, mineralogical texture and composition and wire line logs. The methods and data applied for this study are presented in this chapter

4.2 Sedimentological core study

Core description and core logging was performed on one well, 9/11b-11, located on the East Shetland platform in the Mariner Field East province, UK. Total length of the cored section was 44 ft. long, corresponding to about 13.4 m. The core was logged in feet and then converted to meters after digitalization and stacking of the logs.

4.2.1 Core description

Core logging of well 9/11b-11 was performed at Iron Mountain in the Kirkhill Industrial Estate in Aberdeen, Scotland. The core sample was displayed in 16 different sections, each section ranging from 1-3 ft. The core was logged at a scale of 5cm: 10inches on a standard core description-logging sheet, developed by RWE Dea Norge AS (Appendix A). The scope of the core logging and description was to identify the different facies and facies association for interpretation of the depositional environment. Furthermore, core photos together with wire line logs of wells further west on the East Shetland platform was provided by Statoil. These were used to study the carbonate intervals together with the logged core section to get better understand the lateral distribution and the origin of the carbonates within the Mariner Field.

4.2.2 Digitalization of core logs

Core logs were digitalized in the drawing program Adobe Illustrator CS6. The digitalized logs of the core samples, taken from well 9/11b-11 are presented in Appendix B, log sheets 1-16. In order to get a better overview of the lithological changes and variations within the digitalized logs, the sections were simplified through a stacked log presented in Appendix C.

The intervals of where the core samples are taken from and used for petrographic and mineralogical analysis are marked on the right hand side of the stacked log.

4.3 Petrographical and Mineralogical analysis

Petrographical and mineralogical analysis were done by optical microscopy study of the thin sections, SEM analysis and XRD analysis. The samples used in the petrographic study were collected from well 9/11b-11 provided by Statoil.

4.3.1 Thin section analysis

A total of eighteen thin sections were used in the analysis of the mineral composition and textural parameters of the rock. Statoil provided nine thin sections, with two of the samples (sample 17 and 18) impregnated with blue epoxy. Technical staff, Salahalldin Akhaven at the Department of Geoscience, University of Oslo, prepared the nine remaining thin sections, all impregnated with blue epoxy.

Point counting (modal analysis) of the thin sections was done using a Nikon LABOPHOT-POL petrographic microscope with a Swift automatic counter. Point counting was carried out to estimate the composition and porosity of each sample. However, all the samples had oversized pores related to grain removal during preparation (artificial porosity). Additionally, the samples contained microscopic scaled porosity within the matrix. The latter porosity could not be estimated due to its small-scaled grain size. Porosity was only estimated in areas with good sorting and within the foraminifera, elsewhere it was ignored due to the uncertainty with regards to artificial porosity. A total of 400 points per sample were counted using utilizing both plain polarized light and crossed polarized light. Grain size measurements were performed on each of the samples using the Scope View 3.0 software. These measurements

where plotted in GRADISTAT® Grain Size Analysis Program, which provided both grain size distribution and sorting of each thin section.

The results of the point counting and the grains textural features are displayed in Appendix D, together with the thin sections sample name and interval depth.

In modal analysis, quartz was only differentiated based on crystallinity, and divided into polycrystalline and monocrystalline quartz. The different feldspar grains have not been distinguished and are only counted as K-feldspars due to the small percentage of plagioclase.

Further, the grain shape was determined by Power's (1953) terminology for degree of grain roundness (Figure 4.1).

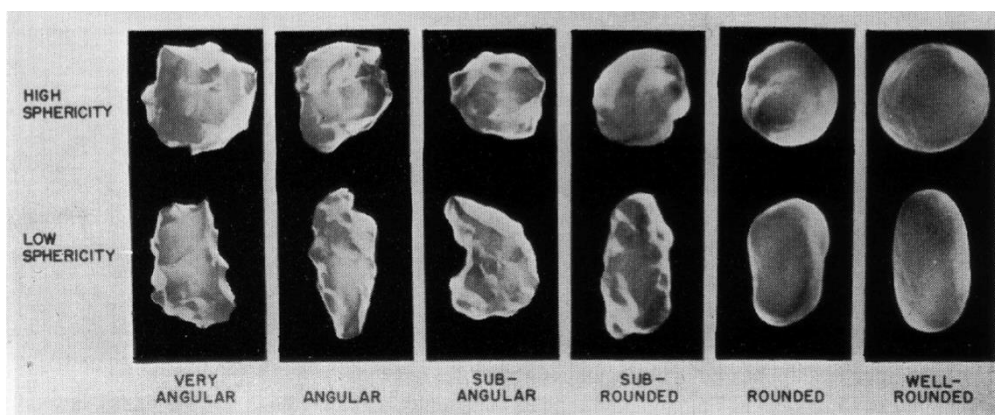


Figure 4.1: Roundness scale for sedimentary particles. Used for determining the rounds of grains in thin sections (Powers, 1953).

Uncertainties related to thin section analysis would be the inexperience and misinterpretation with regards to mineral identification and point counting. In addition, most of the thin sections displayed artificial porosity and artificial fracturing. This may have resulted in overestimation of the porosity and the fractures, mistaken for more mechanically indorsed compaction of the grains. Fifty grains were selected for grain size analysis and should be picked as randomly as possible. However, this is not possible when the measured grains are manually selected. In addition, a larger selection could be needed for more accurate results.

4.3.2 X-ray diffractometry (XRD)

11 core samples were used for the XRD bulk and clay fraction analyses, all of which are derived from well 9/11b-11. Each of the samples were run in the XRD BRUKER D8 ADVANCE instrument for analyzes. The XRD instrument used a diffractometer with an X-ray tube of Cu-K α radiation. This method is based on Bragg's Law:

$$n\lambda = 2d \sin\theta$$

Equation 3.1: Bragg's law of diffraction. N represents an integer, λ is the wavelength of the incident ray, d equals the spacing in the crystal lattice and θ is the angle between the incident ray and the scatter plane (Bragg and Bragg, 1913).

All of the prepared bulk samples were run in XRD in 2-65 degrees 2theta, step size 0.01 degree, 0.3 seconds per set.

XRD Bulk preparation and analysis

Preparations of each bulk sample were performed before the XRD analysis, and was carried out as follows:

- The 11 samples were first disintegrated by hammer, and then crushed by a metal rock crusher into even smaller pieces.
- About 3.5 grams of the crushed sample was then crushed for a third time in an agate mortar.
- 0.5 gram of the total 3.5 grams sample, together with some ethanol was poured into the micronizing container, which held small cylinders of agates staked on top of each other. The sample was then grinded by a micronizing machine (Glen Greston, McCrone Micronizing Mill) for about 30 seconds to pre-contaminate the container.
- After pouring out the pre-contamination material, the 3 grams of crushed sample left were poured into the same container together with about 8ml of ethanol. The samples were grinded in the micronizing machine for 12 minutes to a homogeneous pulverized material.
- The sample was poured into a clean plastic container and put into a heating cabinet to air-dry. After 24 hours the ethanol evaporated, leaving only dry powder.

- The pulverized material was grinded once more in an agate mortar. Then the powder was compacted onto a silicon sample holder using a clean thin section plate with as little force as possible.
- Each sample was then run in the XRD instrument for analysis.

The DIFFRAC.EVA.V2.0 software (EVA) was used to identify the different mineral phases from the given peaks. The “Search/Match” tool in the software was used to identify the reference peaks with the mineral phases using 2Theta- spacing and intensities from the PDF-2 database (Power Diffraction File, ICDD International Center for Diffraction Data). The software DIFFRAC.SUITE TOPAS was then used to quantify the amount of each of the mineral phases found in each bulk sample.

The results are presented in Figure 6.13, which show the sample numbers, rather than the given depth. This is done because the sample represents a depth interval in well 9/11b-11. All the samples are from a shallow depth and are acquired at short sample distances. In addition, two of the samples (sample 17 and 18) were acquired from an unknown interval, and two of the samples (sample 19 and 20) were provided during the process of analyzing. The content of the sample is therefore more emphasized compared to the depth. In Appendix E, a table is presented with all the analyzed samples in XRD with their depth interval and the quantification of the identified minerals.

XRD Clay fraction preparation and analysis

Preparations of each clay fraction sample were performed before run in the XRD instrument for analysis, and was carried out as follows:

- The 11 samples were first hammered into small pieces and then crushed by a metal rock crusher into even smaller pieces.
- 2-3 tablespoons of each sample was mixed with 100 ml Na_2CO_3 in a separate beaker glass and stirred for about 1 minute. Na_2CO_3 was used to chemically loosen the clay particles from each other by charging all the clay particle surfaces into homogeneous negative charged ions. This was the result of the high pH in the sodium, causing the clay particle to repel one another.

- After 24 hours, more Na_2CO_3 was then added to the dispersed mixture, which in turn was put in an ultra-sonic bath for 10-15 minutes. The beaker glass was then set aside for 6 more hours to let the particles settle and only leaving the clay-sized particles ($> 2 \mu\text{m}$) in suspension.
- A tube was filled with distilled water, which carefully siphoned the suspended clay particles left in the water column above 100 ml into a plastic container.
- The suspended clay mixture was added to a Millipore Laboratory Filtration System 3 using a cellulose nitrate membrane filter of pore size $0.45\mu\text{m}$. This type of filtration process was pursued as follows:
 - Between 15 mm to 30 mm of the suspended, material depending on the quantity of the clay particles in the mixture, was syringed into a funnel, which was attached by a clamp to a glass filter holder with the membrane filter on top.
 - A vacuum-filtering flask holding 1 liter, was attached by a tube to the glass filter holder, combined with an attached Chemical Duty Pump of 115V/60 Hz.
 - This filtering instrument was used to vacuum the Na_2CO_3 solution into the connected filtering flask, leaving only clay particles behind on the membrane filter.
- After the filtration, clay particles on the membrane filter was placed on a pyrex glass slide and rolled on by an aluminum cylinder.
- The samples were let to dry for 15-20 minutes before run in the XRD instrument for analysis.

The XRD clay fraction analysis were further treated in three different stages and run in the XRD instrument between each treatment to observe changes of the clay minerals peaks in the diffractogram. The three stages were performed and are as follows:

Stage 1: The samples were treated with an ethylene glycol vapor for 24 hours in a desiccator then run in XRD.

Stage 2: The samples were heated to 350 degrees in an oven for 30 minutes and then run in XRD again.

Stage 3: The samples were heated to 550 degrees in an oven for 30 minutes and then run in the XRD for one last time.

The software used for bulk analysis, DIFFRAC.EVA.V2.0, was also applied to for the clay fraction analysis. However, the tools used for the bulk analysis was not applied here. Each sample, with the air-dried, ethylene glycol and heat treatments where compered separately with one another and then compared with the Clay Mineral Identification Flow Diagram for identification, see Appendix F. The identified mixed clay was quantified using the principles from Watanabe (1981), Wilson (2013) and Moore & Reynolds Jr. (1989) see section 6.5.2.

Uncertainties related to the XRD – analysis would depend on the crystal size, orientation and crystallinity of the studied samples, which will influence the peak intensity and shape of the different mineral phases.

The sensitivity and small step-size of the Lynxeye detector usually produces a detection limit of around 1 – 2 % in multicomponent mixtures. The detection limit is affected by the overlapping of certain mineral phases present in the multicomponent sample, and can thus be difficult to quantify.

4.3.5 Scanning Electron Microscopy (SEM)

Scanning electron microscope generates a high-resolution image, which has the ability to observe microscopic shapes of objects to give information about the surface topography and composition. For scanning electron microscopy, the JEOL JSM- 6460LV electron microscope combined with a LINK INCA Energy 300 (EDS) system from Oxford Instrument was used to analyze 9 thin section and 9 stub samples. Using the BSI (backscattered electrons image) on carbonate coated thin sections, and SEI (secondary electrons image) on gold-coated stub sections, the chemical composition was used to identify the present minerals and their structure.

4.4 Strontium isotope analysis

Strontium isotope analysis (Sr) between ^{87}Sr and ^{86}Sr was applied on ten samples to see if there was any ratio-variation within the carbonates. A technical staff, Yuval Ronen at the Department of Geoscience, University of Bergen provided the results.

4.5 Well correlation and Petrophysical evaluation

4.5.1 Well correlation and interpretation of well- and wire line logs

Statoil provides the majority of the data used in this study. The log depths are measured in total vertical depth (TVD), if not stated otherwise. It should also be mentioned that all of the wells, with exception of well 9/11a-10z and 9/11b-1 (Figure 8.3), are essentially vertical with depths given in meters.

In order to achieve a lateral and vertical distribution of the carbonates within the Maureen Formation, Statoil provided a set of twelve wire line logs to be correlated in petrel® (Schlumberger). The wire line logs for each well included: depth (TVD) in meters, porosity log (PHIE), water- and hydrocarbon saturation log (SWE) and a lithology log of the rocks composition: calcite, shale and sandstone. The set of wire line logs were correlated between well 9/11a-10, 9/11a-10Z, 9/11-3, 9/11-4, 9/11a-9, 9/11a-8, 9/11-2, 9/11a-5, 9/11a-7, 9/11-1 and 9/11a-6, which are listed from east to west (Figure 4.2). Coordinates for all wells used in this study are listed in Appendix G.

Maureen Formation is presented in the data set and correlated against the lithology changes within the formation. The correlated wells also include the lowermost Lista Formation, parts of the eroded Chalk Group along with the uppermost Devonian basement. The main focus was to interpret the chalk beds within the Maureen Formation based on the cored section of well 9/11b-11. Wire line log images of both wells 9/11b-11 and 9/11b-z was also provided by Statoil, but could not be correlated with the other wells due to the lack of correlative data. Both of these two wells are located in the further east section of the Mariner Field, and are the closest ones next to each other (Figure 4.2). Well 9/11b-11 is composed of the thickest and most frequent deposited carbonate beds.

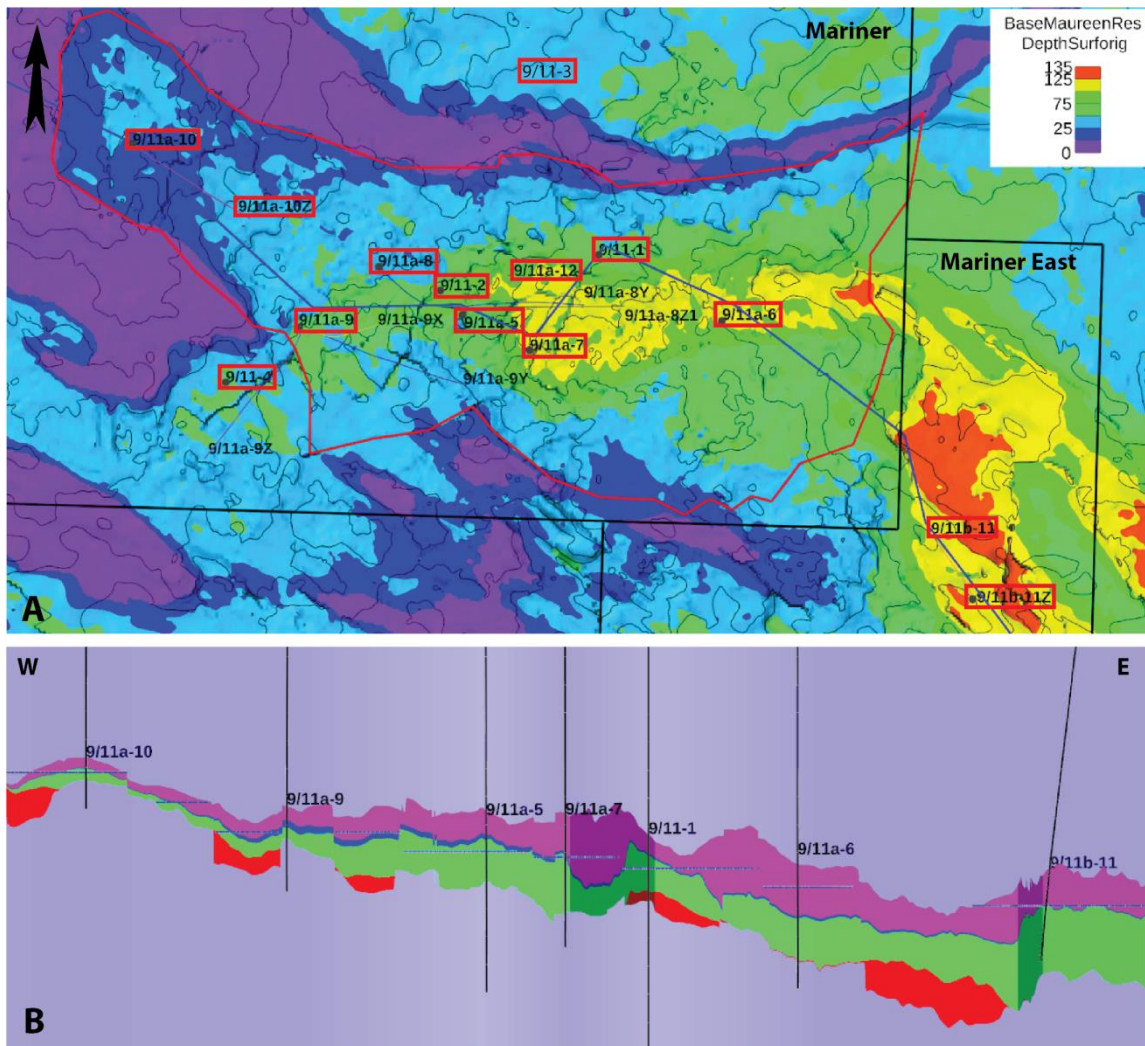


Figure 4.2: A) Thickness map of base Maureen reservoir, with all the exploration wells used for well correlation and/or petrophysical evaluation marked in a red box. B) Cross-section of base Maureen reservoir, illustrating the thickness variation and a relatively small incline of the formation trough Mariner East section to Mariner section on the East Shetland Platform (Statoil, 2014).

4.5.2 Petrophysical analysis

Statoil provided porosity and permeability logs for six of the correlated wells in addition to well 9/11b-11. Petrophysical analysis was carried out based on the relationship between porosity and permeability of the seven wells: 9/11a-10, 9/11-4, 9/11a-9, 9/11a-5, 9/11a-7, 9/11b-11 and 9/11a-10. However, depth for each well was not provided, and the porosities and permeability could not be related according to depth.

Chapter 5: Core description

5.1 Introduction

The core was provided from well 9/11b-11 within the Upper Maureen Sst, where the thickest carbonate intervals are discovered. The sedimentological core-log see Appendix B was used to describe and interpret the depositional environment of the Maureen Formation. From the core description, different facies have been described and associated to a depositional setting (Table 5.1). This is done to improve the understanding of the nature and the source of the carbonate intervals and to provide a brief interpretation of the depositional environment.

5.2 Characterization of facies

Characterizations of the logged core section are divided into seven facies based on lithology, texture and sedimentary- and physical structures. These characterizations are important to determine when establishing a facies. The facies can then be linked to a depositional environment and thereby offer a more lateral interpretation of the distributed sand and carbonate bodies within the Maureen Formation. The facies are summarized in Table 5.1.

Table 5.1: Characterization of the cored intervals and their facies.

Lithology	Facies	Description	Depositional environment
Calcareous sand (CS)	CS1	Mixed sand and chalk with chalk clasts and -veins in various sizes and shapes. Scattered glauconitic clasts, rock fragments, thin mud veins and some deformed mud clasts may appear. (Figure 5.1 A)	Mass flows
	CS2	Mixed sand and chalk with fractured features. Chalk clasts and vein structures in various sizes and shapes. Thin mud veins and scattered glauconitic clasts may appear. Some light purple minerals, within and around the deformed fractured features. (Figure 5.1 B)	Mass flows
	CS3	Soft sediment deformation of chalk within calcareous sandstone layer mixed with small chalk clasts. (Figure 5.1 C)	Semi-consolidated folded layer
Homogeneous sand (HS)	HS1	Structureless homogeneous sand. Partly to poorly consolidate, heavily stained with hydrocarbons. Small chalk clasts mixed within weakly hydrocarbon stained, calcareous sand clasts. (Figure 5.2 A)	Mass flows
	HS2	Structureless homogeneous sand, with crushed shale fragments. Contain various sizes of weakly petroleum stained, calcareous sand clasts and some smaller chalk clasts within. (Figure 5.2 B)	Mass flows
Chalk (C)	C1	Thick chalk layer with some brown-yellowish stained patches. Few mud veins, and some incorporated sand grains. (Figure 5.3 A)	Block slides and/or mass flows
Calcareous clay (CC)	CC1	Crushed calcareous clay beds with small fragments of chalk. Slicken-slide structures, no observation of mineral infill. (Figure 5.3 B)	Reworked calcareous clay by mass flows

5.3 Characterization and interpretation of the core log

The characterized facies observed in the studied core (Table 5.1) will be further described and assessed into a depositional system. From Chapter 2 a short description of the Maureen Formation was introduced. It describes the Maureen Formation to consist of mixed facies with reworked chalk, stripped from carbonate shelf edges and carried out to the basin floor by mass flows. Based on previous literature and the observed features of the logged core section, a proposed depositional environment will be presented for each of the four different lithological intervals from Table 5.1.

Calcareous sand deposits (CS)

The first calcareous sand unit represented in the logged section starts from 6212ft up to 6207ft, see Appendix B, log sheet1. The lower part of this unit consists of dark gray calcareous sand mixed with chalk clasts. In the central part, lamination of white chalk is observed and oriented in a steep angle, most likely a result of the sub-horizontal drilling. The section is cut by a sharp boundary represented by a change in color from dark gray into faint brown colored calcareous sand with less white chalk clasts. The upper section stretches from 6209-6207ft and is defined by another change in color from the brown calcareous sand to light gray calcareous sand, similar to the one described above. Clasts of white chalk are abundant throughout this section, with thicker chalk intervals within the lowermost section. Some thin deformed vein structures, composed of chalk, is also observed in the lower part. The upper part, however, changes slightly with incorporated rounded gray-blackish rock fragments and thicker white chalk clasts.

Next calcareous sand unit is within the interval 6197ft 7inch - 6196ft 3inch and is deposited between two homogeneous sand-rich units (HS)(described below in the homogeneous sand deposits) see Appendix B, log sheet6. The calcareous sand differs from the previous mixed interval with a dark grayish color mixed with both small white chalk clasts and rounded to oval glauconitic clasts. No deformation structures are observed. Two sharp boundaries mark the lower and upper part of this unit. The upper boundary changes from consolidated grayish calcareous sand to stained dark brown, semi-consolidated sand. The lower boundary differs slightly with more consolidated lighter brown stained sand before it shifts into a gray calcareous sand.

The third calcareous sand unit ranges from 6190ft to 6178ft, see Appendix B, log sheet 9. Within the lowermost seven inches, a small-scaled lamination features was observed with thin greenish mud layers interbedded in a light gray calcareous sand unit. The clay layers show a slight inclination, pinching out to the right with a dip between 15-20°. Next seven inches include a thin clay-rich unit (CC) (described below in the calcareous clay-rich beds), marking a change in lithology within the calcareous sand unit. From 6186ft 11inch and up, the calcareous sand is composed of a dark gray unit with some thin, white, deformed chalk veins dominating the lower half. The whole unit is mixed with small-scaled, white chalk clasts, round to oval glauconitic clasts and small amounts of rock fragments. Some parts contain light-green deformed mud veins. The top is marked by an apparent change in lithology and color, shifting from gray calcareous sand to homogeneous dark brown sand, no visual transition is observed.

The thickest calcareous sand unit was logged between 6183 ft 6 inch – 6174 ft (Appendix B, log sheets 11-14), with an interbedded, thin clay-rich unit (CC) of six inches. White chalk clasts dominate the entire calcareous sand unit. The lowermost thirty-five inches starts out with a dark gray color with some brown stains and glauconitic clasts, before it transitions into a lighter gray color. The base is defined by a transition from homogeneous sand (HS) to the calcareous sand unit. Variation in color and texture in this transition indicate mixture of the two lithologies; with more consolidated sand incorporated and small white chalk fragments in the upper part of the homogeneous sand. Further up in the calcareous sand unit, a thick, white three-inch large chalk clast is observed with some light gray mud-veins in the upper left part of it. Small white chalk clasts are observed within the mud-veins. Above the thick chalk clast, calcareous sand shifts into a lighter gray color, containing faint brown patches, deformed white chalk veins, -lenses and some light green mud-veins before it changes into the clay-rich unit (CC). Above the clay-rich unit the calcareous sand is mixed with glauconitic clasts, deformed white to brownish chalk veins, and light-green, thin mud veins. This part was observed between 6180ft – 6177ft and differs from the rest of the calcareous sand unit; with fractures filled with light brown sand and purple minerals. The remaining unit is dominated by deformed white chalk lenses, -veins, some mud clasts and deformed thin green mud-veins. In the central part, soft sediment fold structures of white chalk are observed. The top boundary is defined by a lithology change from calcareous sand to a more homogeneous chalk unit (HS).

Depositional environment: The lithological mixture of sand, carbonate with floating clasts, glauconite and rock fragments imply an absence of turbulent flow with no dynamic sorting of material (Nichols, 2009). The texture and mixture indicate deposition by debris-flow mechanisms. Slump and/or slide deposits might also be prevalent, resulting of deposition of features such as soft-sediment folds, deformed structures and block slides.

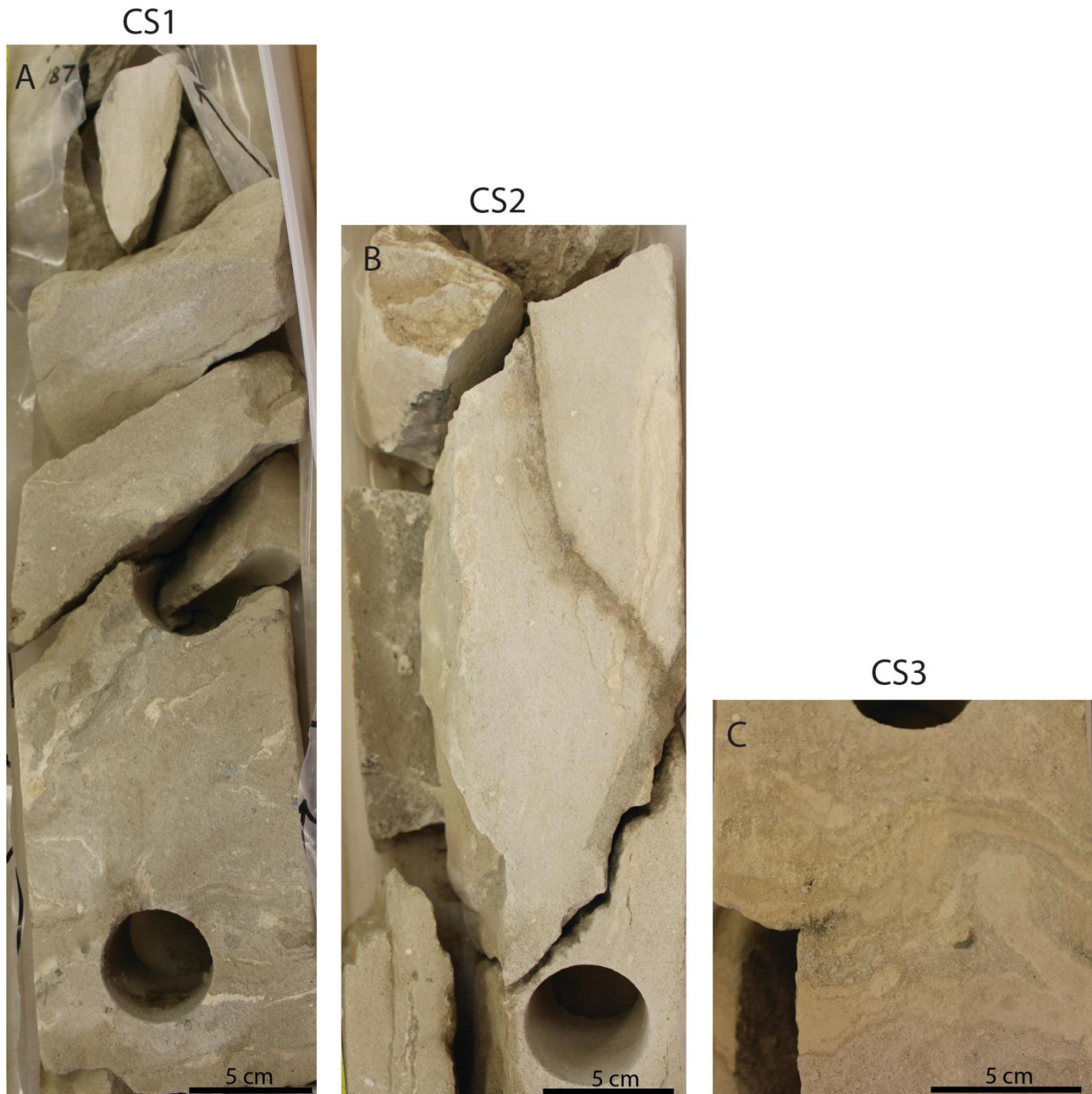


Figure 5.1: Core photos of the calcareous sand facies CS. A) Represents facies CS1. B) Represents facies CS2. C) Represents facies CS3.

Homogeneous sand deposits (HS)

The thickest homogeneous sand layer was logged within an interval from 6207ft-6197ft 7inch, and is divided into two distinctive units, see Appendix B, log sheets 3-6. Within the lower two feet the unit is represented by a dark brown stained, homogeneous sand, mixed with shale fragments and large, faintly stained, calcareous sand clasts. The sand is mostly unconsolidated and the amount of calcareous sand clasts decreases within in the upper part. From 6202ft the section shifts into coarser homogeneous sand, representing the second unit. This sand is slightly darker stained and mostly unconsolidated and characterizes the rest of this unit. However, in the upper eight inches the sand becomes slightly more faintly brown and consolidated and mixed with some calcareous sand.

Between 6197ft 3inch – 6192ft 3inch the second dark brown homogeneous sand-rich unit is represented, see Appendix B, log sheets6-8. This unit is comprised of slightly more consolidated and finer grained sand than the upper part of the previous described homogeneous sand unit. It also differs with a few faintly brown-stained calcareous sand clasts at the bottom. The unit is defined by two sharp boundaries. The lower boundary shifts from a gray calcareous sand into the dark homogeneous sand. The upper boundary increases with a lighter brown color toward the top before it shifts to a white deformed chalk bed.

The third homogeneous sand unit, ranging between 6187ft – 6183ft 6inch (Appendix B, log sheets10-11), is partly consolidated at the bottom with increasing consolidation toward the top. Lithology and texture is mostly the same as the last described homogeneous sand unit, and is represented by two sharp boundaries. The unit is defined by two abrupt boundaries, shifting from light grayish calcareous sand to dark brown homogeneous sand and back into light gray calcareous sand again.

The last logged homogeneous sand unit between 6171ft 9inch – 61688ft (Appendix B, log sheet16) was defined by a boundary shifting from two distinctive lithology; a white chalk-rich unit to the dark brown homogeneous sand with some shale fragments. The fragments were only observed within the lower nine inches and a few faintly stained calcareous sand clasts in upper part. The remaining unit has the same texture as the homogeneous sand unit from 6187ft – 6183ft.

Depositional environment: The homogeneous sand units are composed of fine to medium sand grains with no visual structures. This type of texture and morphology are typical for turbidity currents, transporting suspended material in the water masses by turbulence, and depositing them in graded beds. Such deposition with fine to medium grain-sizes and good sorting could indicate a low-density turbidity current. On the other hand, the homogeneous sand unit mixed with calcareous sand clasts and shale fragments might also indicate a debris flow. Some sections may also be a mixture of debris flows and turbiditic currents.

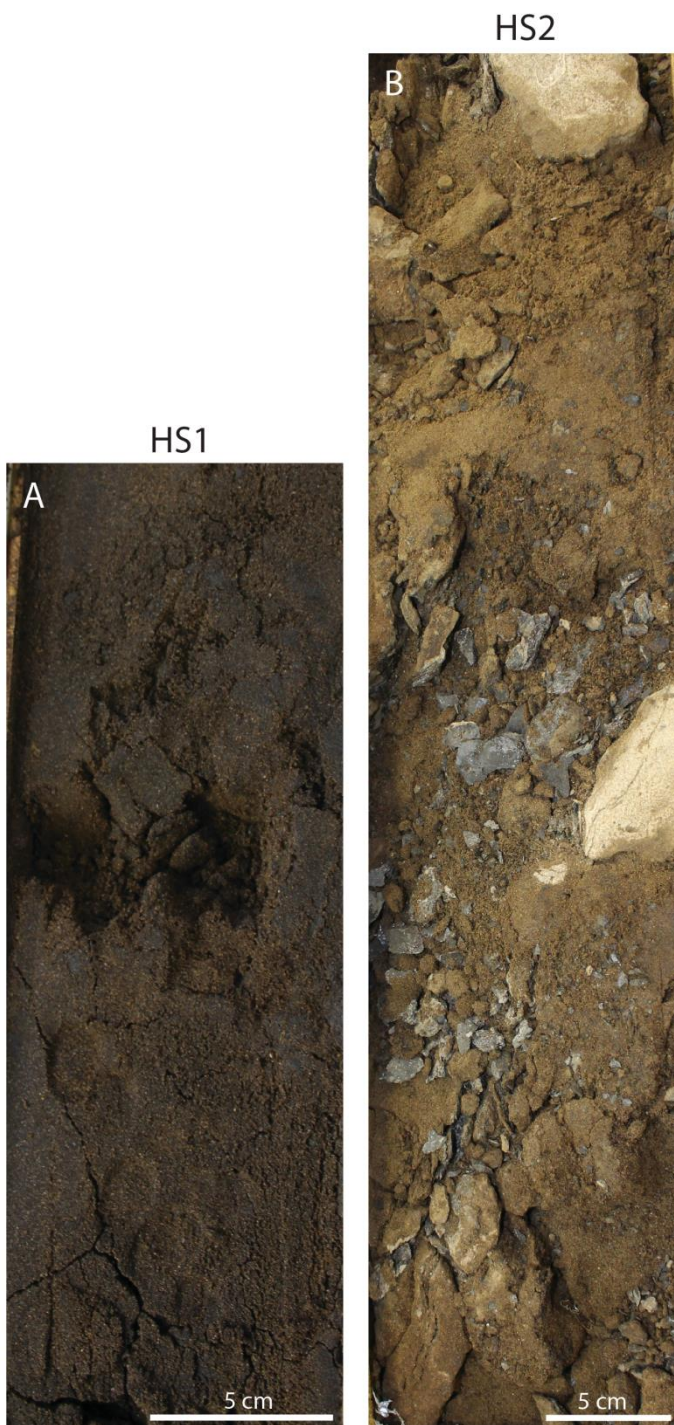


Figure 5.2: Core photos of the homogeneous sand facies HS. A) Represents facies HS1. B) Represents facies HS2.

Chalk-rich beds (C)

The first thick chalk-rich bed was observed between 6192ft 3inch – 6193ft, see Appendix B, log sheet8. Lower part comprises deformed chalk lens and chalk veins into a light gray calcareous sand section. The chalk is white in color with some faint light brown patches. A transition from dark brown to lighter brown sand, then into a thin rim of white chalk, partly stained, to gray calcareous sand, defines the bottom part of the boundary. Further up in the lower part of the chalk-rich unit contain light gray calcareous sand veins and patches. The upper part becomes more homogeneous with some lighter patches, chalk clasts and less incorporated sand. Some parts throughout the whole unit are covered with faint light brown-yellowish patches. Top boundary shifts abrupt from the chalk-rich unit to a light gray calcareous sand unit.

Between 6174ft-6172ft (Appendix B, log sheet15), a second thick chalk-rich unit was observed, mostly composed of homogeneous white chalk with some faint light brown-yellowish patches and some lighter patches of chalk. Some areas show minor fractures filled with light gray mud. The upper part gradually increases with a light gray mud with a silty-sandy light brown-greenish thick vein incorporated. In the upper part of this section, some deformed chalk veins can be observed with some light brown patches at the top. Two distinctive changes in lithology represent the chalk-rich unit. Lower boundary switches from light gray calcareous sand to the white chalk-rich unit, whereas the upper part switches from the light gray-white chalk-rich unit with faintly brown patches to homogeneous dark brown sand. No transition is apparent in neither of the boundaries, and the upper part is missing three inches before it shifts into the dark homogeneous sand.

Depositional environment: The chalk-rich units are deposited in at least two stages; the first stage is a reworked chalk from storm waves or tectonic instabilities, the second stage is most likely represented by block slides. Such flows might be deposited as individual blocks or within a debris flow. It is also possible that they are deposited as a combination of these two mechanisms.

Calcareous clay-rich beds (CC)

Two separate calcareous clay-rich units are observed, located within the described calcareous sand units. First calcareous clay unit is located between 6188ft 11inch - 6189ft 5inch (Appendix B, log sheet9), and the second is located between 6180ft 10inch – 6181ft 4inch (Appendix B, log sheet12). Both units have a same thickness of six inches and share the same textural feature such as containing small fragments of chalk clasts, slicken-slides, with no mineral infill, and a distinctive light green colored bed. The calcareous clay-rich intervals are only represented as rock fragments, and show no visual transition between the calcareous sand below and above its boundaries.

Depositional environment: These calcareous clay units may originate from two different depositional processes; 1) suspended sediments reworked by mass flows 2) reworked allochthonous volcanic ash beds by mass flows.

C1



CC1



Figure 5.3: A) Core photo of the chalk rich layer, facies C1. B) Core photo of calcareous clay, facies CC1.

Chapter 6: Petrographical and Mineralogical Results

6.1 Introduction

Petrographic and mineralogical analysis have been performed on core samples provided from well 9/11b-11, which includes mineral and chemical composition from SEM- and XRD-analysis and textural parameters from modal analysis of thin sections. The scope of these studies is to investigate the origin of the carbonates within the cemented sands, including calcite and chalk, and to understand its unevenly distribution within the formation. This also includes what type of diagenetic modification the core samples have been subjected to during shallow burial diagenesis. Knowledge about the composition and texture of the carbonates might also be helpful in determining the good preserved reservoir quality within the Maureen Formation.

6.2 Composition and texture

Results from point counting classify the overall frameworks composition as a wackestone. Sample 4 and 9, can in some areas be classified as packstone, due to less matrix between the grains and it has an overall grain-supported appearance. Mud within the wackestone is defined as carbonate particles with a grain size < 20 micrometer. By Folk's classification the material of the matrix is defined as a carbonate mud (micritic mud) and along with the high content of fossil fragments it falls within a biomicrite limestone. Based on modal analysis the samples are mostly composed of carbonate mud, with an average of 55,8% see Figure 6.1 A. These results were then plotted into Folk's (1962) triangular diagram Figure 6.1 B, classifying the carbonate in the Maureen Formation as a type II limestone. Accordingly, this indicates a poorly sorted limestone deposited in an environment with weak and/or short-lived currents (Folks, 1962).

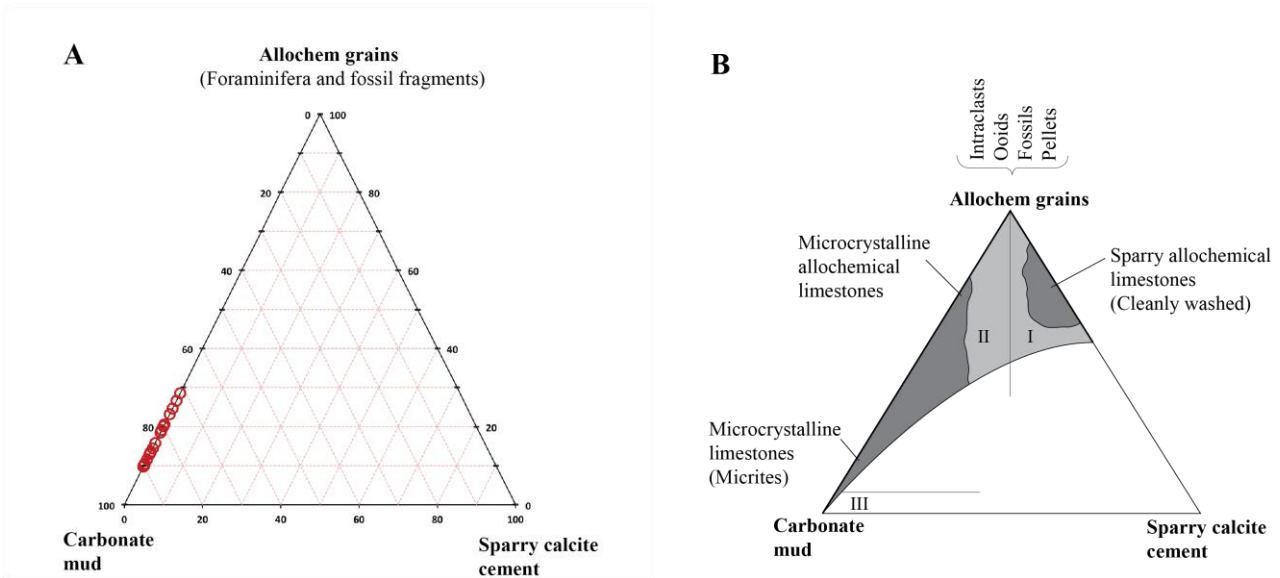


Figure 6.1: A) Samples 1 to 18 plotted in ternary diagram for carbonates. B) Triangular diagram for tree major textural types of limestones. Both figures modified from Folk (1962).

Textural maturity of the sand is within the immature to sub-mature stage. The detrital grains vary from very angular to sub-rounded grains where the majority of the grains are within the sub-angular range (Powers, 1953). The modal analysis show matrix as the dominating material, composing 15% of the total volume. The siliciclastic components in the samples are therefore classified as wackes (Dott, 1964) and are overall poorly sorted. Within the wackes ternary diagram (Figure 6.2), the textural composition is mostly quartz wacke and lithic greywacke.

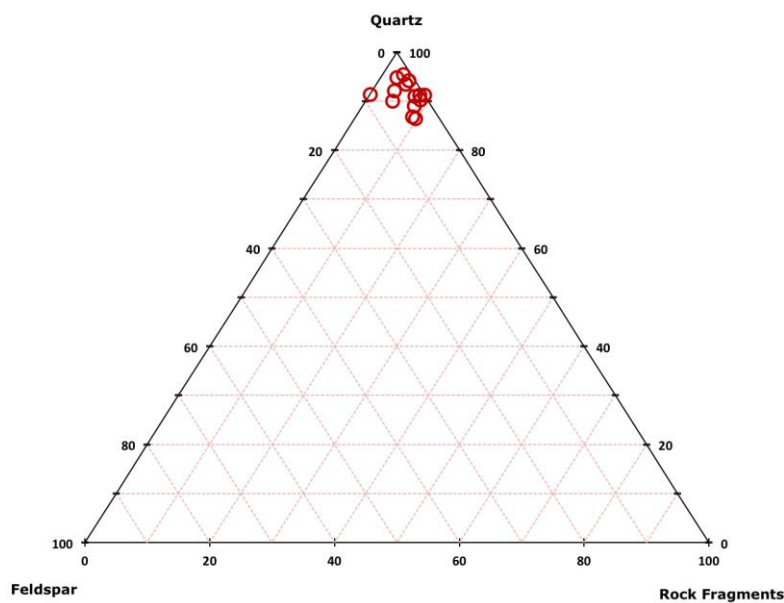


Figure 6.2: Ternary diagram of QFR classification for greywackes. All samples comprising quartz, feldspar or rock fragments are plotted in the diagram introduced by Dott (1964).

Some areas show a better sorting within the samples, such as in sample 4 and 18, which are classified as quartz wackes. These areas are more grain supported, less than 1% matrix, and comprise the highest preserved porosity within all the studied samples. Sample 4 and 18 contain the lowest percentage of carbonate mud, with less than 40% of the total framework.

6.3 Textural parameters and porosity

From Gradistat (see Chapter 4.3.1) the textural parameters of grain size and sorting were calculated. Grain size of the Maureen sands, forams and fossil fragments within the studied samples range between 275 – 111 microns, with an average grain size of fine sand. From the textural parameters, it shows that samples composed of chalk rich units have a better sorting than the mixed calcareous sands, which show a poorly sorted trend. However samples of mixed calcareous sands that contain more chalk than siliciclastic material show an overall moderately sorted trend. The more homogeneous sands, such as sample 4 and 18, are well sorted within areas that are more porous and contain a larger amount of quartz (Figure 6.3 A). However, these two samples also display areas with a more mixed composition dominated by calcareous matrix which classifying these areas as poorly sorted sands, see Figure 6.3 B. In Figure 6.3 C an overview of the transition between good and poorly sorted areas within thin section 18.

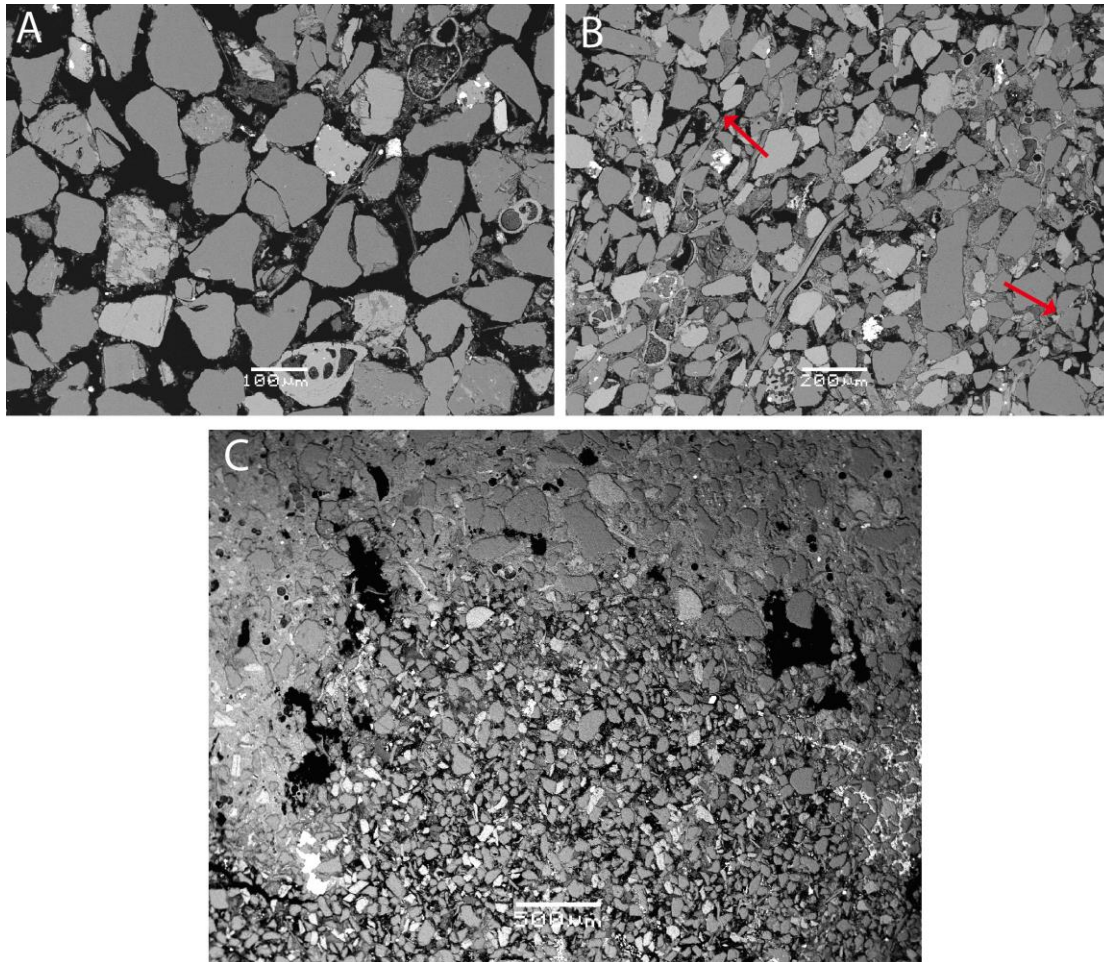


Figure 6.3: SEM image, of thin sections: A) Sample 4, illustrating an area with good sorting and more porous. B) Sample 4, middle part showing a poorly sorted area, with red arrows pointing towards more porous and better-sorted areas. C) Sample 9, an overview of the transition between well and poorly sorted grains. Upper part is matrix supported representing a poorly sorted area. Lower part is grain supported representing more porous sorted area.

The textural parameters are also studied in relation to porosity, which are estimated from modal analysis. Grain size vs. porosity and sorting vs. porosity are presented in Figure 6.4 A and B. They show a moderately good linear correlation, where increasing grain size and sorting corresponds to a decrease in porosity. This signals that poor sorting with large grain sizes will compact more during mechanical compaction and thereby decreasing the porosity. Samples containing a higher quantity of carbonate mud might help preserve the porosity see Figure 6.4 C. However, no estimation between intergranular and intragranular and macro and micro porosity was implemented during modal analysis, which could help determine such relations. Additionally, due to the nature of the thin sections, primary and secondary porosity could not be estimated either. Such differentiation of porosities would have provided a better quantitative data with regards to the compaction history of the Maureen Formation.

Additionally, porosity related to depth shows a feeble relationship, indicating that some mechanical compaction within the carbonate rocks might have taken place during burial with a decrease of porosity (Figure 6.4 D). The two samples that deviate with the highest preserved porosity and lowest amount of carbonate mud are samples 4 and 18 (Figure 6.4 C). This deviation is caused by the textural composition mentioned previous.

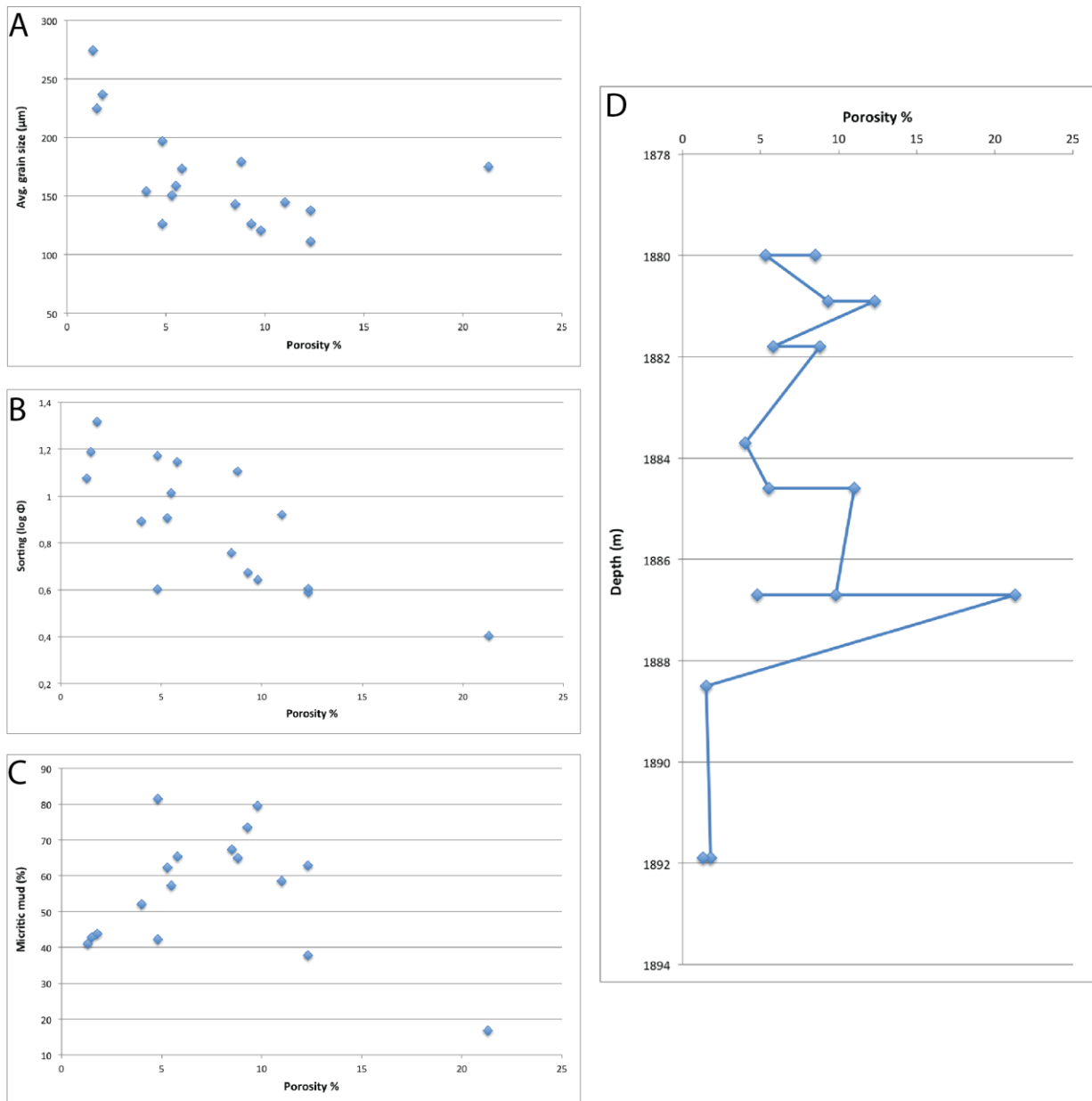


Figure 6.4: A) Calculated average grain size from Gradistat in relation to porosity B) Sorting calculated from Gradistat in relation to porosity C) Relationship between matrix and porosity. D) Porosity in relation to depth, where the depth is given as the highest interval for each sample. Sample 17 and 18 are here excluded due to lack of depth interval.

6.4 Optical mineralogy and SEM

Nine samples have been study through SEM- and optic analysis to establish the composition, texture and structure of the present minerals. Additionally, nine extra thin sections were studied using microscopy to give a better overview and understanding of the how the textural parameters and the grains are distributed in the calcareous sand layers and in the cleaner chalk intervals. Furthermore, the percentages estimated below are derived from the modal analysis (Appendix D).

6.4.1 Framework

Quartz

Quartz grains are the majority of silica minerals dominating the framework with an average of 21.9 %. The grains are mainly round to subangular in shape and vary in size from 400 μm within the framework and down to 5 μm within the matrix. The quartz grains were differentiated based on crystallinity, where the monocrystalline grains dominating the larger quantity of the framework with about 19,8%. Polycrystalline quartz is less represented in the cleaner chalk intervals, and has an average of 2,1%.

Feldspar

The feldspar grains are mostly rounded and vary in size. The majority of the feldspar grains observed in SEM shown as brighter colored K-feldspar with some darker albite patches, see Figure 6.5 A. The types of feldspar were distinguished by their EDX spectrum. The pure feldspar grains consist predominantly of K-feldspar, however minor amount of pure plagioclase grains can also be observed from the EDX results. Distinction between K-feldspar and plagioclase was not implemented in the modal analysis due to the generally low amount of feldspar grains 0,6%, and the mixture of both feldspar and albite, which could not be distinguish from another.

In the more chalk rich layers the amount of feldspar is observed to be small to absent, whereas the K-feldspar grains appeared more frequently in the calcareous sand layers. Additionally most of the thin sections display oversized pores, most likely a result of grain removal during preparation (Figure 6.5 B, C). The existence of oversized pores creates a false

interpretation of secondary porosities associated with feldspar precipitation. The oversized pores were therefore not taken to account during modal analysis.

Mica

Micaceous flakes are observed in small quantities of muscovite grains. The muscovite grains were distinguished by their birefringence in the cross polar light. Some grains have been subjected to minor grain modification observed through SEM, where authigenic pyrite has filled in parts of the muscovite grain structure see Figure 6.5 A. Other mica grains observed through SEM and EDX show indications of small-scaled intergrowth of less K-rich composition (most likely kaolinite) that appears as darker tone constituents within the lighter tone muscovite. However, the less K-rich mineral is most likely a detrital grain. Additionally, chalk rich layers show lower mica content than the remaining samples. Overall content of mica grains included in the framework is relatively small, with about 0,4 %.

Glauconite

Glauconitic grains were observed through nearly all of the samples, with about 0,5% of the total detrital grains, except in the chalk-rich layers. The grains vary in size from 10-200 μm , and appear in two distinctive forms, round and angular shaped. In the microscope through cross-polar light, the grains were easily observed due to their distinctive green color and their fine granular texture see Figure 6.5 D. In plane polarized light they also appear green, but with a slightly more faded color. In SEM the morphological features varied and seemed to be partly dissolved and thereby creating secondary porosity. However, these features are most likely due to grain removal during preparation (Figure 6.5 B, C) and not compaction driven mechanisms. Additionally, due to the small amount and scattered nature of the glauconitic grains, they were not detected in the XRD Bulk analysis.

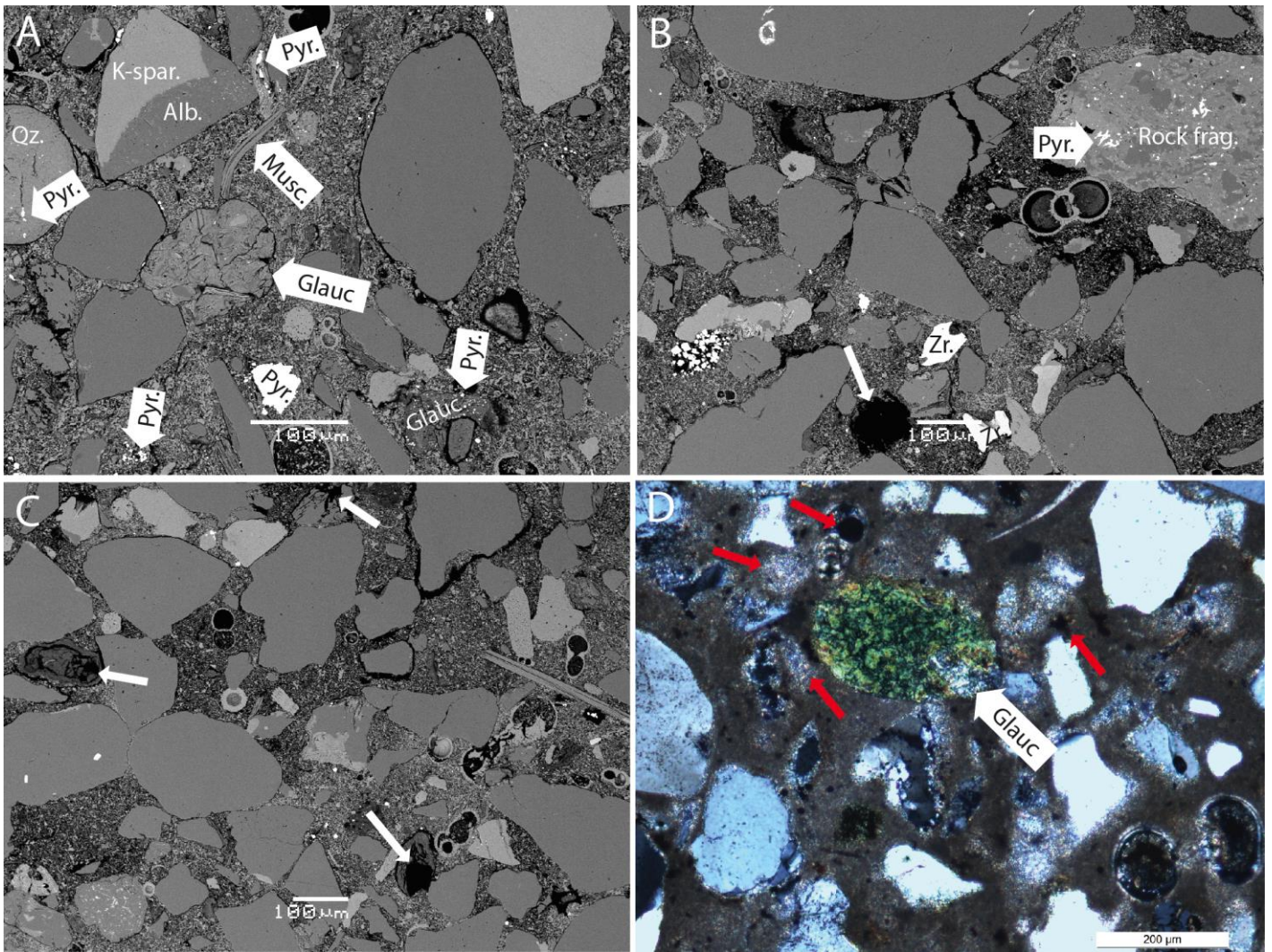


Figure 6.5. A) Sample 2, SEM image of thin section showing a lighter colored K-feldspar (K-spar.) with darker albite (Alb.) patch, some deformed muscovite grains (Musc.) and a rounded glauconitic grain in the center (Glauc.). Accessory mineral pyrite (Pyr.) within the matrix and framework. B) Sample 3, SEM image of thin section. Accessory mineral within the framework zircon (Zr.), arrows pointing at grain removal. A) and B) Pore filling pyrite within grain structure similar to that of quartz (QZ.), muscovite (Musc.), glauconite (Glauc.) and rock fragments (Rock frag.). C) Sample 3, SEM image of thin section. Arrows pointing at grain removal, such as glauconitic and feldspar grains. D) Sample 3, through optical microscope image in cross-polar light. Arrows pointing at overlaying micritic chalk matrix and dark spots representing carbon coating. Green colored glauconitic grain (Glauc.) in center.

Carbonate

Carbonate grains, that are part of the framework is represented by detrital bioclast, such as foraminifer, crushed mollusks (of a previous aragonite shell) and other fossil fragments. They vary in size and shape and are most abundant in the chalk-rich layers. The primary shells of the organisms are mainly composed of low Mg Calcite, which makes these bioclast highly stable during diagenesis. There is also no evidence of pore-filling carbonate cementation within any of the studied samples. However, some minor indications of epitaxial cement on the interior chambers of a few foraminifera have been observed in SEM see Figure 6.6, though this might have originated from a previous diagenetic instability.

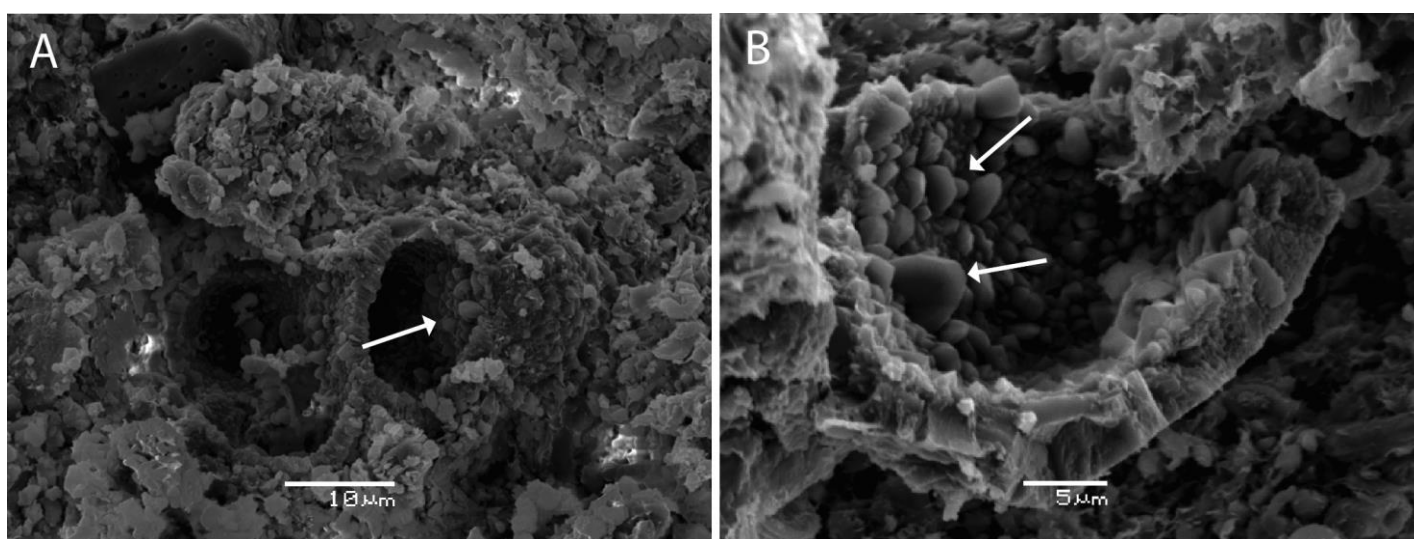


Figure 6.6: SEM images of stub samples: A) Sample 10, showing a foraminifer with crystalized calcite (epitaxial cement) on interior (white arrow). B) Sample 2, showing a fragmented foraminifer with some crystalized calcite on interior (epitaxial cement), see arrows.

Other remarks:

The detrital grains, especially quartz and feldspar, show minor fractures, which are filled with pyrite. Other grains however were hard to identify in the microscope, due to limiting factors such as overlaying micritic chalk matrix which partly or completely covered the grains surface and thick layering of carbon coating covering the grains with dark spots (Figure 6.5 D). Additionally, no evidence of mineral leaching and no indication of quartz overgrowths were observed during SEM and microscopy.

Other detrital minerals that have been detected are rutile, apatite, zircon and monazite (Figure 6.5 B). These minerals appear scattered within small quantities and are predominantly absent in the chalk rich layers

6.4.2 Clays

Identification of the clays was based on the XRD Clay fraction analysis see section 6.5.2. The amount of clay was relatively small in the studied thin sections, and the interstratified clays (I/S) found from XRD Clay fraction analysis was difficult to identify in EDX. The EDX could only show the major elements of the mixed clay layer Si, Al, K, Ca, Mg, and Fe. From stub sample in SEM analysis, webby to filamentous morphology with small-scaled bridges across pore of the I/S was observed (Figure 6.7 A, B). The I/S acts as a thin rim on top of the micritic matrix making it difficult for the electron beam to separate the mixed-layer from the underlying and surrounding material. Additionally, the compositional ratio between the amount of K, Ca and Fe varied greatly. Most of the Ca might results from contaminants from the surrounding calcite bioclasts, whereas feldspar and quartz fragments might have affected the other components. The I/S clay was therefore studied using the combined information from XRD and SEM analyses. In the chalk-rich layer the I/S clay was poorly represented.

Other clay minerals detected were illite and kaolinite. The illite is identified in most of the samples through XRD as illite/muscovite, but was not separated as the minerals share the same d-spacing value of 10Å. In SEM and in the microscope they can be distinguished by their different morphology and birefringence. However, the illite content proved hard to quantify in modal analysis due to its scattered nature, small grain size and low concentration. Kaolinite has generally been observed in small quantities within some of the muscovite vein structures. The mineral was identified from XRD analysis through most of the samples, with one exception being the clean chalk layer, sample 5. Additionally, another clay mineral was observed through SEM and EDX with an unusual morphology, containing the components Si, Al, Mg, K and Fe see Figure 6.7 C, D. This detrital clay appears scattered and is only present as a discontinuous rim around some of the grains. The EDX spectrum varies for the unidentified clay, and because of a thin rim, it was difficult to determine its composition using EDX. Furthermore, the overall primary components that were detected was Si, Al and Mg, which suggest that the clay might be composed of a mix of clay mineral, potentially of smectite, illite, kaolinite and chlorite. However, through XRD clay fraction analysis (Chapter 6.5) a small quantity of illite was detected, which could be the potential source for this rim.

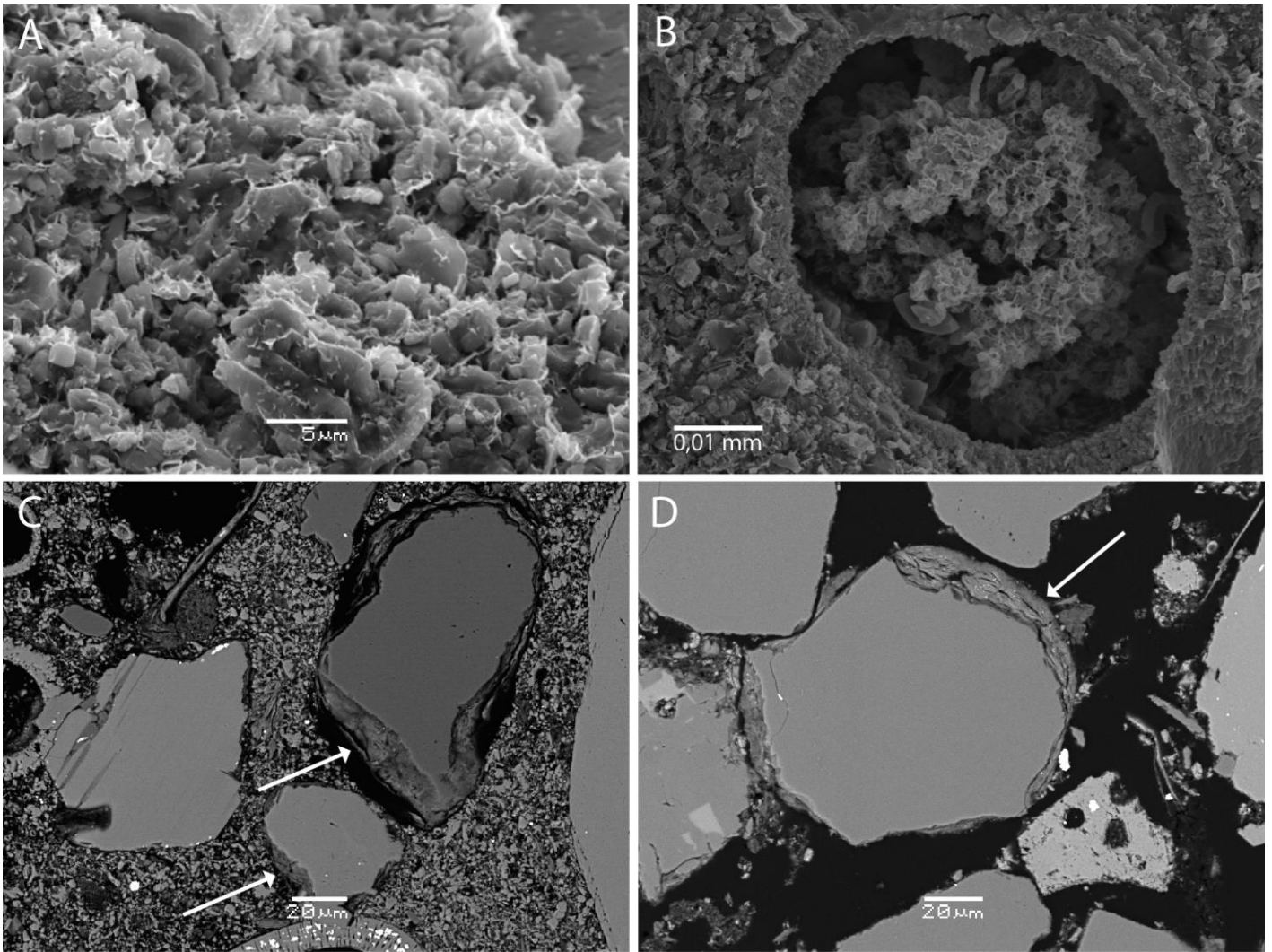


Figure 6.7: A) Sample 2, and B) Sample 2, represented in SEM images from stub samples showing detrital mixed layered I/S mixed within the micritic chalk matrix. C) Sample 2, SEM image from thin sections showing rim of detrital mixed clay mineral around detrital quartz grains, see arrows. D) Sample 4, SEM image from thin sections showing a close up of the detrital mixed clay mineral around quartz grain.

6.4.3 Matrix

In cross polar light, the overall matrix has a brownish color, but some areas appear either as brighter interference colors, close to or around the grains, or as darker brownish stained color within the matrix (Figure 6.8 A). The matrix is rich in calcium and silicon, a result of the high content of carbonate mud, mainly composed of calcite bioclasts, and the mixture of non-calcareous minerals (Figure 6.8 C). Non-calcareous minerals have been observed in SEM to consist of small fragments of fine-grained detrital quartz, feldspar and mica, glauconite, clay minerals and authigenic pyrite (Figure 6.8 B). However, it is not possible to distinguish matrix composition in modal analysis due to the particle size is $\leq 10\mu\text{m}$. Samples 4 and 18 are generally grain supported and contains less carbonate mud and microfossils. In microscopy, the two samples deviates from the other studied thin sections with porous sand and an overall

darker brown color within the matrix and within the pore space. This dark brown film occupying the pore space is most likely caused by heavy oil, which makes it difficult to separate the matrix from porosity. However, the matrix and the pore space could be distinguished from each other using SEM. SEM analysis shows that the more open pore space appears within the good-sorted sections and the matrix fills the pores within the less sorted sections. This approach was used to separate the porosity from matrix during point counting (Figure 6.8 D). Additionally, some particles within the micritic matrix show physical contact and areas that are less porous might indicate that these sections have been partly recrystallized (Figure 6.8 B). It has only been observed internal cementation within the matrix.

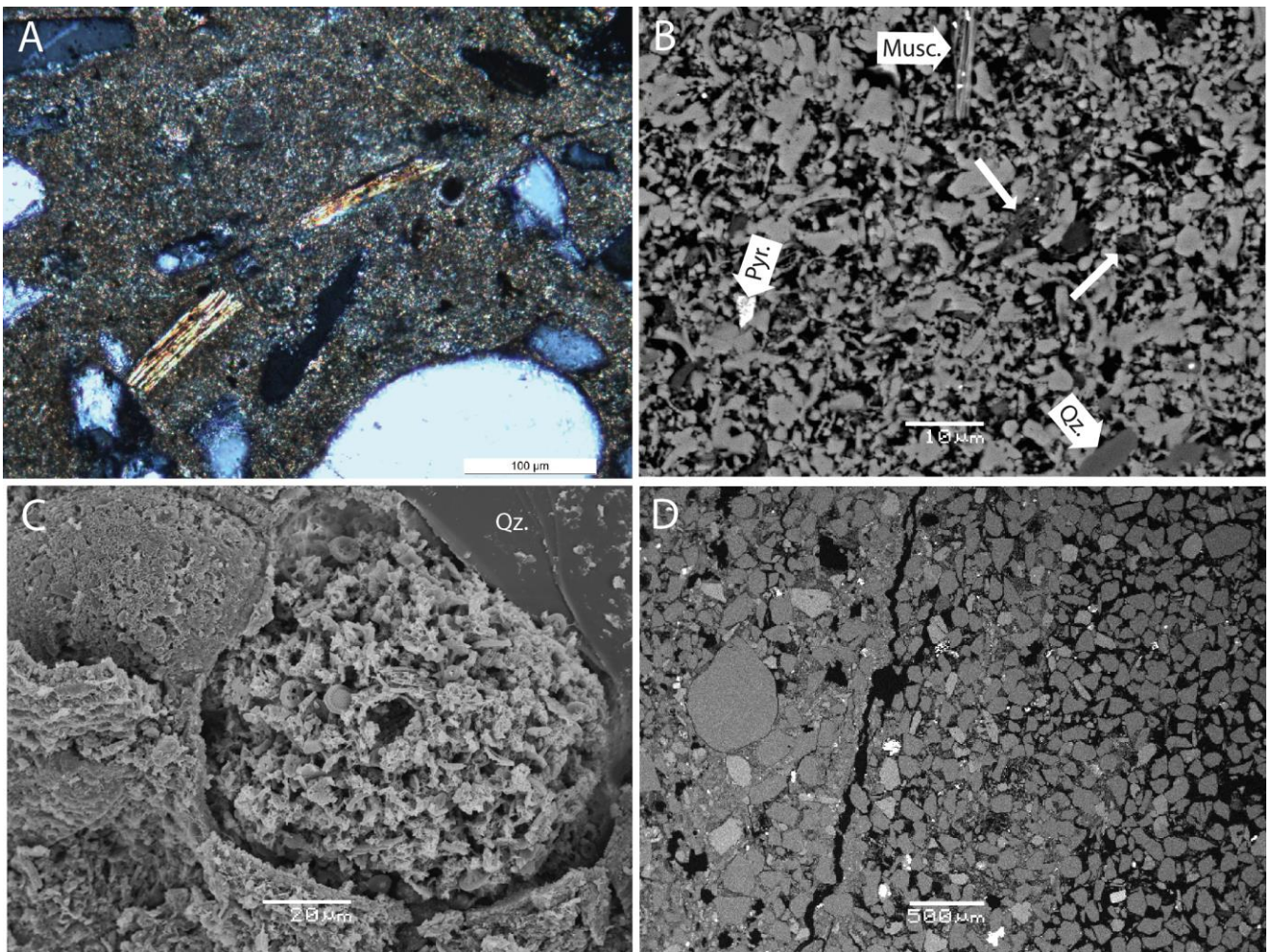


Figure 6.8: A) Sample 18, through optical image in cross-polar light shows micritic chalk mud, within the framework with a dark brownish color. B) Sample 10, SEM image of thin section shows a close up of the matrix, can observe carboniferous mud mixed inn with detrital grain fragments such as quartz (Qz.) and muscovite (Musc.). Pyrite (Pyr.) and some clay veins (marked with arrows) with small bridges across the pore space within the matrix were also observed. C) Sample 2, SEM image of stub sample showing matrix surrounding part of a quartz grain (Qz.) and filling inn part of a foraminifera. Note the webby clay structure within the matrix. D) Sample 4, through optical image in plane polarized light showing the transition from good sorting (right side) to poorly sorting with matrix around the grains (left side). Displacement of grains in the central area and some grain removal to the left should also be noted.

6.4.4 Cement

Pyrite

Authigenic pyrite is detected throughout all of the samples, but is less evident in the clean chalk layers. Pyrite is observed in various forms, within the matrix as framboidal aggregates (Figure 6.9 A), as pore filling constituents within fractures and most often next to or within the structure of muscovite grains as cubic crystals.

Halite

Authigenic halite is only detected in a few of the samples, scattered and in small quantities. The crystals observed are most likely not primary components of the sampled rock, but contamination during removal of the core samples. It could either be the result from crystallization during drying of saline formation brine when exposed to the surface, or due to contamination from the drilling mud (Figure 6.9 B).

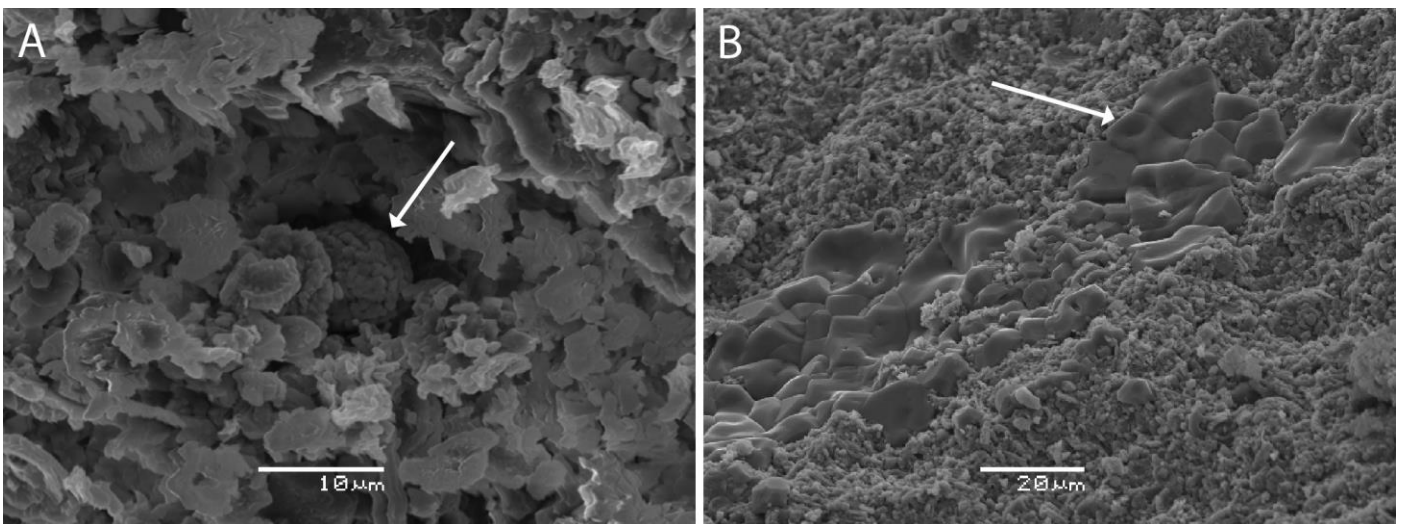


Figure 6.9: SEM image of stub samples: A) Sample 3, arrow pointing to a framboidal pyrite aggregate mixed within the matrix. B) Sample 6, arrow pointing to halite crystals.

6.4.5 Fossils

In all of the studied thin sections different fossils have been observed varying in size and shape, see Figure 6.10 A, B. Some are well preserved while others have been altered due to crushing, either by mechanical compaction or by transportation. The fossils act as part of the framework or within the micritic chalk matrix. Micritic chalk is observed within all of the studied samples where the main components include nanofossils and microfossils. The most abundant microfossils observed in the samples are foraminifers, while coccoliths comprise the nanofossils. The coccoliths are fine-grained particles derived from decaying nanoplanktons and constitute the greater part of the matrix. Foraminifera are observed to be part of both the framework and the matrix as crushed fragments. The primary fossils that have been identified through microscopy, SEM and EDS are described below and will be used to provide information about the paleoenvironment and the extent of their textural modification during deposition and diagenesis.

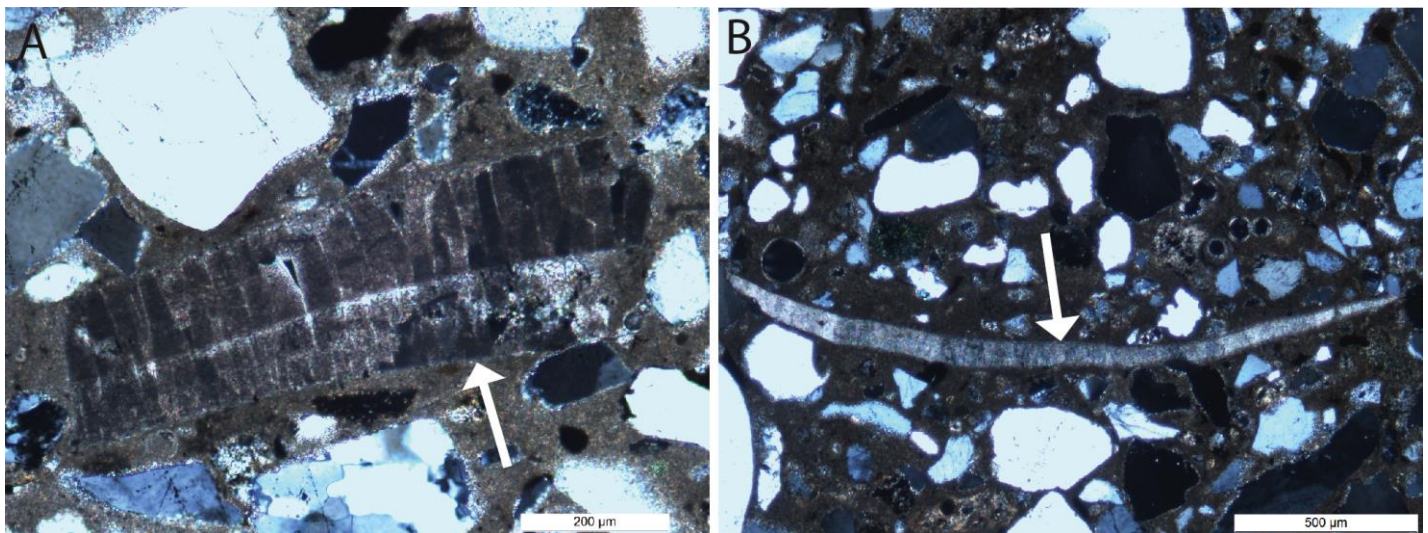


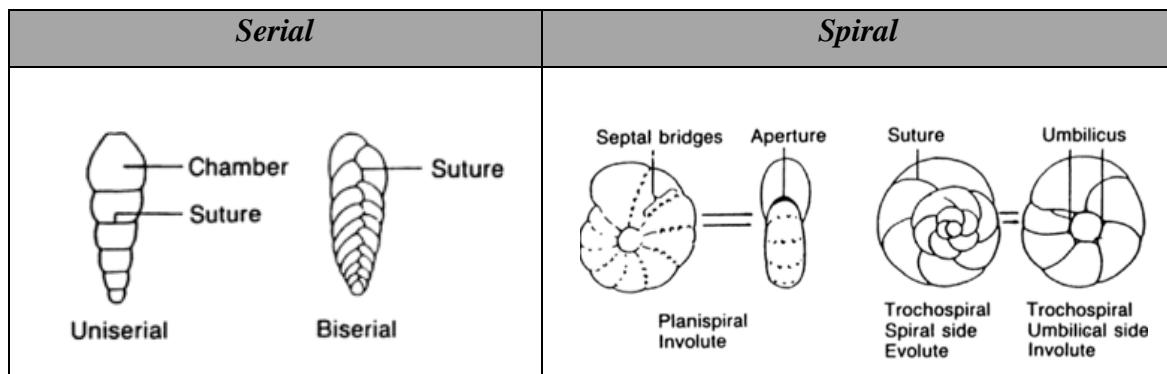
Figure 6.10: Optical image in cross-polar light: A) Sample 1, prismatic fossil fragment with complete calcite cementation of the mould, most likely mollusk (white arrow). B) Sample 3, fossil fragments, most likely part of an ostracode (white arrow), with a few surrounding planktonic foraminifera composed of calcite chambers in various sizes.

Foraminifera

The composition and wall structure of foraminifers are important parameters in the classification of the species in the group. Observations made through microscopy and SEM does not provide enough information about their morphology to classify them further. However, the observed foraminifera can be divided into two groups: carboniferous- and agglutinated foraminifera, where foraminifera with calcareous chambers are the more abundant ones.

The foraminifera range in size from 50 to 200 μm , are most abundant in the chalk rich layers. They occur with two basic patterns; serial and spiral. The two observed serial forams are generally characterized as uniserial, appearing as a string of beads, and biserial appearing with an additional set of string of beads, see Table 6.1. Forams of spiral structures have mainly been observed as planspiral forming as a coil of rope in a single plane, however some trochospiral are also observed forming a helical spiral, see Table 6.1 (Doyle, 1995).

Table 6.1 : Illustration of the two basic patterns of foraminifera found in the studied samples with their single and multi-chambered foraminiferal tests (modified from Doyle, 1995).



Carboniferous foraminifera in this study are primarily of planktonic origin (Figure 6.11 C, D), however smaller quantity of benthic forams has also been observed (Figure 6.11 A, B). The planktonic shell consists mainly of low-Mg calcite. The benthic forams are also calcareous, however, some have also been detected with an arenaceous (agglutinated) structure. This type of structure is only characterized within the benthonic mode of life and is composed of mineral grains (Doyle, 1995). In the studied samples they appear less frequent and more scattered compared to the planktonic calcareous forams.

The planktonic foraminifera are only of marine origin, and abundant in open marine waters. They are free-floaters, commonly known as living in symbiosis with green algae, and are limited to the photic zone. The planktonic organisms are restricted to marine water and are not able to survive in brackish waters or near suspension of clay particles.

The benthic foraminifera are not as restricted to these conditions, causing planktonic species to be good indicator for paleobathymetry (Hanken et al., 2010). The foraminifera are often used for interpreting changes in paleoclimate through geological time, due to their sensitivity to temperature, salinity and oxygen (Doyle, 1995). The main species of the planktonic group

are from the family *Globigerinidae*, where some has a distinctive feature formed as balloon-shaped structure with spiky surfaces, which is typical for Globigerids (Figure 6.11 C, D). This type of planktonic foraminifera is commonly found in the upper water column and most common in the oceanic sediments. Some of the forams are also detected as a flattened keeled chamber, typical for Globorotalids, which are most common in the lower part of the water column and are good for stratigraphic markers.

The benthic foraminifera are most likely from the family *Rotaliidae*, however some might originate from the *Nodosariidae* family (pers.comm, Jenő Nagy, 2014). The benthic forams are typically detected along the marginal to abyssal plan, but can also be found in deep ocean waters. Additionally, the arenaceous benthic foraminifer provides the widest geographical distribution of the forams due to its ability to survive below the carbonate compensation depth (CCD) (Doyle, 1995).

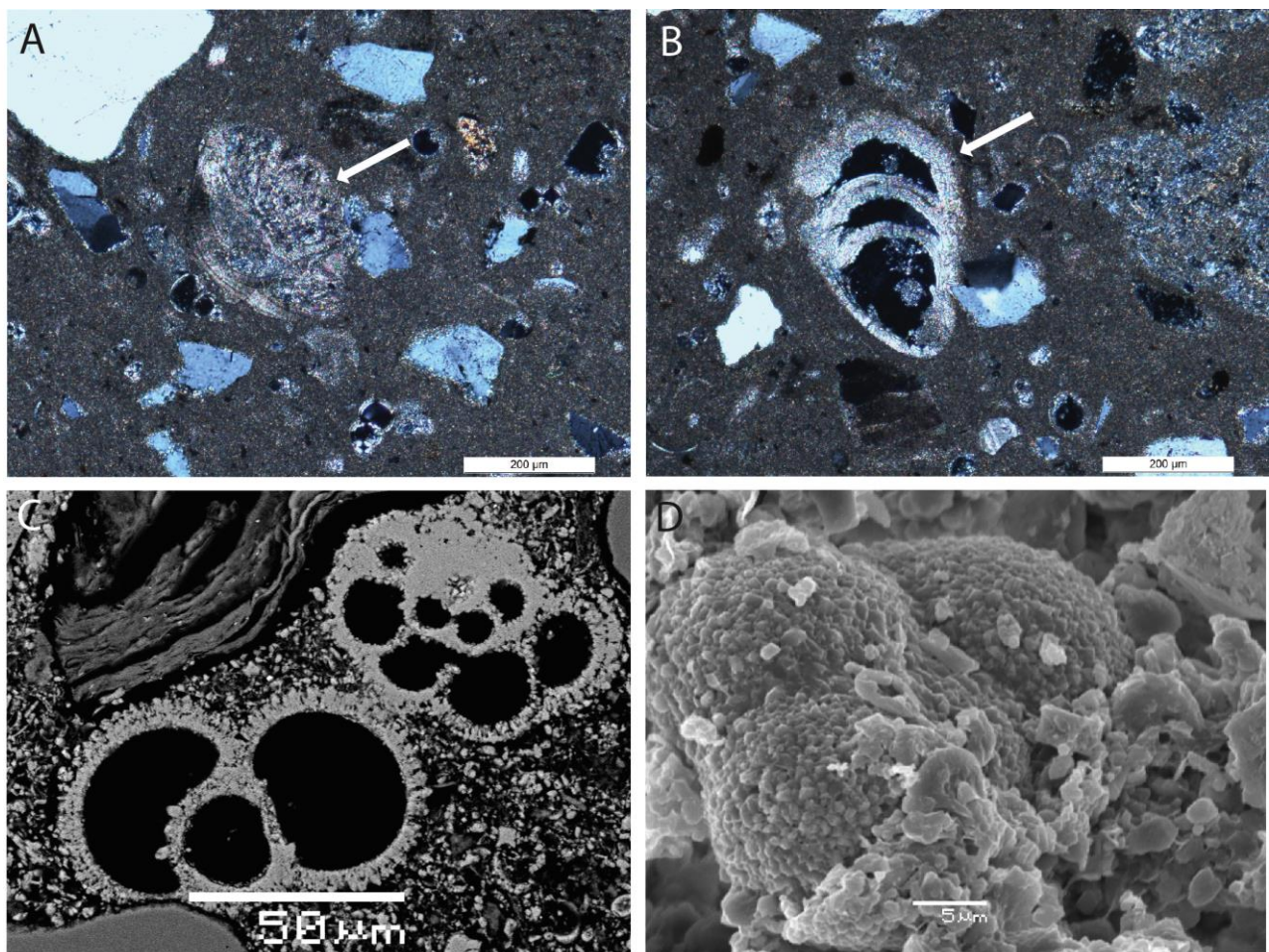


Figure 6.11: A) Sample 8, through optical image in cross-polar light shows a benthic serial foraminifer. B) Sample 9, through optical image in cross-polar light shows a benthic trochospiral foraminifer. C) Sample 3, SEM image of thin section showing two planktonic foraminifera, where the bottom foram represents a Globigerids. D) Sample 1, SEM image of stub sample showing a planktonic planspiral foraminifer, also representing a Globigerids.

Coccoliths

The observed coccoliths vary in shape and size. Most of them are circular while some are oval shaped, and they range in size from 5 - 10 μm . The assembled plates forming the sphere range in size from 0.5 – 1 μm , and some appear as individual crystallites (Hanken et al., 2010). The coccoliths skeletal texture and structure could only be clearly observed through the stub samples in SEM due to their small size. Three different skeletal shapes with different morphological features have been observed in the studied samples: wagon-wheel shaped, discos shaped and oval shaped with a perforated center (Figure 6.12 C, D, E, F). Several of coccoliths are well preserved (Figure 6.12 A), while the majority has been partly or fully disaggregated to small platy crystals, 0.25 - 1 μm during deposition (Figure 6.12 B). Well-preserved coccoliths show little signs of diagenetic modification, however, some samples show slightly more deformed particles indicating a low percentage of dissolved calcite and recrystallized chalk.

The coccoliths are also free- floaters and important organisms to the paleoecology due to their very specific requirements and their abundance in open marine waters. These requirements include sensitivity to temperature, existence only in the photic zone and important contributors for deep basinal and distal shelf sediments. They are only able to live within normal marine saline waters, away from suspended clay particles (Hanken et al., 2010).

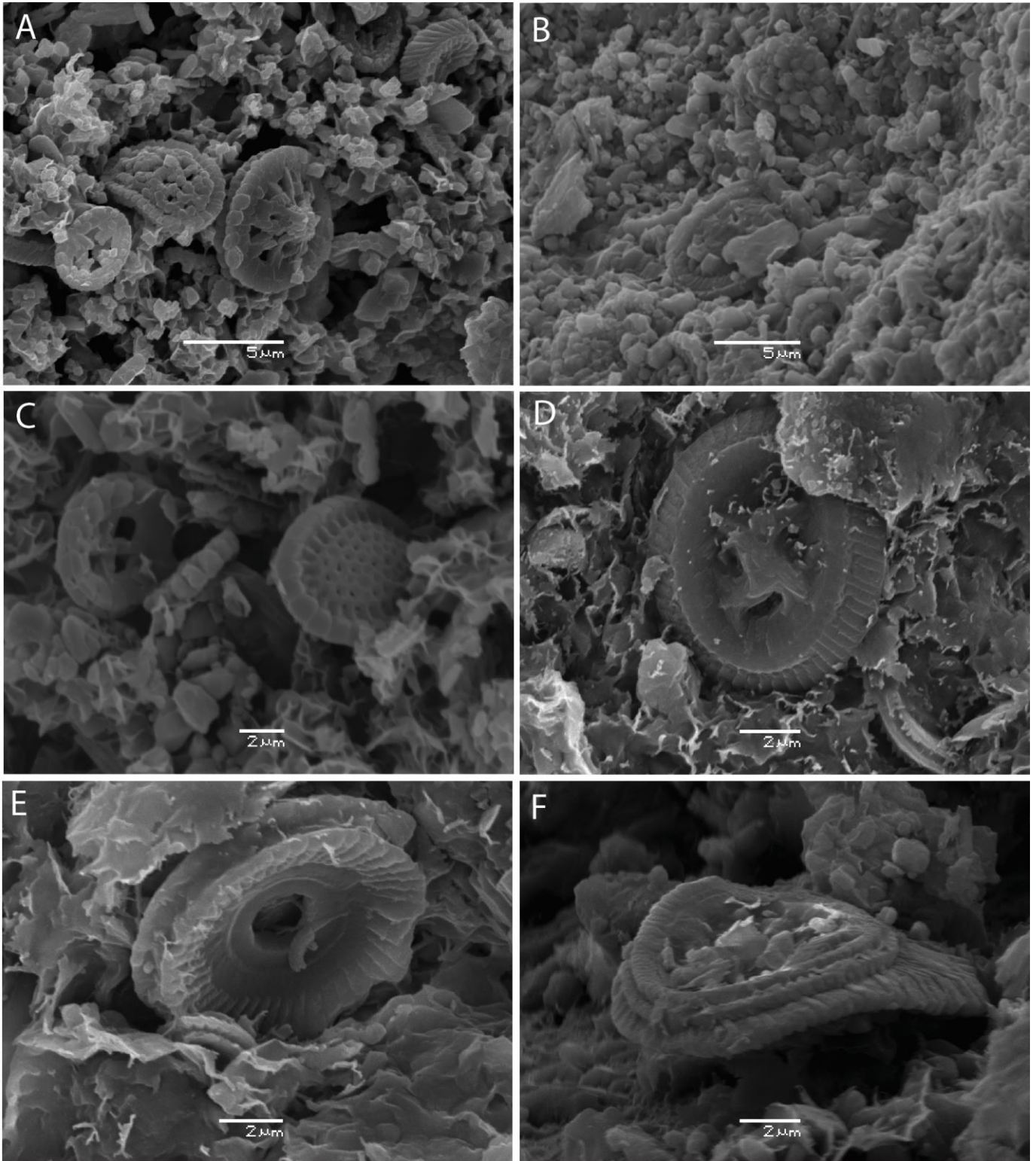


Figure 6.12: Sem image of stub samples: A) Sample 10 and B) Sample 6, illustrating the various shapes of the coccoliths, some with assembled plates and others as individual crystallites that have been disintegrated. C) Sample 2 shows two different morphological features, to the left wagon-wheel shaped, to the right coccoliths with a perforated center. D) Sample 4, close up of a wagon-wheel shaped coccoliths. E) Sample 4 and F) Sample 3, discos shaped coccoliths.

6.5 X-Ray Diffraction (XRD) analysis

Identification and quantifications of eleven selected samples were applied both through bulk analysis and clay fraction analysis. Nine of the samples were also used for optical microscope and SEM analysis. These samples represent the general variation of the lithological changes within the cored section and contained the largest proportion of rock material provided for this study. These samples out of 18 were therefore chosen for the X-ray analysis. The two last samples, 19 and 20 were provided later on from two different lithological sections within the cored well 9/11b-11.

6.5.1 XRD Bulk

An overview of the bulk mineralogical composition is presented in Figure 6.13. It displays a quantification of the total amount of minerals detected in the upper part of Maureen Sandstone strata (Sst) from well 9/11b-11. The source of error in the bulk quantification is shown in Appendix E together with the table of numerical XRD bulk result. Note that a high XRD% in source of error for a mineral phase, in relation to the minerals content, implies a lower compatibility with the quantitative model for that mineral phase.

The overall trend within the upper part of Maureen Sst shows a high content of calcite, with an average of 34.1 XRD%. These calcite-rich samples show a zero to minor amount of clay minerals. An exception to this trend is the homogeneous sandstone intervals with more silica prone minerals, and less calcite, containing the lowest XRD value at 1.5%. Additionally, these samples also contain a small percentage of clay content. The clay content presented in Figure 6.13 will be discussed and presented in section 6.5.2. The results observed from the XRD bulk quantification has been subdivided into four different groups based on their overall mineral content.

Mixed calcareous layer (Sample 1, 2, 3, 6, 7 and 8)

The amount of calcite and quartz observed in the mixed layers shows a wide variation of these contents, Figure 6.13. Sample 6 and 7, which are the more chalk rich layers, has the highest XRD percentage of calcite compared to the other samples from the mixed layers. Both samples contain more than 60 XRD% calcite of the total mineral content. The

remaining XRD% consists of siliciclastic material, where quartz exhibits the highest values represented with around 20 XRD% of the total amount. Sample 1, 2, 3 and 8, are the more sand-rich calcareous layers which has a content of quartz from around 40-60 XRD%. However, the calcite is still highly represented with an amount of 20 to almost 40 XRD% of the remaining mineral content. Additionally the amount of feldspar is observed to follow the trend of the quartz content, high amounts of quartz is associated with higher amount of feldspar and vice versa. Traces of pyrite can be observed throughout all of the mixed layers varying from 1 to 3.5 XRD%.

Homogeneous sand layer (Sample 4, 9 and 10)

The homogeneous sand layers contain more than 50 XRD% quartz and a total content of siliciclastic material of more than 80 XRD%. Sample 4 and 9 contain the highest amount of calcite, with values from 8 to 15 XRD%. This corresponds well with the physical observation of the two samples, which are more consolidated than sample 10. The quartz content of sample 4 shows the highest XRD% with a value of 60.7, whereas sample 9 contains the least amount of quartz, 50.5 XRD%, but the highest amount of calcite, 14.7 XRD%. Sample 10 has the lowest amount of calcite present with only 1.5 XRD%. The same sample shows a value of more than 95 XRD% of siliciclastic material, where 51.4 XRD% of this represents quartz. This sample is also the most fine-grained homogeneous sand layer of all the studied samples, and the least consolidated one. Additionally, the amount of feldspar shows no visual trend with the amount of quartz and therefore breaks with the pattern from the samples in the mixed layers.

Chalk-rich layer (Sample 5)

The only observed homogeneous chalk layer from the studied XRD samples is sample 5. It shows from Figure 6.13 that this layer contains the highest amount of calcite with a value of 91.5 XRD%, and the lowest quantity of siliciclastic material with a total amount of 8.2 XRD%. Of the total siliciclastic material, 7.6 XRD% is quartz with the remaining muscovite/illite containing the lowest amount of all the studied samples. There is no observed feldspar in this sample.

Clay rich layer (Sample 11)

Sample 11 is also the only studied sample comprised of a clay-rich unit. The amount of quartz is fairly low, 10.5% XRD, however the sample contains the highest amount of feldspar, 18.8 XRD% within the quartz-feldspar ratio compared to other studied samples. Total amount of siliciclastic material is 76.9 XRD%, with the muscovite/illite representing the most abundant mineral, with a value of 29.2 XRD%. Additionally, sample 11 is observed with the highest quantity of halite, 2.9 XRD%, compared with the other studied samples. Other minerals that are represented in sample 11 are calcite (4.1 XRD%) and anatase (2.8 XRD%), which is only detected in this sample.

Well 9/11b-11

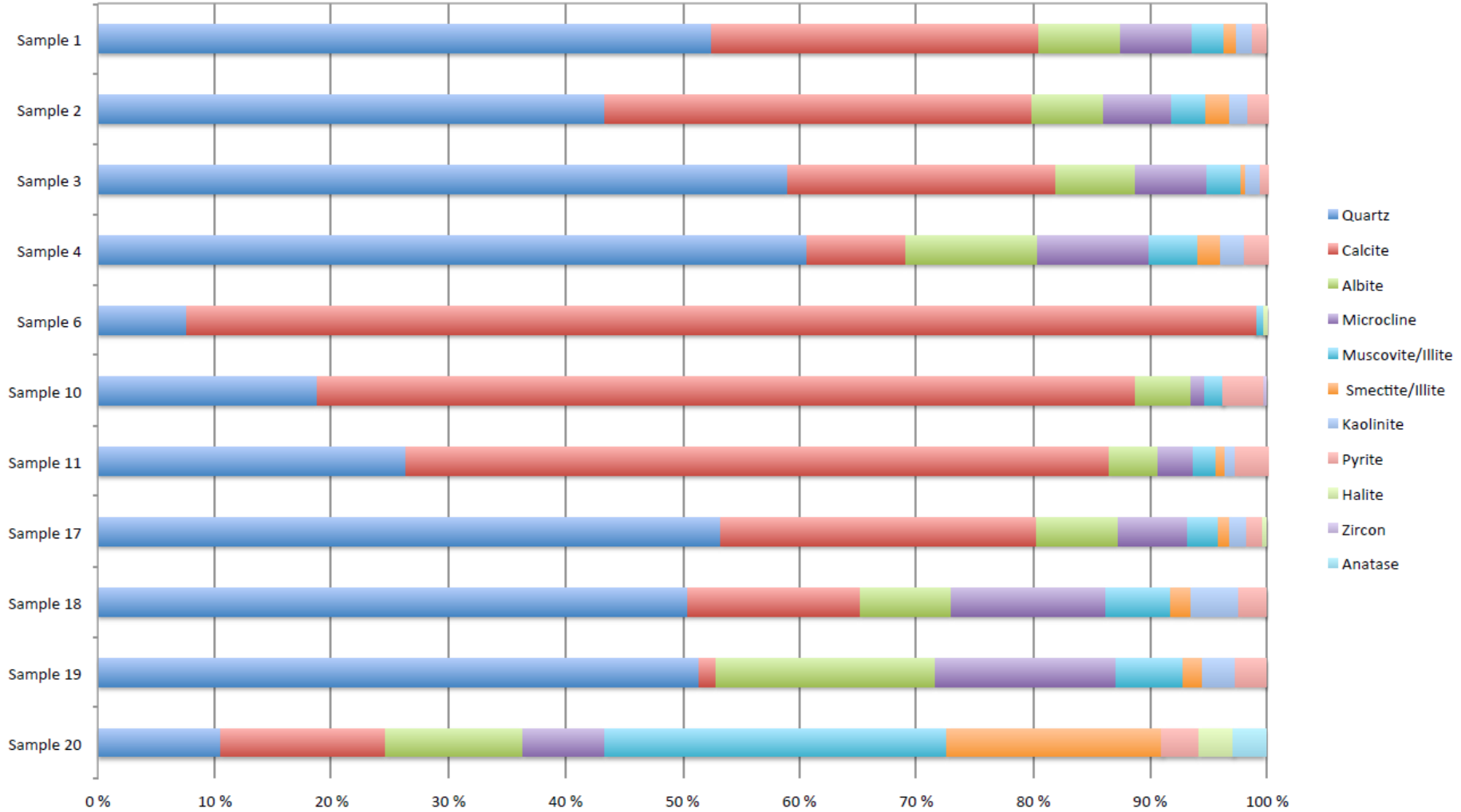


Figure 6.13: XRD Bulk results of each eleven samples from the quantification of the individual mineral phases.

6.5.2 XRD Clay fraction

As the amount of clay found in XRD Bulk analysis represent a minor portion of the total mineralogical content, only the results from XRD Clay fraction will be presented in this section. Minerals identified in this study are illite, kaolinite and mixed layer of illite/smectite (I/S). The clay minerals identified in this section will only relate to the clay fraction analysis and not the bulk fraction analysis.

The XRD Clay fraction analysis involves clay-sized particles of less than 2 μm . Particles that are non-clay minerals such as quartz, feldspar, carbonate etc. might also be present due to contamination during crushing of the samples or due to the same grain size as clay particles such as micritic mud. However, the air-dried clay minerals produce their first 001 peak between 30 and 5 \AA , while minerals such as quartz, calcite and feldspar, which are present in these samples have their first peaks above 5 \AA , separating the clay minerals from the non-clay minerals. Furthermore, the clay mineral could only be identified by its mineral group such as smectite and not the type of mineral due to the 060 reflections, which also mark contributions from the non-clay minerals within the samples.

Identification of the Clay Minerals

I/S is the most abundant mineral identified through all the studied XRD clay fraction samples. The mixed layer was revealed by its wide air-dried (AD) peak at $\sim 14.4\text{\AA}$, shifting to a higher spacing of $\sim 16.7\text{\AA}$ after ethylene glycol (EG) treating and collapsed to a peak at $\sim 10\text{\AA}$ after heated to 350 $^{\circ}\text{C}$. After heated to 550 $^{\circ}\text{C}$ the peak slightly collapsed with a slight reduced intensity. The 001 illite peak was revealed at $\sim 10\text{\AA}$ during AD and after EG treating. When heated to 350 and 550 $^{\circ}\text{C}$, the peak was destroyed. Kaolinite was identified using the same procedure as illite, thereby detected with its 001 peak at $\sim 7.1\text{\AA}$ during AD, EG treatment and after 350 $^{\circ}\text{C}$ heat treatment. However, after heated to 550 $^{\circ}\text{C}$ the peak was destroyed.

Mixed-layered illite/smectite

The mixed-layer I/S is distributed within the matrix, and is a controlling factor for reservoir quality. The type of clay mineral that is present will affect the reservoir properties differently, and is therefore essential to distinguish them from another. The diffraction patterns can detect the presence of a clay mineral, but cannot be used to estimate the percentages of each mineral in a mixed clay layer. However, one can estimate a virtual proportion of the I/S present by calculating the reflection patterns between 002 and 003 that were treated with EG to calculate each samples $\Delta 2\theta_1$ and $\Delta 2\theta_2$ values (Table 6.2).

Table 6.2: Based on Watanabe's (1981) and Wilson's (2013) approach between peaks in rang of: $5.1 - 7.6^\circ \Delta 2\theta$ (l_1), $8.9-10.2^\circ \Delta 2\theta$ (l_2) and $16.1-17.2^\circ \Delta 2\theta$ (l_3) were applied to measure $\Delta 2\theta_1$ and $\Delta 2\theta_2$ values, represented by the angular difference between $l_2 - l_1$ and $l_3 - l_2$. The $\Delta 2\theta_1$ and $\Delta 2\theta_2$ values are plotted in Figure 6.14.

Sample	$l_2 - l_1$	$\Delta 2\theta_1$	$l_3 - l_2$	$\Delta 2\theta_2$
1	15.956 - 10.436	5.52	10.436 - 5.277	5.15
2	15.953 - 10.404	5.54	10.404 - 5.267	5.13
3	15.987 - 10.471	5.51	10.471 - 5.373	5.12
4	15.974 - 10.356	5.61	10.356 - 5.258	5.09
6	15.922 - 10.345	5.57	10.345 - 5.302	5.04
7	15.975 - 10.482	5.49	10.482 - 5.281	5.20
8	15.975 - 10.444	5.53	10.444 - 5.378	5.06
9	15.985 - 10.470	5.4	10.470 - 5.315	5.15
10	15.913 - 10.442	5.48	10.442 - 5.314	5.12
11	15.949 - 10.322	5.62	10.322 - 5.253	5.06

The calculated values were then plotted in the Watanabe's diagram (1981), (Figure 6.14) placing all the samples of $\Delta 2\theta$ values within the structural type $g=0$, concluding with a smectite content between 85-95%. The $\Delta 2\theta$ was then used to estimate the percentage of illite using the table presented in Table 6.3. The I/S was estimated to contain less than 20% illite. Based on the results, the I/S layer is estimated to contain 80-90% smectite and consequently 10-20% illite. However, the quantities of the clay minerals might vary within a small fraction, as the Watanabe's diagram is design for a fixed I/S layer that might differ from the one detected in this study.

% Illite	001/002		002/003		° $\Delta 2\theta$
	d(Å)	2 θ	d(Å)	2 θ	
10	8.58	10.31	5.61	15.80	5.49
20	8.67	10.20	5.58	15.88	5.68
30	8.77	10.09	5.53	16.03	5.94
40	8.89	9.95	5.50	16.11	6.16
50	9.05	9.77	5.44	16.29	6.52
60	9.22	9.59	5.34	16.60	7.01
70	9.40	9.41	5.28	16.79	7.38
80	9.64	9.17	5.20	17.05	7.88
90	9.82	9.01	5.10	17.39	8.38

Table 6.3: $\Delta 2\theta$ Values for estimating illite percent after treated with EG from mixed layer I/S. Modified from Moore & Reynolds Jr., 1989.

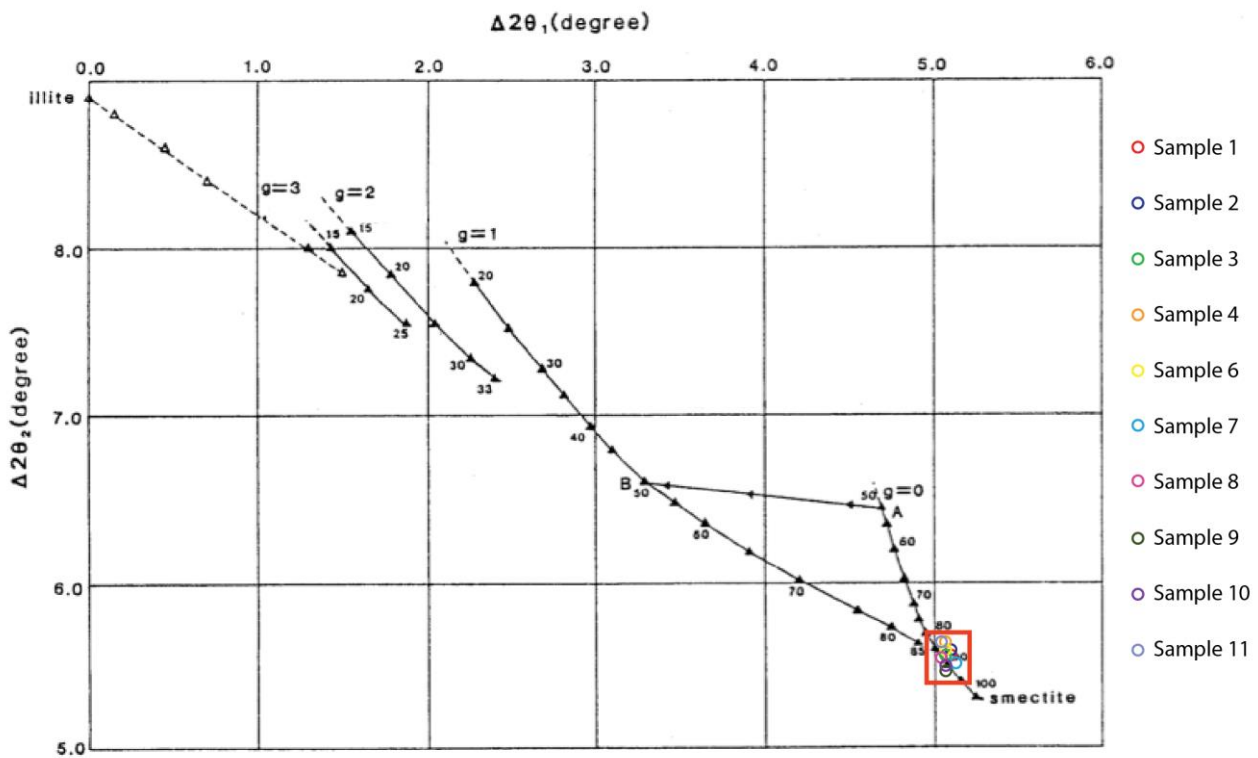


Figure 6.14: Identification diagram of I/S for Cu.k α radiation. The black triangles on the curve indicate the percentage of smectite with the g letter corresponding to a proposed I/S structural type, see Watanabe 1981 for further reading. All studied samples containing I/S are plotted within the red square in the diagram based on the $\Delta 2\theta_1$ and $\Delta 2\theta_2$ values from Table 6.3. The samples are plotted with a smectite content between 85-95%. Modified from Watanabe, 1981.

Chapter 7: Strontium isotope analysis

Strontium isotope analysis

The reason to perform the Sr-isotope analyses was to find out if the studied core interval had been influenced by ground water influx.

The strontium isotope composition in water is developed through dissolution of minerals and ion exchange reactions. The $^{87}\text{Sr}/^{86}\text{Sr}$ ratio is obtained from a rock when water interacts with the minerals as it flows through an aquifer (Frost & Toner, 2004).

The seawater has two different “feeders” of strontium into the seawater, which has made the strontium isotope ratio vary through the geological time record. Continental weathering is the main contributor of ^{87}Sr , which is derived from granitic rocks, by the decay of rubidium to ^{87}Sr . Dissolution of basaltic rocks at mid-oceanic ridges, produces strontium with a low $^{87}\text{Sr}/^{86}\text{Sr}$ ratio because of the potassium and rubidium in the basaltic rocks (Bjørlykke, 2010). A high-resolution seawater $^{87}\text{Sr}/^{86}\text{Sr}$ ratio from the last 100 Ma (Figure 7.1) was used by Richter et al. (1991) to relate the Sr isotopic variations in seawater to the collision of the Indian and Asian continents.

The results from Sr-isotope analyses are presented in Table 7.1. The strontium isotopic values shows that these samples are consistent with marine origin during Late Danian to Early Thanetian age (Figure 7.1). This confirms that during the deposition of the Maureen Formation from well 9/11b-11 where not under influence by meteoric flushing. It should be mentioned that sample 7 deviates slightly from the other samples due to the higher content of clay.

Table 7.1: Results from the Sr-isotope analysis, provided by the University of Bergen.

Sample	$^{87/86}\text{Sr}$	2S error	$^{87/86}\text{Sr}$ corrected
1: 6190-6193 ch+s	0,707851	0,000009	0,707853
2: 6190-6193 ch	0,707855	0,000009	0,707857
3: 6183-6186 ch+s	0,707879	0,000009	0,707881
4: 6183-6186 ch+s	0,707872	0,000009	0,707855
5: 6180-6183 ch+s	0,707863	0,000009	0,707846
6: 6180-6183 mud+ch	0,708481	0,000008	0,708464
7: 6174-6177ch+s(gl+mud)	0,70789	0,000009	0,707873
8: 6174-6177 ch+s	0,707872	0,000009	0,707855
9: 6171-6174 ch	0,707826	0,000009	0,707809
10: 6168-6171 ch+s	0,707844	0,000009	0,707847

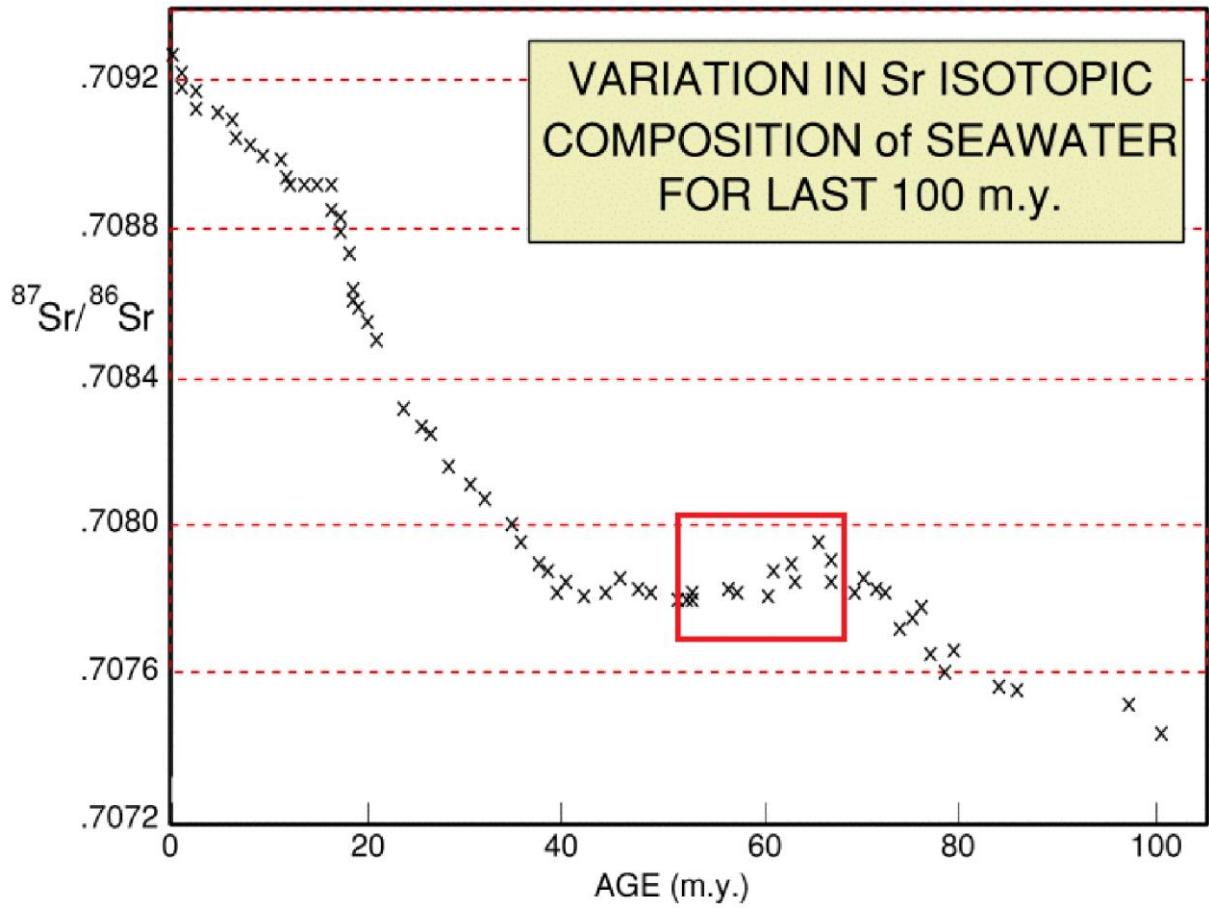


Figure 7.1: Showing the variation in the Sr-isotopic composition in seawater during the last 100 Ma. Values from Danian to Thanetian age are highlighted in red square (ca. 0.7078). After Richter et al. (1992).

Chapter 8: Well correlation and petrophysical results

8.1 Introduction

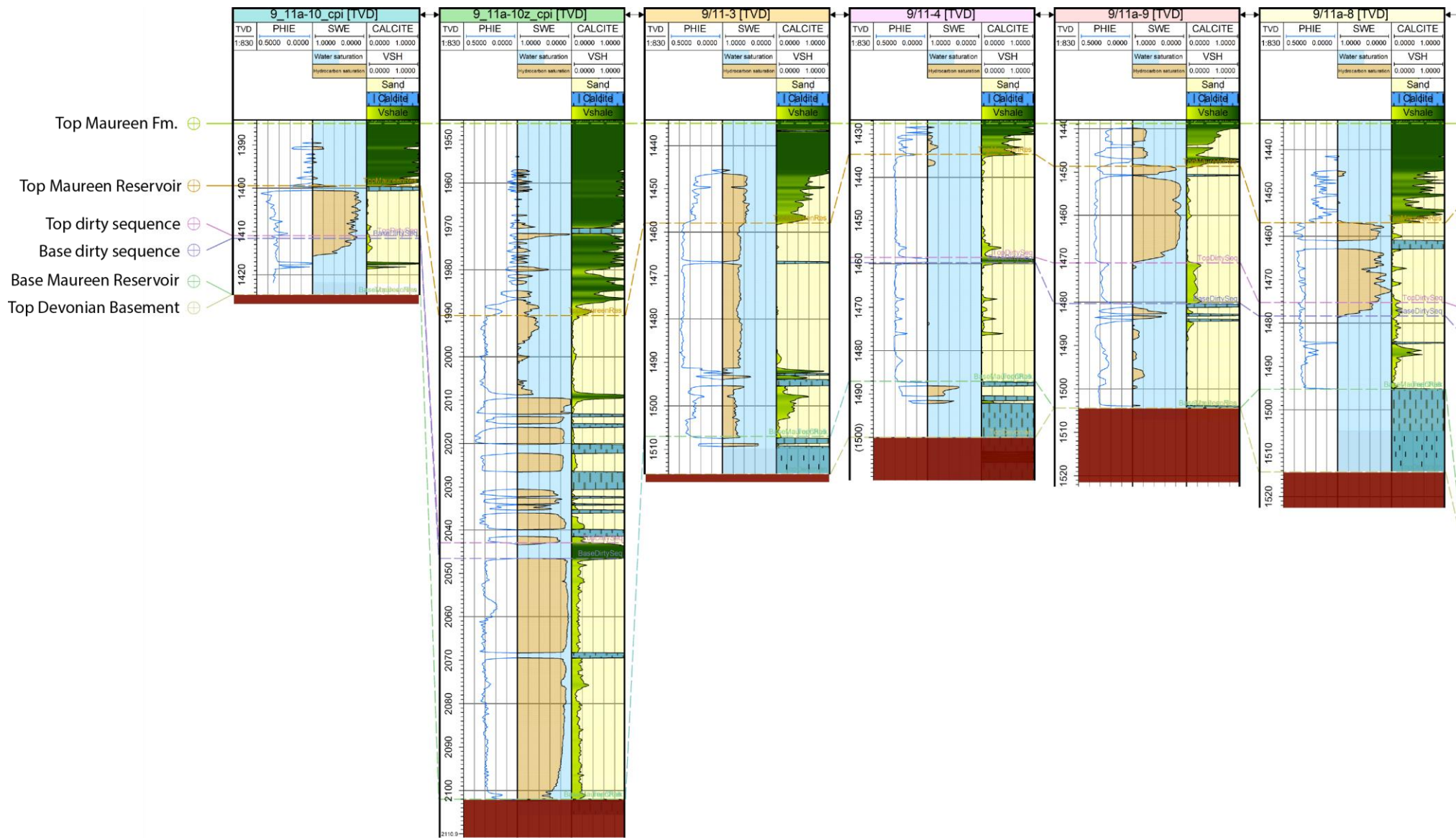
Well correlation has been performed together with evaluations of petrophysical properties by use of wire line logs and core plug data presented in Chapter 4.5. The main purpose of this chapter is to:

- i) Study the lithostratigraphic framework of the Maureen formation based on core data.
- ii) Identifying occurrences of carbonate intervals both laterally and vertically using correlated wells, wire line logs and seismic images.
- iii) Use core plug data to investigate zones with high and low porosity and permeability to correlate with physical properties within the formation.

8.2 Well correlation

Well correlation was applied to visualize the lithostratigraphic framework and observed the vertical variations and the lateral extent of the chalk within the Maureen Formation. Eight wells, 9/11-4, 9/11a-9, 9/11a-8, 9/11-2, 9/11a-5, 9/11a-7, 9/11-1 and 9/11a-6 are presented in Figure 8.1 and correlated based on their similarities of the electrical logs, such as curves, shapes, magnitude and their lithology. Reference point for all the wells are flattened at the correlated horizons for Top Maureen Formation. Distances between each well varies from no more than 157 m to 2624 m, giving a relatively broad lateral extent of the occurrences of the carbonate intervals. Depths and correlated horizons of each well are presented in Appendix G.

The thicknesses of the Maureen reservoir, defined by the horizons Top Maureen reservoir and Base Maureen reservoir in the well logs, vary in all wells but generally become thicker towards the east. The Maureen Formation is relatively thin on the East Shetland platform, a result of exposure of major erosion over time (Mudge & Copestake, 1992).



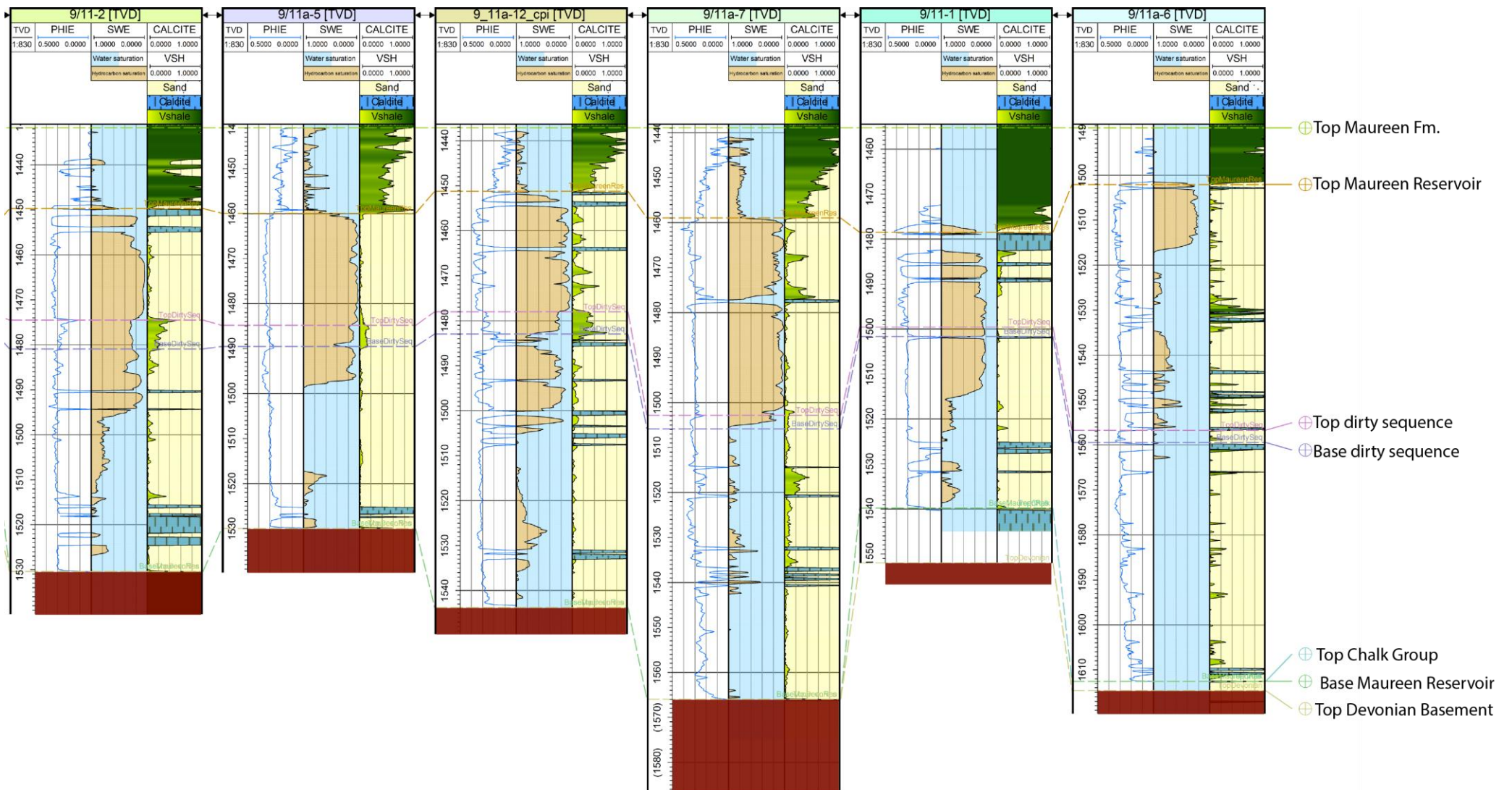


Figure 8.1: Well correlation of seven horizons comprising the Mauren Formation, Chalk Group and Devonian basement.

8.3 Characterization of the carbonate intervals: combining well correlations and wire line logs from Mariner east.

Well correlation presented in Figure 8.1, together with a time structure map and a seismic lines image of the East Shetland platform (Figure 8.2, 8.3), gives a general overview of the lithology, the depositional pathways and the bathymetry. From well correlation it can be observed that the carbonate intervals occur more frequently in the distal areas compared to the more proximal westward areas on the East Shetland platform. These linear features of the carbonate intervals seem to coincide well with the west to eastward fairways with thicker deposited sediments in the more distal parts. Though, some of the shallower, more proximal areas also appear to contain some thinner intervals of carbonate. From the time structure map it can be observed that some of the wells have been deposited in shallower areas, exposing these sections to more erosion. Such shallow areas will then result in a larger proportion of cleaner sandstones and a lower sand to carbonate ratio. Well 9/11a-10z, which contains sediments deposited further west in the Mariner field, shows an overall trend of thick sandstones and carbonate deposits. This well shows an area where sediments have been deposited in a trough and is consequently able to accumulate more sediment compared with the other nearby wells. Figure 8.3 illustrates the bathymetry in the area where well 9/11a-10z is located.

Deposition of the carbonate intervals seems to be influenced both by the bathymetry and how far they are transported. In the more marginal or distal areas such as in well 9/11b-11 and 9/11b-z (Appendix H), the carbonate intervals seem to become more frequent and are deposited in thicker units. These areas are located at the edges of an elongated depression on the seafloor located in the southeastern section of the time structure map (Figure 8.2). The depression seems to be wider compared to other parts further west, and suggest a low angle slope, causing deposition of the sediments within a more constrained area. Additionally, these two wells are located in the Mariner east section in the Mariner Field (Figure 4.2), and are controlled by a deeper bathymetry, resulting in a larger depocentre than further west in the more proximal parts. Time structure map Figure 8.2 is used to estimate distances between well 9/11b-11 and 9/11b-z.

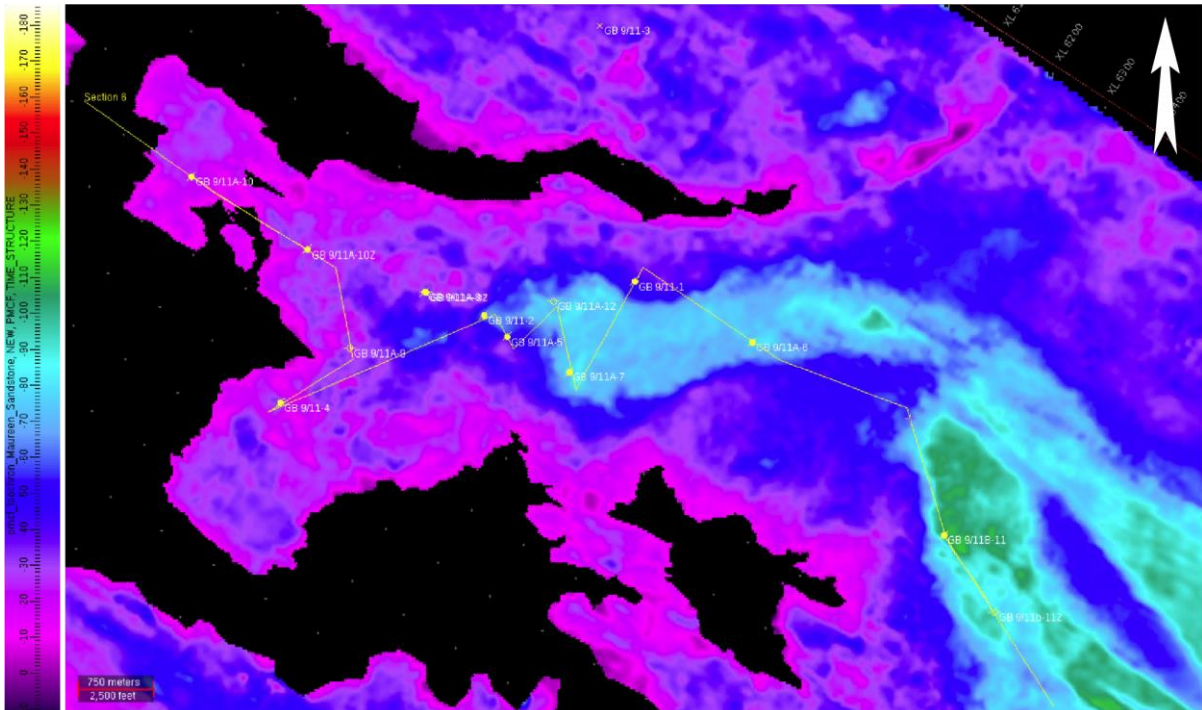


Figure 8.2: Time structure map of the Mariner field. Most of the well logs from well correlation are presented in the western area. Both wells from Mariner East are present (Statoil, 2014).

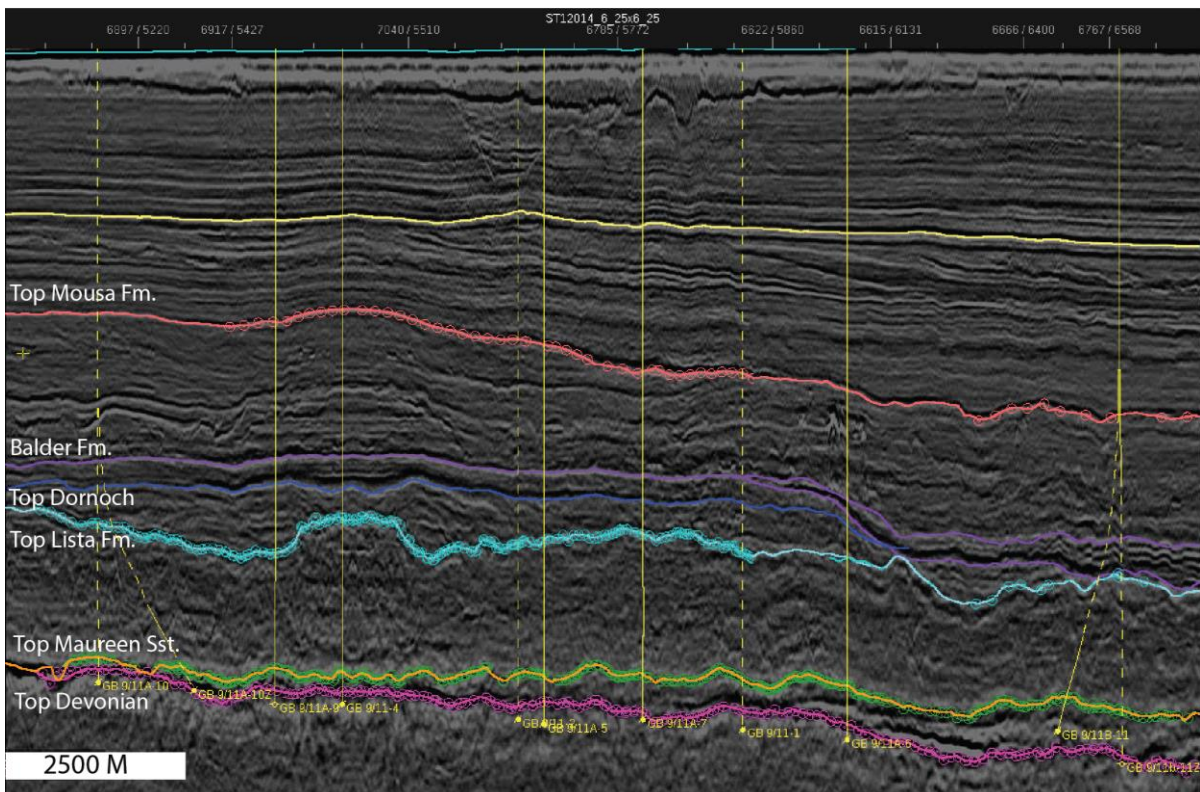


Figure 8.3: Seismic section of the Maureen Formation, located on the East Shetland Platform with some wells presented. The horizontal lines mark the boundaries between Paleocene formations (Statoil, 2014).

7.4 Petrophysical analysis

Porosity and Permeability

Porosity and permeability are of great importance with regard to reservoir quality. The relationship between wells 9/11a-10, 9/11-4, 9/11a-9, 9/11a-5, 9/11a-7 and 9/11b-11 is presented in Figure 8.4. Similar signature can be observed, where increase of permeability corresponds to increase of porosity. However, some wells deviates from this trend such as 9/11a-9 and 9/11a-5, which are separated into two sections indicating two separate reservoirs. 9/11a-7 also deviates from the other cores with a high-constant permeability with an increase in porosity.

It can also be noted that the porosity and permeability from well 9/11b-11 is more scattered and contains the lowest porosity and permeability values within the wells (Figure 8.4, red circle). The low values could be a result of by several factors; such as heavier calcite cementation, thicker and more repeated chalk intervals and textural variations. The grain size can be seen in relation to the depositional fairways, where decreasing grain size often corresponds to more distal areas further away from the source.

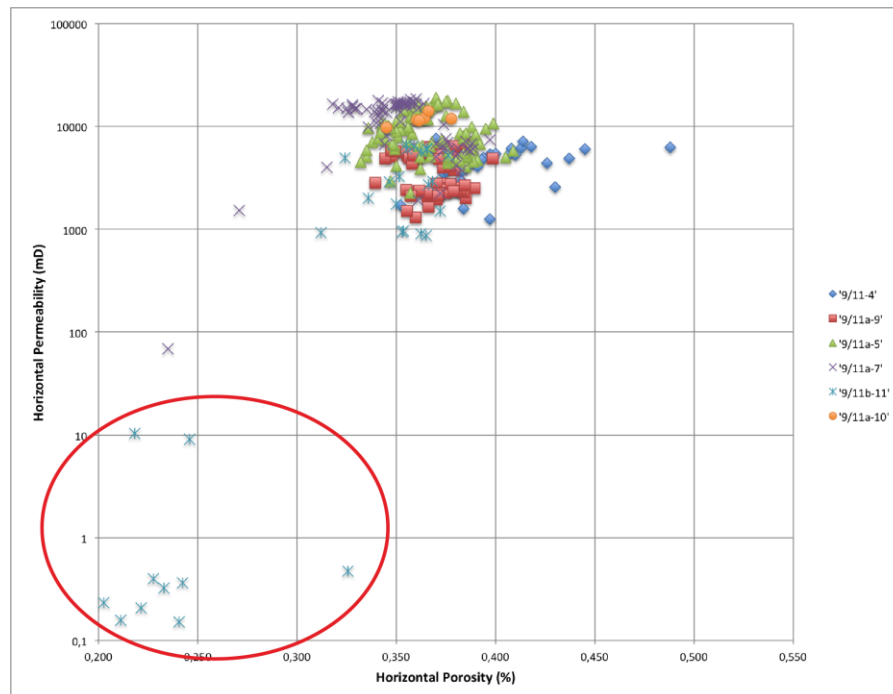


Figure 8.4: Relationship between porosity and permeability from five wells. 9/11-4, 9/11a-9, 9/11a-5 and 9/11a-7 are from the Mariner area and 9/11b-11 is from the Mariner east area. Not the red circle marking the lowest values of well 9/11b-11.

Porosity and Permeability of well 9/11b-11

Horizontal and vertical plots of porosity and permeability were provided with depth interval, from the cored section of well 9/11b-11. These were plotted to see changes in the lithology, between the carbonate intervals and the homogeneous sand layers. The low permeable zones and the lower porosity (Figure 8.5 A,B,C,D red ellipses) represent the carbonate intervals. The homogeneous oil stained sand layers represents the higher permeable zones and porosity. It can be noted that some of the homogeneous sand sections display a lower permeability in comparison to the porosities, indicating some chalk or clay mixed within the section.

Further, the chalk rich layers (Figure 8.5 C,D green ellipses) show a relative high porosity, which is expected due to its particle size and shape. They also represent the majority of porosity of the carbonate intervals. However, the permeability is relative low, from 11 mD and below, which is represented for all the carbonate intervals (Figure 8.5 A,B).

From the plots, the average permeability is estimated at 2022 mD with a preservation of porosity at 28,9 %.

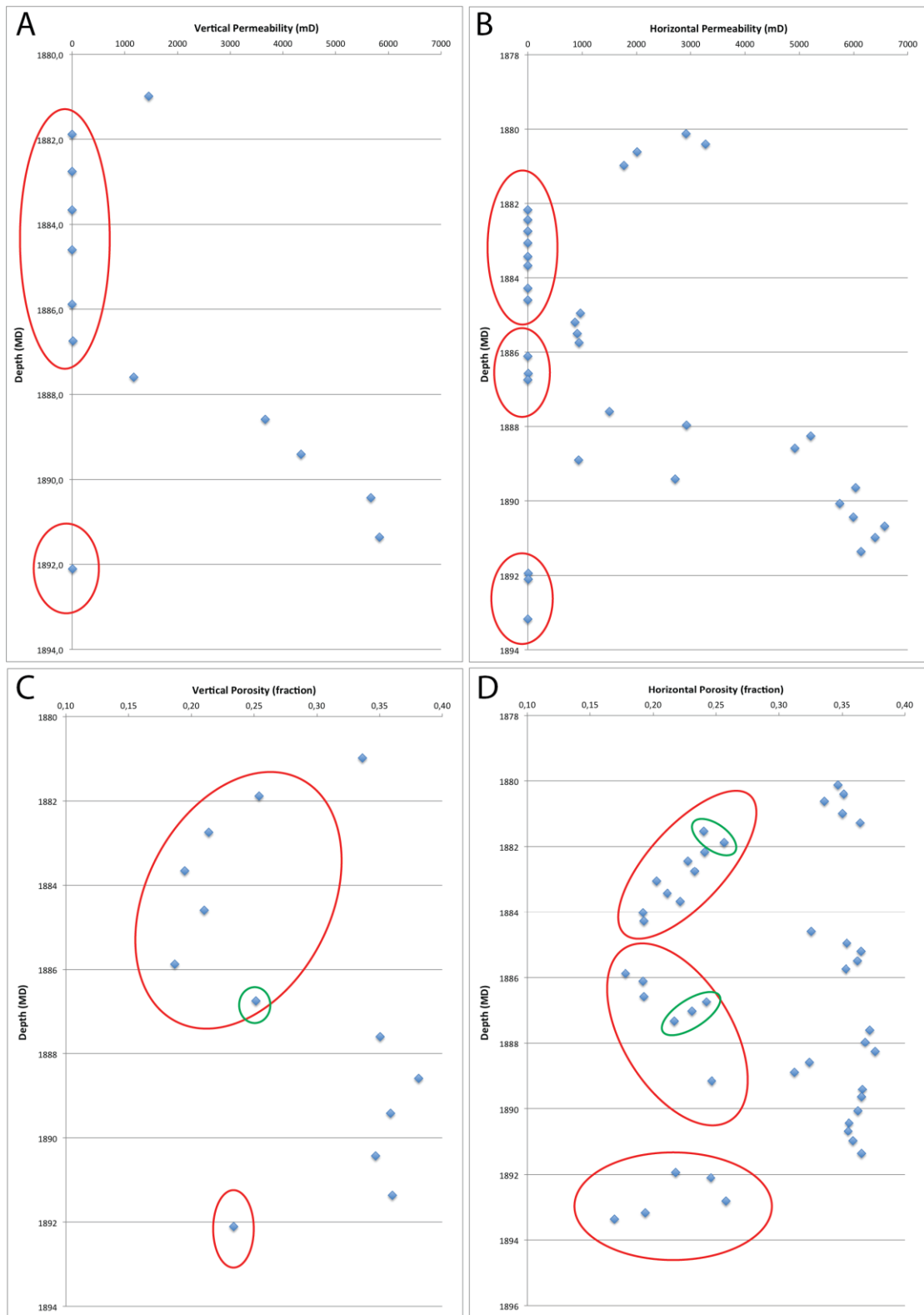


Figure 8.5: Porosity and permeability plots of well 9/11b-11. A) Vertical permeability distribution. Red ellipses indicate carbonate intervals within low permeable zones. B) Horizontal permeability distribution. Red ellipses carbonate intervals within low permeable zones. C) Vertical porosity distribution. Red ellipses indicate carbonate intervals with relative high porosities, and green ellipse indicates chalk-rich zones. C) Horizontal porosity distribution. Red ellipses indicate carbonate intervals with relative high porosities, and green ellipse indicates chalk-rich zones.

Chapter 9: Discussion

9.1 Depositional environment

Late Danian – Early Thanetian age represents the period prior to the deposition of the Maureen Formation. During this time the sediments were deposited on a gently easterly dipping slope resulting from tectonic tilting of the Shetland- Scotland uplift (Ahmadi et al., 2003). Combined with the effect of a rise in the relative sea level, the site created accommodation space for a depositional fan system. This system gave rise to the facies distribution investigated from the cored section, well 9/11b-11. Reworking of older chalk deposits with a surge of clastic inflow are the general compositions of the facies, which will be discussed.

9.1.1 Facies distribution

Homogeneous sand facies

The homogeneous sand deposits makes up the thickest units of the cored section (Appendix B) and the correlated well units (Figure 8.1). These thick sand bodies are defined as facies HS1 and are characterized by structureless sand-rich units characteristic for turbiditic fan deposits. According to Mitchum et al. (1993), Shanmugam et al. (1996) and Den Hartog Jager et al. (1993) such massive sand deposits were typical products of the Paleocene submarine fan currents. Deposition of well-sorted, fine to medium grained sand defines such successions and has resulted in good reservoir qualities throughout the North Sea.

From well correlation, it is observed that these thick sand bodies are distributed over large areas on the East Shetland Platform. However, the platform is only shown as a slightly eastward dipping shelf on the seismic section (Figure 8.3). Such submarine flows can be initiated at very low angles. This means that the slope it self does not have to be the main controlling factor of these sediment flows, but rather the source of the material and its hydrodynamic condition during transportation (Den Hartog Jager et al., 1993). Further, at the lower boundaries within the cored facies of homogeneous sand units (HS1), crushed shale fragments mixed with calcareous sand clasts are detected representing facies HS2. Deposition of the HS2 is rather a mixed and disaggregated sand unit, but contain more or less the same textural features as the homogeneous sand facies HS1. This mixture is most likely a result of a debris flow event. However, even though the HS2 and HS1 facies are deposited from two different flows, they might also be related to one another. This can be initiated by an increase of fluid content within a debris flow, which transforms into a low-density turbidity current

(Shanmugam et al., 1996). Such transitions might have been the case for these two homogeneous sand facies.

Calcareous sand facies

Facies associated with the heterogeneous calcareous sand deposits suggests a more complex submarine depositional system. The calcareous units within the studied cored section of well 9/11b-11 were divided into three separate facies: CS1, CS2 and CS3. All three facies are composed of five main textural features: a large mixture of siliciclastic material, rip-up clasts of chalk, deformed chalk lenses and veins, small pebbly rock fragments and glauconitic clasts. These sediments also contain a high content of matrix and show little internal stratification, which are typical for gravity flow systems (Shanmugam et al., 1996 & Watts et al., 1980). Even though the three facies have more or less the same lithological texture, they show some variety of how they were deposited through gravity flows.

Facies CS1 is most likely a mixture of slump and debris flow. This is seen by large amounts of deformed mud and chalk clasts with minor deformed vein structures, which are typically for slump deposits (Shanmugam et al., 1996). Facies CS3 is a thin unit identified by soft sediment deformed chalk within calcareous sand, most likely related to slumping by dewatering or slope instabilities related to tectonics. The deformed structures within these facies indicate rapid deposition, mixing water fluids within the sediments resulting in high, unstable pore pressures. Rotational movements together with fluid-escapes are often the case of such internal deformation structures found within these facies (Ortner, 2007).

Facies CS2 is a more typical debris flow deposit with less deformed structures. However, CS2 deviates somewhat from the other facies by containing structures resembling sand injections. These sand injections are most likely derived from fluidized sand (Jonk, et al. 2005) of the underlying homogeneous sand layer (HS). Tectonic movements might also have affected them after deposition. Furthermore, these textural features are typically found within the Maureen Formation across the North Sea (Kilhams et al., 2014).

Chalk-rich facies

The facies identified as purer chalk (C1) within the cored section, could be related to several depositional processes such as: in situ pelagic rainfall during progradational high stands, reworked chalk from storm deposits or processes related to mass flows. Within the Maureen Formation most analyses has indicated in situ pelagic deposition for pure chalk facies, though such layers have been cored closer to the base of the formation (Kilhams et al. 2014), rather than the top as it is in this studied core log. Biostratigraphic analysis provided by Statoil estimate these units to have originated from an older chalk material, dated prior to the deformed chalk lenses and chalk matrix, identified within the calcareous sand deposits. For these chalk units to be older but still be deposited above younger chalk material and sand deposits, the C1 facies had to have been consolidated before transportation into the deeper parts of the shelf/ basin floor. Therefore, these units must have been transported as whole blocks and not as in situ marine “rain” or reworked suspended material. The blocks have most likely originating from unstable edges of re-activated older faults, described in Chapter 2. The peak of the East Shetland Platform uplift was during mid-Thanetian (Ziegler, 1990b), which could have loosened semi consolidated and consolidated blocks from structural highs on the platform, transporting and depositing the sediments at a later stage within the uppermost parts of the formation. Some of these chalk units have also been dated within a few of the correlated well sections 9/11a-10, 9/11a-7 and 9/11a-6 (Figure 8.2), but this does not mean that all of the carbonate layers was deposited by older re-worked chalk and block slides.

Well correlation reveals layers containing carbonate, but does not differentiate their origin. This could mean that some chalk rich layers throughout the well column might originate from a younger, insitu deposited pelagic chalk. Further, such layers might be related to the ones observed in the uppermost part of the more proximal well logs: 9/11a-10, 9/11a-10z, 9/11-2 and 9/11a-12 (Figure 8.1), where a large transgression initiated by a sea level rise was dominating the area with the deposition of pelagic mud. This will then indicate that even after deposition of the thick Maureen sands, pelagic rainfall of chalk was still part of the depositional environment. If these intervals are identified, they can easily be correlated with one another and might even be distributed over a larger area.

Clay-rich facies

Facies CC1, composed of a green mud-prone layer mixed with minor chalk clasts and chalk matrix, represents the thinnest unit identified in the cored section of well 9/11b-11. These layers are associated with periods of little siliciclastic input, deposited from suspended material containing smectite rich clay identified through XRD analyses (Chapter 6.5). Some of these mudstones have been identified as volcanic ash, deposited as hemipelagic mud across the North Sea. These volcanic muds have been traced and correlated across the Atlantic Ocean (Simonsen & Toft, 2006). However, in this study the cored sections of these layers contain larger amounts of siliciclastic material, then what is expected for such ash beds. Tough, the layers could be locally reworked ash beds, resulting from low-turbulent flows. The latter proposal might explain the incorporated siliciclastic material, the minor amount of chalk clasts and the chalk matrix within.

Interpreted depositional environment

As a result from the discussed facies above, the depositional environment is interpreted to reflect poorly organized and rapid slope system dominated by high-density gravity flows within a submarine fan environment. Several authors (Ahmadi et al., 2003, Deegan & Scull, 1977, Chandler and Dickinson, 2003, Gatliff et al., 1994, Kilhams et al., 2012, Mudge & Bliss, 1983, Johanson, 1987, Surlyk et al., 2003) have interpreted the deposition of Maureen Formation within in the North Sea to result from slumps, debris flows and turbidities. However, further studies of the carbonate successions closer to the Shetland shelf and within the northern part of the North Sea is needed to fully understand their occurrences.

9.2 Origin of carbonate beds and Maureen sands

Carbonate beds

Carbonate beds are investigated within the cored sections of well 9/11b-11 (Appendix H) and through well correlations presented in Figure 8.1 of the Maureen Formation. Samples from different cored sections have been dated as mentioned, and are collected from the Chalk Group of Tor Formation. This formation is of Maastrichian age and consists of homogeneous white to pale gray allochthonous chalk, deposited from downslope mass movements of primary pelagic or older resedimented chalk. The chalk ooze was deposited in an epicontinental sea, where intrabasinal highs, such as the East Shetland Platform were no

deeper than 150 m (Surlyk et al., 2003). The coccospheres were therefore deposited in a relative shallow marine environment, which might have been a result of some well-preserved coccoliths and the high proportion of calcareous rich planktonic and benthonic foraminifera. However, the majority of the samples observed through petrographic analysis show a large amount of calcite crystals originated from disintegrated coccoliths. This is most likely related to reworking of the Tor Formation, influenced by local fault-controlled subsides (Nøttvedt et al., 1995 and Surlyk et al., 2003), redepositing the chalk and further disintegrate the coccoliths. The Chalk Group presented in the well correlation (Figure 8.1), has most likely only consisted of the Tor Formation. Evidence of the younger Ekofisk Formation (Danian age) is highly unlikely according to documented occurrences, where the Ekofisk Formation has its erosional limits throughout the UK sector (Surlyk et al., 2003), such as on the East Shetland Platform. However, deposition of younger chalk further up in the Maureen stratigraphy should not be neglected.

Paleocene sediments

Deposition of large accumulation of clastic material during Paleocene is most likely associated to the mentioned East Shetland Platform and the Scottish Highlands uplift (Underhill, 2002). However, coincidence between regional extensive regressive-transgressive sedimentary cycles together with subsidence from the tectonic uplift is highly preferred as the main contributor for the sedimentary supply (Mudge & Bujak, 1996). Calculations of this uplift have been suggested to be less than 1km (Den Hartog Jager et al., 1993), resulting in an easily tilting of the East Shetland Platform providing supply of coarse clastics, dominated by quartz arenite with some alternated volcanic rocks. The sediments were first transported eastwards by fluvial-deltaic systems into a shallow marine shelf, before being reworked (Cutts, 1991). The sedimentary transport direction was generated in a distinct western to eastern fairway (Kilhams et al., 2014), controlled by the relict bathymetry seen in Figure 8.2.

9.3 Distribution and dimension of carbonate intervals

The Chalk Group, overlaying older Devonian rocks on the East Shetland Platform are more or less absent today. The formation that once was deposited along intrabasinal highs were eroded and redeposited into the more distal basinal areas, such as the Viking Graben (Johanson, 1987).

In Mariner Field, some of the Chalk Group overlaying old red Devonian rocks is still preserved as thin layers within a few of the wells presented in Figure 8.1. The larger extent and dimension of the reworked chalk are mostly distributed within the more distal basin floors within the North Sea. Tough, some thick units are observed within wells from the East Shetland platform. These units are most likely controlled by the bathymetry and occur within areas that have accumulated thicker sediment packages located within depressions and/or troughs on the platform. Such areas are presented and identified in seismic sections (Figure 8.3), and time structure map (Figure 8.2).

The underlying Devonian basement is rather stable to weathering, compared to the overlying Chalk Group, which in turn will erode the platform in a more horizontally direction. As a result, the carbonate sediments have be transported further down the slopes and re-deposited in the lowest part of the more distal areas on the East Shetland Platform. When the chalk is eroded away within the subsea channels, the thicker intervals of clastic sand will dominate the succession. Due to stable weathering of the Devonian rock, the channels will gradually by avulsion erode the rims of the channel, depositing chalk intervals again. If such an occurrence is the case, this might be an explanation to why there is an erosive unconformity between the Maureen Formation and the underlying Devonian basement, and why the Chalk group is mainly absent on the East Shetland Platform today. However, these possesses are most likely a combination of earlier reworked and redeposit chalk from upper Cretaceous and reactivation of older fault blocks on the platform during early Paleocene together with the erosive submarine channels.

The carbonate intervals observed from well correlation and core logging have most likely behaved in tree different ways: (i) as consolidated or semi consolidated block slides, (ii) as rip up clasts from underlying semi consolidated chalk and (iii) as unconsolidated material mixed in as micritic matrix. From wire line log 9/11b-11 (Appendix H) and well correlations

(Figure 8.1) the base of the Maureen Formation show relative frequent carbonate cemented intervals, with in upward increase in clastic sediments. A dirty sequence is present in the middle part as the input of clastic material increase towards the top with incorporated carbonate intervals in the upper most succession. The upper part of the latter is covered by massive shale, representing the overlaying Lista Formation. Even though the carbonate intervals show some degree of depositional reoccurrences, the difference in consolidation has led to spread and unevenly distribution of the chalk intervals.

Correlation of the upper carbonate intervals

In the upper part of the Maureen reservoir carbonate intervals can be followed within the well correlations (Figure 8.1) and wire line logs (Appendix H), and might be continuous successions.

The two wells 9/11a-9 and 9/11a-6 (Figure 8.1) are lined up perpendicular to the shelf (Figure 4.2) and show some similar features, both with a thin carbonate interval in the upper part of the formation. The more distal well, 9/11a-6, shows a slightly thinner carbonate bed, which may indicate a decrease in the flow regime. If these intervals were to be connected, it would imply that the vertical distribution of these carbonate beds are relatively large, within a 5,9 km distance. However, due to the large distance between the wells the correlation of the relatively thin carbonate beds is less probable. Such relations and trends can also be observed in well 9/11-2 and 9/11a-12. However, these wells are located closer to one another, approximately 750 m, making a correlation more likely. This will indicate that the vertical extent of the debris flows could have occurred over a great area.

In the more distal parts of Mariner East, well 9/11b-11 and 9/11b-z (Figure 4.2) are located relatively close to one another; about 800 m. The carbonate interval from the upper part of the formation display similar thicknesses and could therefore presumably represent part of the same debris event. However, the carbonate intervals within well 9/11b-z, which is the more distal well of these two, is located on a higher relief. The offset between the two thicker upper carbonate intervals is about 350 m, which means that they can not correlate with one another and are most likely not from the same depositional flow. In addition, latter well also show a higher amount of dirty sequence towards the top compared to well 9/11b-11, and less carbonate intervals, which presumably is due to different currents and depositional flows.

Overall, the well correlation of all the studied logs from Figure 8.1 and wire line logs of well 9/11b-11 and 9/11b-z (Appendix H) show corresponding intervals of carbonate beds within the upper part of Maureen Formation. These beds are most likely deposited approximately in a same time period prior to the peak uplift off the East Shetland Platform. However, due to an uneven relief, see in the time structure map and in the seismic section (Figures 8.2 and 8.3) these intervals are most likely not from one, but several flow event. With limited diagenetic input in the upper sections of the formation, these flows have most likely overlapped and merged within some areas. Though, they might be partly continuous, but due to the relief of the platform it is unlikely that they are continuous over a large area.

It should also be mentioned that the Maureen formation is deposited onto old rifts, which were reactivated during the East Shetland Platform uplift. This has most likely created uneven structural highs on the platform, which have most likely affected the lateral distribution of flow event deposits. However, with limited data and core information of the correlated wells it is difficult to interpret a clear distribution of the carbonate sections. Though, it can be assumed that the carbonate beds show a better vertical- compared to lateral connection. In addition, a net thickness map, such as one made of the Outer Moray Firth basin by Killhams et al. (2014), of carbonate prone layers would provide a better understanding of their occurrences and their lateral and vertical dimensions within the Maureen Formation.

9.4 Diagenetic modification of carbonate intervals

The carbonate examined within the Maureen Formation has been identified as calcite, primarily composed of biologically derived low-Mg calcite (CaCO_3). All of the studied thin sections comprise a micritic chalk matrix mixed within the clastic sediments. However, some of the samples are also taken from a purer chalk unit where the clastic input is more or less absent.

9.4.1 Mechanical compaction

From thin section- and SEM analysis, the clastic grains are mostly dominated by quartz, with an average of 19,2%. These grains exhibit various sizes and show very little degree of grain breakage and show little to no contact between the framework grains or grain- to grain dissolution. There is also a large quantity of microfossils, such as foraminifera, that are well

preserved. However, some fossil fragments do show some degree of fracturing, but this is most likely the effect of transportation mechanisms, such reworking of older chalk deposits and mass flows.

9.4.2 Chemical compaction

The chalk occurs as a micritic matrix within the framework, which classified these samples as greywackes. From thin section analysis it was difficult to estimate the amount of micritic chalk matrix due to their small grain size ($<10\mu\text{m}$). Further studies of modification of chalk are therefore mainly supported on SEM analysis.

The effects of fine grain-to grain contact will reduce the overburden compaction at an early stage, as the stress per contact is relatively low. Small plates of coccoliths with a significant proportion of planktonic foraminifera, represents the bulk of the studied samples. These nanofossils and microfossils are composed of low-Mg calcite, which makes them chemically stable during early diagenesis (Bjørlykke, 2014). However, even though the chalk is fairly stable, dissolution of low-Mg calcite grains can occur if a sufficient linear pressure is applied to increase the solubility of calcite, commonly through increase the overburden (Mapstone, 1975). From thin sections and stub samples in SEM, minor dissolution of calcite is observed within the pore space. Some grain contacts have been observed in addition to areas that exhibit a higher degree of compaction within the matrix.

Studies from the North Sea chalk show that early lithification is common and result in a fairly stable framework. It has also suggested that the Danian chalk and Maastrichtian chalk could be divided into a three basic modes of chalk lithification; (1) spot-welding between grain-to grain contact, (2) selective overgrowth on calcite grains and (3) pore filling sparry calcite with stylolite seams (Mapstone, 1975). This diagenetic scheme is presented as an early diagenetic stage moving to a late diagenetic stage due to increase of burial depths and temperature. Such lithification pattern is often found through chalk studies in the North Sea, such as the Ekofisk Field, the Tor Field, Maureen Field etc.

The studied carbonate samples within the upper part of Maureen Formation show very little diagenetic modification. It has been observed that some of the grain contacts within the chalk matrix have exceeded a minimum threshold of localized dissolution of low-Mg calcite between the grains. Such modifications can typically be seen during early diagenesis, as been

presented above during a spot-welding diagenetic stage, where pressure-dissolution has occurred at sharp point contacts but within a confined area (Neugebauer, 1973). However, evidence of any further diagenetic modification such as calcite overgrowth, stylolite seams, calcite cementation within the framework or recrystallization of calcite crystals to larger aggregates have not been detected in any of these samples. This might be due to the rapid burial, where the sediments had a limited time of exposure, reducing the time for lithification on the seafloor and effects of bioturbation and due to the majority of chemical stable organisms composed of low-Mg calcite. In addition, an early hydrocarbon entry into the carbonate intervals could also explain the absence of further chemical dissolution and precipitation within these layers (Vagle & Brasher, 1996).

Further, other modification within the studied samples can be seen on fossil fragments of ostracodes and mollusks, where calcite has replaced an earlier aragonite or high-Mg calcite by neomorphism (Folk, 1965). In addition, it has also been observed some epitaxial cement on the interior of foraminifera. However, these processes might reflect inherited modifications from the first depositional cycle, which prevailed during re-deposition of mass flow events. This assumption is based on the low percentage of diagenetic modification and the lack of ground water flow through the sediments during burial, indicated by strontium isotope analysis presented in Chapter 7.

From these observations it can be concluded that the samples support the theory of pressure dissolution between smaller grain contacts, stabilizing the framework at an early stage. This has reduced the mechanical compaction and preserved most of the primary composition of the carbonate framework. In addition, it has led to little grain modification and a large quantity of well-preserved micro fauna. Further, the amount of carbonate that could be precipitated is limited by the minimal variability of cations, such as Ca^{++} , Mg^{++} and Fe^{++} . Unless significant amounts of calcium are released from non-carbonate minerals, very little new calcite will be precipitated (Sigal & Bjørlykke, 1987). In addition, early hydrocarbon emplacement will prohibit or reduce dissolution and precipitation of CaCO_3 in carbonate, which in turn will prohibit any further chemical compaction (Vagle & Brasher, 1996).

9.5 Origin and source of clay minerals

The clay minerals found in samples from well 9/11b-11 within the Maureen Formation were analyzed as three different minerals: (i) mixed layered illite/smectite (I/S), (ii) illite and (iii) kaolinite. These clay minerals will be discussed based on SEM-, EDX- and XRD analysis.

Illite/ smectite

The interstratified mixed layered I/S was observed and quantified within the pore filling chalk matrix and as thin calcareous clay beds. Result from SEM and EDX analysis shows an iron-rich mixed layered clay mineral, with a webby morphology (Figure 6.7). The high iron content is explained by a high content of smectite, calculated from XRD clay fraction results. The smectite comprises about 90% of the mixed clay layer, with the remaining 10% composed of illite. Such interstratified clay minerals are typically found within the North Sea, where the smectite content tend to decrease with increasing burial depth, and is gradually replaced by mixed- layer minerals (I/S) and illite (Bjørlykke & Jahren, 2010). Initiations of interstratification of clays are often caused by illitization of smectite see Chapter 3.3.

Further, the carbonate samples from well 9/11b-11 within the upper part of Maureen Formation were tested through strontium isotope analysis (Chapter 7). The results showed that the carbonate intervals within these samples have not been under influence of any ground water flow during deposition or through the burial history.

Based on the results given, and the fact that the samples from this study are taken from burial depths of less than 1800 meters, with a corresponding temperature of only 46° C, these clay minerals are most likely not of authigenic origin. In addition, thin section observations support the theory of a detrital origin as no weathering was observed on the feldspar or mica grains. Initiation of such mixed layered I/S reactions within this formation at such low temperatures is therefore unlikely. It should also be mentioned that the diffuse and chaotic morphology of these clay minerals, analyzed though thin sections and stub samples in SEM, does not support any authigenic origin.

Distribution and source of illite/smectite

The high iron content found in the I/S is characteristic of volcanic ash but it can also originate from other sources within the region (Peltonen et al., 2008). However, given the time period

of deposition for these sediments, volcanic ash is considered a plausible explanation to the source of these smectite-rich clay deposits. The origin of the mixed layered I/S is most likely from detrital clay minerals and not from modification during burial diagenesis. Due to their occurrences within the Maureen Formation, both as calcareous mud layers and within the micritic matrix, they are most likely derived from reworked, older pelagic clays transported by mass flows.

Illite

Illite, identified and quantified from XRD analysis, is present in small quantities within all of the studied samples with an average of 5,4%. Nevertheless, the percentage of illite is slightly higher in the calcareous clay layers (Figure, 6.13). The differentiation between authigenic illite and detrital illite is difficult to determine based on XRD results, due to interferences of clastic illite and muscovite (Bjørlykke, 1998), which share the same 10Å peak. From SEM analysis and microscopy there has not been made any clear observation of authigenic illite. In addition, the micritic matrix within the studied samples makes it even more difficult to identify illite as the pore filling matrix has a chaotic appearance and very small grain size <10 µm.

Moreover, based on the burial depth and temperature mentioned above, with no past or present influx of groundwater influencing these sediments, it is highly unlikely that precipitation of illite has occurred post deposition. Therefore, the quantified illite has most likely originated as detrital clay, and can often accumulate as a result of flooding events. Illitization of kaolinite is considered a destructing process with regards to permeability in deeper buried reservoirs (temperatures from approximately 130 ° C) due to its fibrous and pore bridging morphology (Bjørlykke, 1998). Due to the shallow burial depths and thereby also the relatively low temperature in addition to the low amounts found in XRD analysis, the illite incorporated in the Maureen formation is not believed to have any significant effect on the reservoir quality. Further discussion on modification of illite and its effect on reservoir properties are therefore excluded in this study.

Kaolinite

From XRD bulk results, a small proportion of kaolinite was quantified through all of the samples containing homogeneous- and calcareous sand, an average of 1,4% (Figure 6.13). Autigenic kaolinite is usually precipitated at an early diagenetic stage, due to unstable minerals such as feldspar and micas, which are easily dissolvable when in contact with meteoric water (Bjørlykke, 1998).

From the reactions presented in chapter 3.2, the absent of groundwater flows, as mentioned earlier, will prevent dissolution of these cations. The precipitation of kaolinite is consequently more or less neglected within these samples and is most likely not of authigenic origin. It should also be mentioned that no distinctive morphological features, such as pseudo-hexagonal plates, was observed (Wilson & Pittman, 1977). This further confirms the belief that the kaolinite is most likely of detrital origin and that the kaolinite is transported by mass flows from more proximal areas, which again dominates the deposition of the studied sediments.

9.6 Other minerals

Pyrite and glauconitic pebbles were found within the majority of the samples.

In respect to diagenetic alteration, these minerals have little impact on reservoir quality, but rather indicates what type of chemical reactions that were provided during deposition. In addition, glauconite is also a good indicator of what type of sedimentary environment the formation was deposited in, due to their commonly growth within a shallow marine environment. However, the sediments from well 9/11-b 11 within the Maureen Formation are distal deposits, which means that these glauconitic clasts are pebbles transported from proximal parts of the East Shetland Platform out to the shelf within mass flows.

9.7 Consequences for reservoir quality within the Maureen Formation

Prediction of carbonate intervals distributed within a reservoir is important to address when in production of hydrocarbons, due to carbonate intervals can form barriers to fluid flow during production. It is therefore important to understand when and how they were formed within reservoirs. The carbonates composition is dominated by coccoliths, and due to their shape and structure it makes them more impermeable compared to pure siliciclastic sand. It is

therefore of great interest to investigate the relation between the permeability of the reservoir sands and the carbonate intervals. This discussion will be based on the data provided from the cored section of well 9/11b-11 with focus on the homogeneous oil-stained sand facies and the carbonate facies described in Chapter 5.

The vertical and horizontal permeability plots in Figures 9.1 and 9.2 shows a clear trend, with drastic decrease in permeability within the calcareous sand and chalk rich intervals (with depth?). The vertical permeability in the carbonate intervals varies between 0,1-11 mD, were the lowest value most likely represents incorporated clay within the calcareous sand layers. The horizontal permeability of the carbonate intervals range between 0,1-10 mD, and show the same consistency with a lower permeability presumably associated with more incorporated clay (Figures 9.1 and 9.2). From these results, the more clay incorporated in the layers, the more difficult for fluid to flow, especially in a vertical direction due to thin laminations and veins of clay within the layer. However, it should be noticed that the chalk rich layer within log sheet 8 (Appendix B) shows the highest vertical permeability, 11 mD, of the carbonate intervals, with a corresponding horizontal permeability of only 0,362 mD. The higher vertical permeability might be due the previous re-worked material from the Tor Formation, which might have partly improved the permeability. In addition, these chalk rich layers were deposited in a consolidated to semi-consolidated state, as block slide from structural highs. This has resulted in little silicalstic input, less then 8%, and might also have aided in preservation of vertical permeability (Sample 5) and less incorporated clay.

It has also been observed that a calcareous sand layer has relative similar vertical permeability (6,69 mD) and horizontal permeability (9,04 mD) values (Figures 9.1 and 9.2),. The layer is interbedded between homogeneous oil stained sand units, and is less compacted then the other section seen through thin section analysis (Sample 3). This is most likely due a lower amount of matrix (42,8%), a higher amount of quartz grains (60%) and a lower amount of calcite (22%) (Figure 6.13). This might have resulted in better a horizontal and vertical connection calcareous layer.

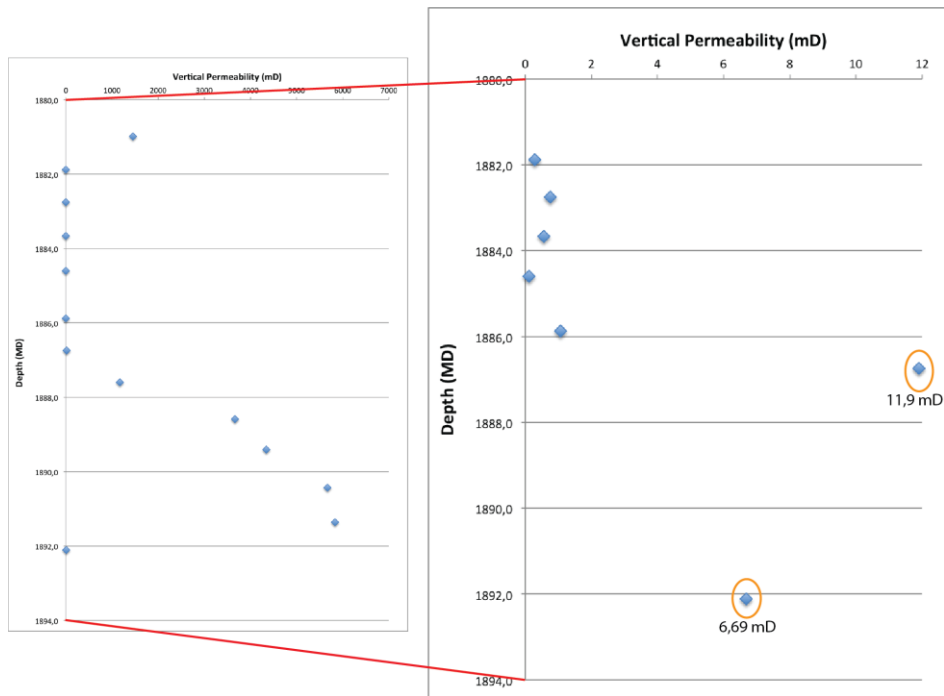


Figure 9.1: Vertical permeability of well 9/11b-11 of the carbonate intervals. Distribution of the lowest vertical permeability, with more incorporated clay closer to zero.

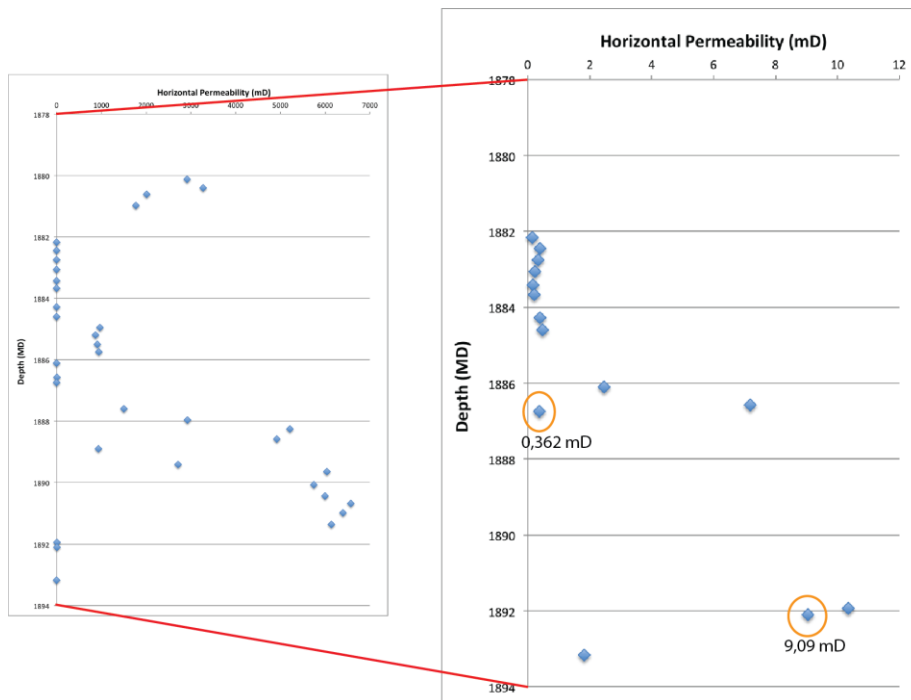


Figure 9.2: Horizontal permeability of well 9/11b-11 of the carbonate intervals. Distribution of the lowest horizontal permeability, with more incorporated clay closer to zero.

Further, in Figure 8.4 all wells with measured horizontal porosity and permeability variation from the correlated log was plotted, (depth was dot provided for these plots). Well 9/11a-7 has a relatively constant permeability with an increase of porosity. From the correlated log in Figure 8.1, the composition is relative homogeneous, and has very little incorporated carbonate intervals. However, within the upper part, a thin carbonate layer can be detected, which is possibly way a few of the permeability plots of this well deviates some from the rest. On the other hand, it still has a high permeability and do not seem to impact the reservoir sandstone. Well 9/11a-9 and well 9/11a-5 are split into two sections, one with a higher permeability and one with a slightly lower permeability. From the well correlation in Figure 8.1 these two section have the thickest dirty sequence section. These sections have a higher amount of clay, which might be the reason for the separations between the porosity, and permeability plots. A depth interval of these plots would help understand these separations better. In addition, well 9/11b-11 is the well that deviates the most, with a larger proportion of low permeability and porosity (Figure 8.4, marked with a red ellipse). These low permeable sections are most likely related to the carbonate intervals discussed above, with more input of clay within the calcareous layers the less permeable they get.

Overall, the carbonate intervals within the upper part of well 9/11b-11 seem to have an generally low permeability with an average of 3,05 mD in vertical- and 2,4 mD in horizontal permeability. It also seems that the more mixed the calcareous layers are, with respect to higher amount of clay clast and veins, the less permeable the layers are, especially within the vertical direction. However, even though the carbonate intervals are less permeable than preferable, the carbonate intervals do not seem to correlate well over a large distance within the reservoir sands due to the bathymetry. In addition, some of the wells such as 9/11a-7 do not show large diversity in permeability within the carbonate interval. The reservoir contains heavy oil, which means that the viscosity is high and if hydrocarbons were to migrate into the carbonate intervals it would most likely not be retained within the tight layered section. Nevertheless, additional permeability and porosity data on the carbonate intervals would increase the understanding of how the carbonate intervals related to the reservoir sand.

Chapter 10: Conclusion

CONCLUSION

- Slump, debris flows and turbiditic currents are the main depositional processes in the Maureen Formation, which is seen through the chaotic variations in grain sorting and distribution of deformation structures.
- Biostratigraphical analysis (By Statoil) dates the chalk to upper Maastrichian, reworked Tor Formation. The chalk is derived from i) consolidates or semi-consolidated block slides, ii) rip-up clast and ii) unconsolidated micritic matrix.
- The lateral and vertical discontinuity from the well correlation is mainly caused by subsidence of the Shetland platform, reactivation of old faults and the nature of the gravity flows. In combination with the difference in consolidation, this has resulted in an unevenly and mixed distribution of the carbonate intervals seen in the Maureen Formation.
- The thermal uplift of the Scotland Shetland region towards the early Palaeocene caused a broad exposure of the chalk group and a subsequent increase deposition of reworked chalk through gravity flows. The carbonate beds seen in the upper part of the formation, from the wells in this study, is believed to result from several flow events. These beds are consequently interpreted to be discontinuous over a larger area, but show relatively good lateral connectivity within shorter distances.
- The reworked chalk consists primarily of coccoliths and foraminifera, and is composed of low-Mg calcite making them fairly chemical stable. Their small grain size, the large quantity of micritic chalk, minor grain-to-grain dissolution and early hydrocarbon entry has reduced the effect of mechanical and chemical diagenesis. Together with large amounts of siliciclastic sediments it has resulted in preservation of high porosity (average of 28,9 %) and permeability (average of 2022 mD) in well 9/11b-11.
- The carbonate intervals show an overall low vertical and horizontal permeability, and fluid flow of heavy oil through these layers might not be so efficient. However, given sections with less clay and chalk clasts incorporated in the calcareous layers, the intervals might work better as fluid pathways.

References

- Adda, G. W. 2012: Hydrocarbon generation and migration from Jurassic source rocks in the northern North Sea. Unpubl. MSc. Thesis. *Norwegian University of Science and Technology*. 88.
- Ahmadi, Z., Sawers, M., Roberts, S. K., Stanworth, B., Kugler, K., Kristensen, J. & Fugelli, E. 2003: Paleocene. In: Evans, D., Graham, C., Armour, A. & Bathurst, P. (Eds.), *The Millennium Atlas: Petroleum Geology of the Central and Northern North Sea. The Geological Society of London*, Ch. 14, 235-389.
- Badley, M., Price, J., Dahl, C. R. & Agdestein, T. 1988: The structural evolution of the northern Viking Graben and its bearing upon extensional modes of basin formation. *Journal of the Geological Society*, 145, 455-472.
- Berg, E. A., Silcock, S. & Østbo-Bjastad, B. 2013: Next step in offshore heavy oil-Mariner Reservoir Development. SPE Offshore Europe Oil and Gas Conference and Exhibition. *Society of Petroleum Engineers*.
- Bjørlykke, K. 1994: Fluid-flow processes and diagenesis in sedimentary basins. *Geological Society, London, Special Publications*, 78(1), 127-140.
- Bjørlykke, K. 1998: Clay mineral diagenesis in sedimentary basins – a key to the prediction of rock properties. Examples from the North Sea Basin. *Clay Minerals*, 33, 15-34.
- Bjørlykke, K. 2010: Sedimentary Geochemistry. In: Bjørlykke, K. (Ed.), *Petroleum Geoscience – From Sedimentary Environments to Rock Physics. Springer*. Ch. 3, 87-111.
- Bjørlykke, K. & Jahren, J. 2010: Sandstone and Sandstone Reservoirs. In: Bjørlykke, K. (Ed.), *Petroleum Geoscience – From Sedimentary Environments to Rock Physics. Springer*. Ch. 4, 113-140.
- Bjørlykke, K., Jahren, J., Mondol, N. H., Marcussen, Ø., Croize, D., Peltonen, C. & Thyberg, B. 2009: Sediment Compaction and Rock Properties. *AAPG International Conference and Exhibition*, Cape Town, South Africa.
- Bjørlykke, K. & Aagaard, P. 1992: Clay minerals in North Sea Sandstones. *SEPM Special Publications*, 47, 65-80.
- Bjørlykke, K., Aagaard, P., Egeberg, P. K. & Simmons, S. P. 1995: Geochemical constraints from formation water analysis from the North Sea and the Gulf Coast Basins on quartz, feldspar and illite precipitation in reservoir rocks. *Geological Society, London, Special Publications*, 86, 33-50.
- Boles, J. R. & Franks, S. G. 1979: Clay Diagenesis in Wilcox Sandstones of Southwest Texas: Implications of Smectite Diagenesis on Sandstone Cementation. *Journal of Sedimentary Petrology*, 49, 55-70.

- Bowman, M. B. J. 1998: Cenozoic. In: Glennie, K. W. (Ed.) *Petroleum geology of the North Sea: basic concepts and recent advances*. Blackwell Publishing. Ch. 10, 350-375.
- Bragg, W. H. & Bragg, W. L. 1913: *The Reflection of X-rays by Crystals*. The Royal Society, 88, 428-438.
- Brasher, J. E. & Vagle, K. R. 1996: Influence of Lithofacies and diagenesis on Norwegian North Sea Chalk Reservoirs. *AAPG Bulletin*, 80, 746-769.
- Chandler, P. M. & Dickinson, B. 2003: The Maureen Field, Block 16/29a, UK Central North Sea. *Geological Society, London, Memoirs*, 20, 587-601.
- Chilingar, G. V., & Larsen, G. 1983: Introduction. In: Chilingar, G. V., & Larsen, G. (Eds.), *Diagenesis in Sediments and Sedimentary Rocks*. Elsevier Scientific Publishing Company, 2, Ch. 1, 1-16.
- Christiansson, P., Faleide, J. I. & BERGE, A. 2000: Crustal structure in the northern North Sea: an integrated geophysical study. *Special Publication - Geological Society of London*, 167, 15-40.
- Cutts, P. 1991: The Maureen Field, Block 16/29a, UK North Sea. *Geological Society, London, Memoirs*, 14, 347-352.
- Deegan, C. T. & Scull, B. J. 1977: A standard lithostratigraphic nomenclature for the Central and Northern North Sea. *Report of the Institute of Geological Sciences, 77/25; NPD Bulletin No.1*.
- Dominguez, R. 2007: Structural evolution of the Penguins cluster, UK northern North Sea. *Geological Society, London, Special Publications*, 292(1), 25-48.
- Dott JR, R. H. 1964: Wacke, Graywacke and Matrix--What Approach to Immature Sandstone Classification?. *Journal of Sedimentary Research*, 34 (3), 625-632.
- Doyle, P. 1996: Microfossils – Foraminifera. In: *Understanding Fossils – An Introduction to Invertebrate Palaeontology*. Wiley. Ch. 16, 278-289.
- Faleide, J. I., Bjørlykke, K. & Gabrielsen, R. H. 2010: Geology of the Norwegian continental shelf. In: Bjørlykke, K. (Ed.), *Petroleum Geoscience – From Sedimentary Environments to Rock Physics*. Springer. Ch 22, 467-499.
- Feazel, C. T., Keany, J. & Peterson, R. M. 1985: Cretaceous and Tertiary Chalk of the Ekofisk Field Area, Central North Sea. In: Roel, P. O. & Choquette, P. W. (Eds.), *Carbonate Petroleum Reservoirs*. Springer, Ch. 31, 497-507.
- Folk, R. L. 1962: Spectral subdivision of limestone types – Classification of Carbonate Rocks. *Amer. Assoc. Pet. Geol.* 62-84.

Folk, R. L. 1965: Some aspects of recrystallization in ancient limestones. In: Pray, L. C., and R. C. Murray (Eds.), *Dolomitization and Limestone Diagenesis. Soc. Econ. Paleont. and Mineral. Spec. Publ.* 13, 14-48.

Frost, C. D., & Toner, R. N. 2004: Strontium Isotopic Identification of Water-Rock Interaction and Ground Water Mixing. *Groundwater*, 42(3), 418-432.

Gabrielsen, R.H., Færseth, R.B., Steel, R.J., Idil, S. & Kløyvan, O.S. 1990: Architectural styles of basin fill in the northern Viking Graben. In: Blundell, D.J. & Gibbs, A.D. (Eds.), *Tectonic Evolution of the North Sea Rifts. Clarendon Press, Oxford.* 158-179.

Gatliff R. W., Richards P. C., Smith K., Graham, C. C., McCormac, M., Smith, N. J. P., Long, D., Cameron, T. D. J., Evans, D., Stevenson, A. G., Bulat, J. & Ritchie, J. D. 1994: The Geology of the Central North Sea. *British Geological Survey United Kingdom, Offshore Regional Report*, HMSO, London.

Hanken, N. M., Bjørlykke, K., Nielsen, J. K. 2010: Carbonate Sediments. In: Bjørlykke, K. (Ed.), *Petroleum Geoscience – From Sedimentary Environments to Rock Physics. Springer.* Ch. 5, 141-200.

Heald, M. T. 1956: Cementation of Simpson and St. Peter sandstones in parts of Oklahoma, Arkansas, and Missouri. *The University of Chicago Press*, 64, 16-30.

Hillis, R. R. 2001: Coupled changes in pore pressure and stress in oil fields and sedimentary basins. *Petroleum Geoscience*, 7, 414-425.

Houseknecht, D. W. 1987: Assessing the relative importance of compaction processes and cementation to reduction of porosity in sandstones. *AAPG bulletin*, 71, 633-642.

Jager, D. D. H., Giles, M. R., & Griffiths, G. R. 1993: Evolution of Paleogene submarine fans of the North Sea in space and time. In: Parker, J. R. (Ed.), *Geological Society, London, Petroleum Geology Conference series. Geological Society of London.* Vol. 4, 59-71.

Jonk, R., Hurst, A., Parnell, J., Mazzini, A. & Fallick, A. E. 2005: Origin and timing of sand injection, petroleum migration, and diagenesis in Tertiary reservoirs, south Viking Graben, North Sea. *AAPG Bulletin*, 89, 329-357.

Kilhams, B., Hartley, A., Huuse, M. & Davis, C. 2012: Characterizing the Paleocene turbidites of the North Sea: the Mey Sandstone Member, Lista Formation, UK Central Graben. *Petroleum Geoscience*, 18, 337-354.

Kilhams, B., Hartley, A., Huuse, M. & Davis, C. 2014: Characterizing the Paleocene turbidites of the North Sea: Maureen Formation, UK Central Graben. In: McKie, T., Rose, P. T. S., Hartley, A. J., Jones, D. W. & Armstrong, T. L. (Eds.), *Tertiary Deep-Marine Reservoirs of the North Sea Region. Geological Society, London, Special Publications*, 403. First published online February 6, 2014, <http://dx.doi.org/10.1144/SP403.1>.

Knox, R. & Holloway, S. 1992: 1. Paleogene of the central and northern North Sea. In: Knox, R. W. O'B. & Cordey, W. G. (Eds.), *Lithostratigraphic nomenclature of the UK North Sea. British Geological Survey Nottingham.*

Lyngsie, S. B., Thybo, H. & Rasmussen, T. 2006: Regional geological and tectonic structures of the North Sea area from potential field modelling. *Tectonophysics*, 413, 147-170.

Mapstone, N. B. 1975: Diagenetic history of a North Sea chalk. *Sedimentology*, 22, 601-614.

Martinsen, O. & Nøttvedt, A. 2008: Norway rises from the Sea; Palaeogene and Neogene (Cenozoic) – the modern continents take shape: 66-2,6 Ma. In: Ramberg, I. B., Bryhni, I., Nøttvedt, A., Rangnes, K. (Eds.), *The Making of a Land – Geology of Norway. Norwegian Geological Association*, Ch. 14, 442-479.

Mitchum, R. M., Sangree, J. B., Vail, P. R. & Wornardt, W. W. 1993: Recognizing sequences and systems tracts from well logs, seismic data, and biostratigraphy: Examples from the Late Cenozoic of the Gulf of Mexico. In: Weimer, P & Posamentier, H. (Eds.), *Siliciclastic Sequence Stratigraphy: Recent Developments and Applications. Amer Assn of Petroleum Geologists; illustrated edition edition (May 1994)*. Ch7, 163-197.

Mondol, N. H., Jahren, J. & Bjørlykke, K. 2013: Elastic properties of clay minerals. *Society of Exploration Geophysicists*, 27(6), 758-770.

Moore, D. M. & Reynolds, R. C. 1989: X-ray Diffraction and the Identification and Analysis of Clay Minerals. *Oxford university press Oxford*.

Morse, J. W. & Mackenzie, F. T. 1990: Interactions Between Carbonate Minerals and Solutions. In: *Geochemistry of Sedimentary Carbonates*. Elsevier Science Publishers, Ch. 2, 39-85.

Mudge, D. & Bliss, G. 1983: Stratigraphy and sedimentation of the Palaeocene sands in the Northern North Sea. *Geological Society, London, Special Publications*, 12, 95-111.

Mudge, D. C. & Bujak, J. P. 1996: An integrated stratigraphy for the Paleocene and Eocene of the North Sea. *Geological Society, London, Special Publications*, 101, 91-113.

Mudge, D. C. & Copestake, P. 1992: Lower Palaeogene stratigraphy of the northern North Sea. *Marine and Petroleum Geology*, 9, 287-301.

Nichols, G. 2009: Deep Marine Environments. In: *Sedimentology and stratigraphy*. Wiley – Blackwell, Ch. 16, 247-262.

Neugebauer, J. 1974: Some aspects of cementation in chalk. *Spec. Publs int. Ass Sediment*, 1, 149-176.

Nøttvedt, A., Gabrielsen, R. & Steel, R. 1995: Tectonostratigraphy and sedimentary architecture of rift basins, with reference to the northern North Sea. *Marine and Petroleum Geology*, 12, 881-901.

Nøttvedt, A. & Johannessen, E. P. 2008: The source of Norway's oil wealth; Late Jurassic – a sea of islands emerges; 161-146 Ma. In: Ramberg, I. B., Bryhni, I., Nøttvedt, A., Rangnes, K.

(Eds.), *The Making of a Land – Geology of Norway*. Norwegian Geological Association, Ch. 12, 384 – 417.

Offshore – Technology. 2014: Mariner Area Development, North Sea, United Kingdom [online]. Available: <http://www.offshore-technology.com/projects/mariner-area-development-north-sea-uk/> [accessed

Ortner, H. 2007: Styles of soft-sediment deformation on top of a growing fold system in the Gosau Group at Muttekopf, Northern Calcareous Alps, Austria: slumping versus tectonic deformation. *Sedimentary Geology*, 196, 99-118.

Peltonen, C., Marcussen, Ø., Bjørlykke, K. & Jahren, J. 2008: Mineralogical control on mudstone compaction: a study of Late Cretaceous to Early Tertiary mudstones of the Vøring and Møre basins, Norwegian Sea. *Petroleum Geoscience*, 14, 127-138.

Powers, M. C. 1953: A new roundness scale for sedimentary particles. *Journal of Sedimentary Research*, 23(2), 117-119.

Ravnås, R., Nøttvedt, A., Steel, R. & Windelstad, J. 2000: Syn-rift sedimentary architectures in the Northern North Sea. *Geological Society, London, Special Publications*, 167, 133-177.

Roberts, A. M. & Yielding, G. 1991: Deformation around basin-margin faults in the North Sea/mid-Norway rift. *Geological Society, London, Special Publications*, 56, 61-78.

Richter, F. M., Rowley, D. B. & DePaolo, D. J. 1992: Sr isotope evolution of seawater: the role of tectonics. *Earth and Planetary Science Letters*, 109 (1992), 11-23.

Saigal, G. C. & Bjørlykke, K. 1987: Carbonate cement in clastic reservoir rocks from offshore Norway – relationships between isotopic composition, textural development and burial depth. In: Marshall, J. D. (Ed.), *Diagenesis of sedimentary sequences*. Geological Society Special Publications, 36, 313-324.

Scoffin, T. P. 1987: Carbonate grains. In: *An Introduction to Carbonate Sediments and Rocks*. Blackie, Ch. 4, 15-52.

Shanmugam, G., Bloch, R., Mitchell, S., Damuth, J., Beamish, G., Hodgkinson, R., Straume, T., Syvertsen, S. & Shields, K. 1996: Slump and debris-flow dominated basin-floor fans in the North Sea: an evaluation of conceptual sequence-stratigraphical models based on conventional core data. *Geological Society, London, Special Publications*, 103, 145-176.

Simonsen, L. & Toft, J. 2006: Texture, composition and stratigraphy of volcanic ash beds in lower Palaeocene chalk from the North Sea Central Graben area. *Marine and petroleum geology*, 23, 767-776.

Skovbro, B. 1983: Depositional conditions during chalk sedimentation in the Ekofisk area Norwegian North Sea. In: Kaasschieter, J. P. H. & Reijers, T. J. A. (Eds.), *Petroleum Geology of the Southeastern North Sea and the Adjacent Onshore Areas*. Springer Netherlands. 169-175.

Surlyk, F., Dons, T., Clausen, C.K. and Higham, J. 2003: Upper Cretaceous. In: D. Evans, C. Graham, A. Armour and P. Bathurst (Eds.), *The Millennium Atlas, Petroleum Geology of the Central and Northern North Sea*. London, *The Geological Society, London*. 213–233.

Underhill, J. 2001: Controls on the genesis and prospectivity of Paleogene palaeogeomorphic traps, East Shetland Platform, UK North Sea. *Marine and petroleum geology*, 18, 259-281.

Watanabe, T. & Sato, T. 1981: Expansion characteristics of montmorillonite and saponite under various relative humidity conditions. *Clay Science*, 7, 129-138.

Watanabe, T. 1988: The structural model of illite/smectite interstratified mineral and the diagram for its identification. *Clay Science*, 7, 97-114.

Watts, N., Lapre, J., Van Schijndel-Goester, F. & Ford, A. 1980: Upper Cretaceous and lower Tertiary chalks of the Albuskjell area, North Sea: Deposition in a slope and a base-of-slope environment. *Geology*, 8, 217-221.

Wilson, M. D., & Pittman, E. D. 1977: Authigenic clays in sandstones: recognition and influence on reservoir properties and paleoenvironmental analysis. *Journal of Sedimentary Research*, 47(1), 3-31.

Wilson, M. J. 2013: Mixed – layer Clay Minerals. In: *Clay Minerals*. *The Geological Society*, 392-599.

Ziegler P. A. 1978: Northwestern Europe: tectonics and basin development. *Geologie Mijnbouw*, 57(4), 589-626.

Ziegler P. A. 1990: Geological atlas of western and central Europe. *Geological Society*.

http://www.statoil.com/en/NewsAndMedia/News/2014/Pages/20Dec_Mariner.aspx

Appendix A – Log Template

SHEET _____ OF _____

FIELD: _____
 WELL: _____
 REF. DEPTH: _____
 CORE DIAMETER: _____
 INTERVAL: _____

CORE DESCRIPTION









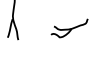



FORMATION: _____
 AGE: _____

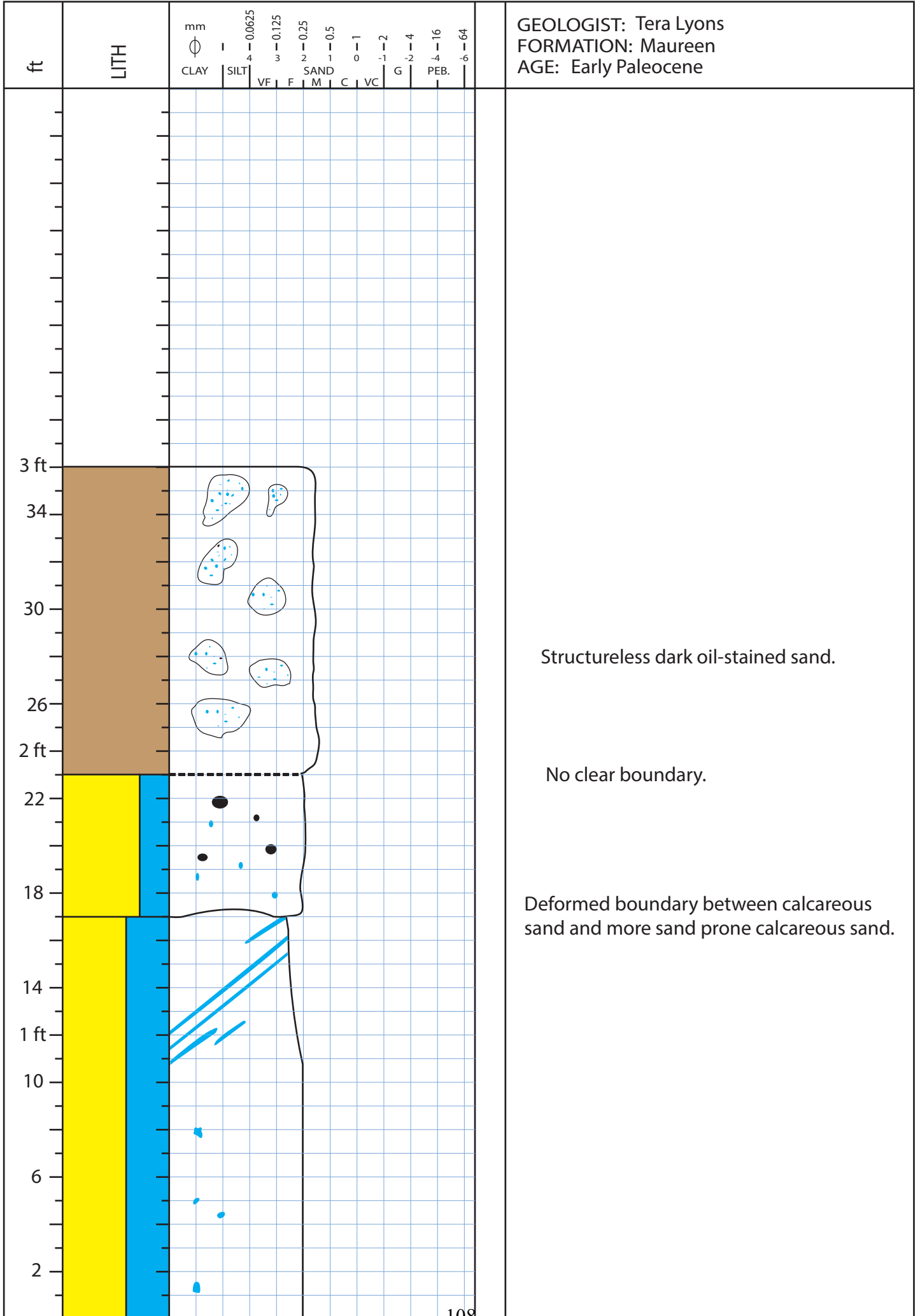
SCALE: _____
 DATE: _____
 GEOLOGIST: _____

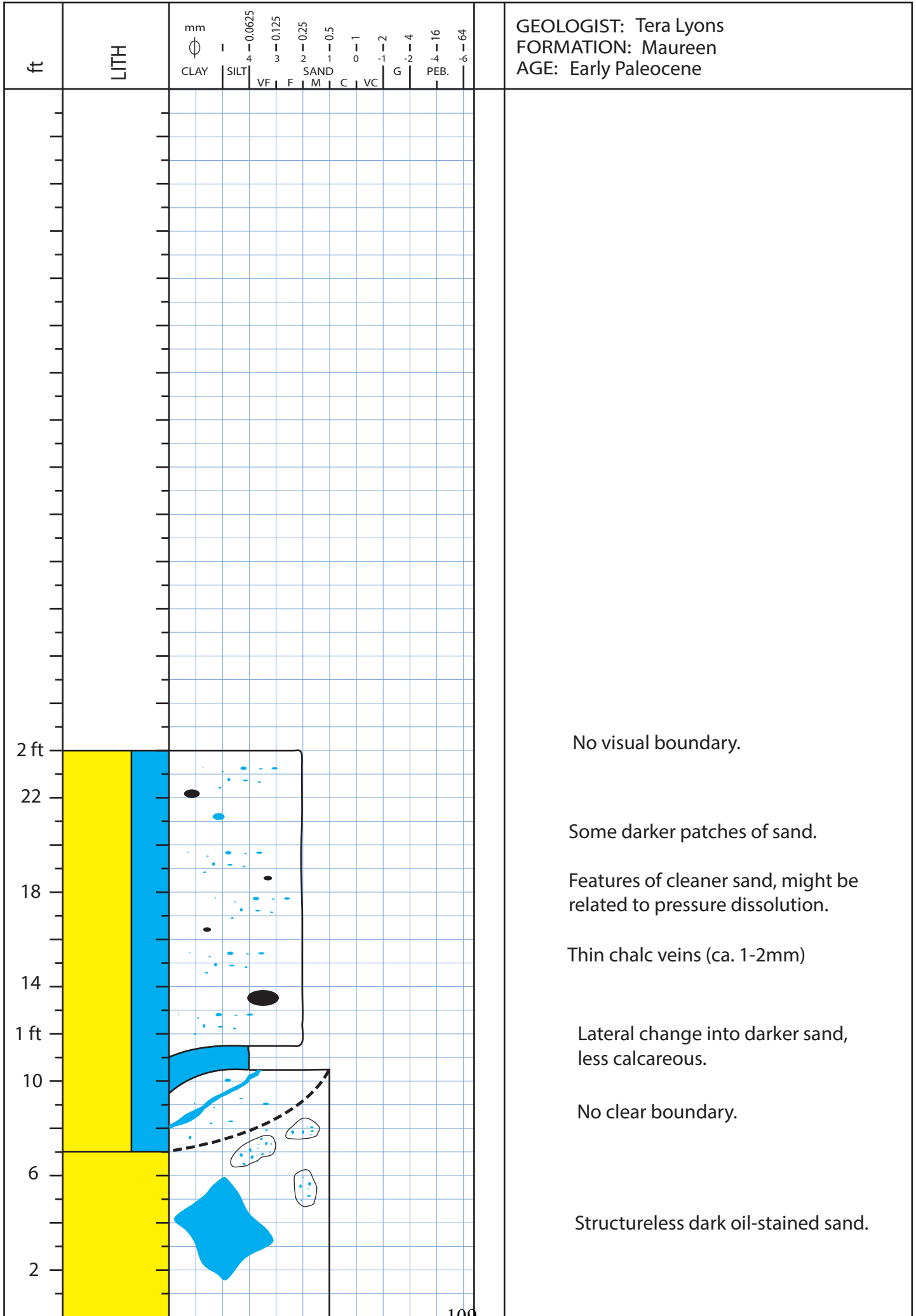
CHRONOSTRATIGRAPHY	LITHOSTRATIGRAPHY	RESERVOIR ZONE	CORE NO.	LOG DEPTH (mMD RKB)	CORE DEPTH	LITHOLOGY	GRAIN SIZE AND SEDIMENTARY STRUCTURES	COLOURS AND STAINING	STACKING PATTERN	SUBENVIRONMENT/FACIES	DEPOSITIONAL ENVIRONMENT	REMARKS, DESCRIPTION AND INTERPRETATION																																		
							<table border="0" style="font-size: small; width: 100%;"> <tr> <td>Clay</td> <td>1000</td> <td>8</td> </tr> <tr> <td>Silt</td> <td>0.0025-4</td> <td></td> </tr> <tr> <td>Very Fine Sand</td> <td>0.025-0.05</td> <td>4</td> </tr> <tr> <td>Fine Sand</td> <td>0.05-0.25</td> <td>3</td> </tr> <tr> <td>Medium Sand</td> <td>0.25-0.5</td> <td>2</td> </tr> <tr> <td>Coarse Sand</td> <td>0.5-1</td> <td>1</td> </tr> <tr> <td>Very Coarse Sand</td> <td>1-2</td> <td>0</td> </tr> <tr> <td>Gravel</td> <td>2-8</td> <td>-1</td> </tr> <tr> <td>Pebbles</td> <td>8-16</td> <td>-2</td> </tr> <tr> <td></td> <td>16-32</td> <td>-3</td> </tr> <tr> <td></td> <td>32-64</td> <td>-4</td> </tr> </table>	Clay	1000	8	Silt	0.0025-4		Very Fine Sand	0.025-0.05	4	Fine Sand	0.05-0.25	3	Medium Sand	0.25-0.5	2	Coarse Sand	0.5-1	1	Very Coarse Sand	1-2	0	Gravel	2-8	-1	Pebbles	8-16	-2		16-32	-3		32-64	-4						
Clay	1000	8																																												
Silt	0.0025-4																																													
Very Fine Sand	0.025-0.05	4																																												
Fine Sand	0.05-0.25	3																																												
Medium Sand	0.25-0.5	2																																												
Coarse Sand	0.5-1	1																																												
Very Coarse Sand	1-2	0																																												
Gravel	2-8	-1																																												
Pebbles	8-16	-2																																												
	16-32	-3																																												
	32-64	-4																																												

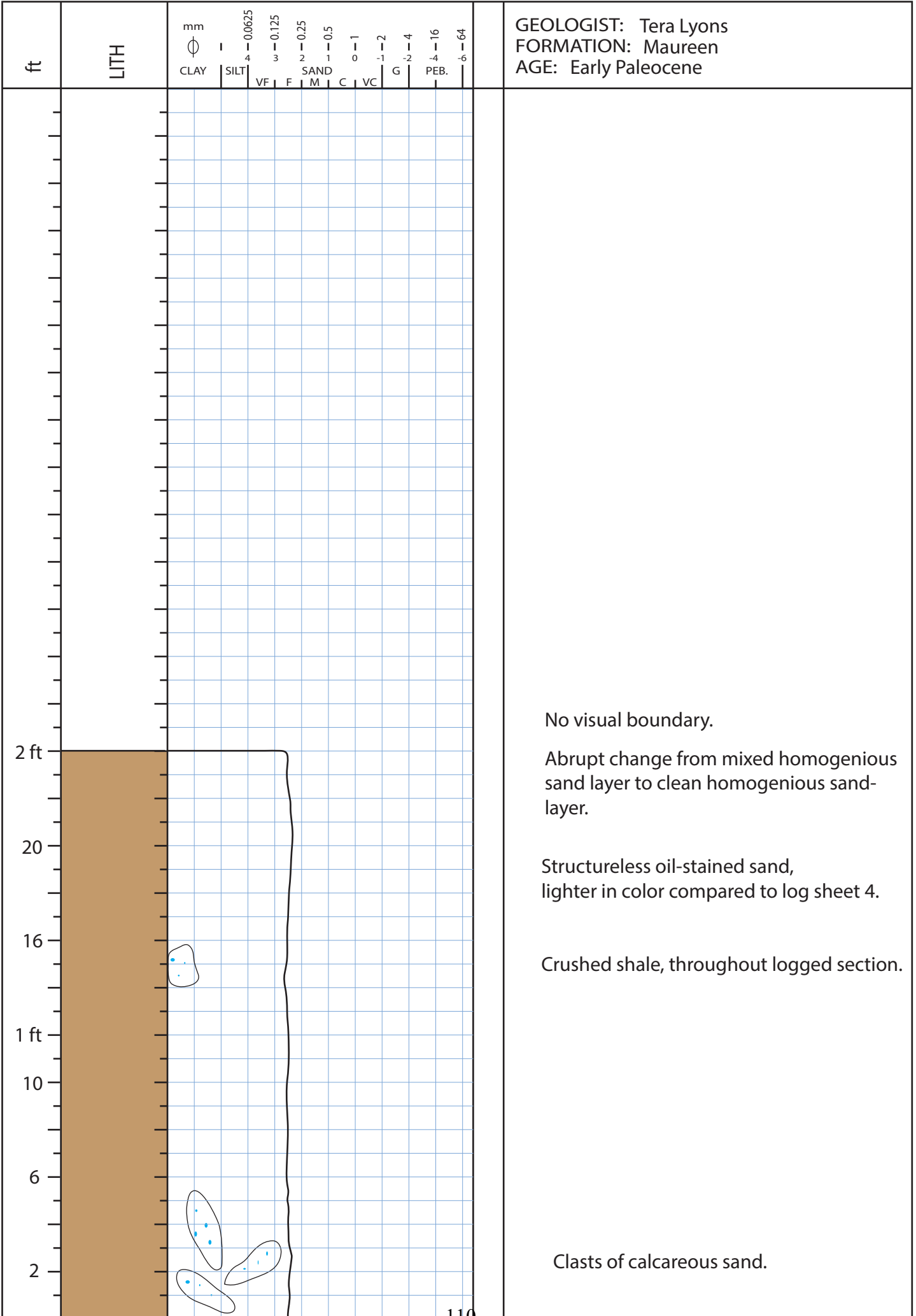
Appendix B – Sedimentary core logs

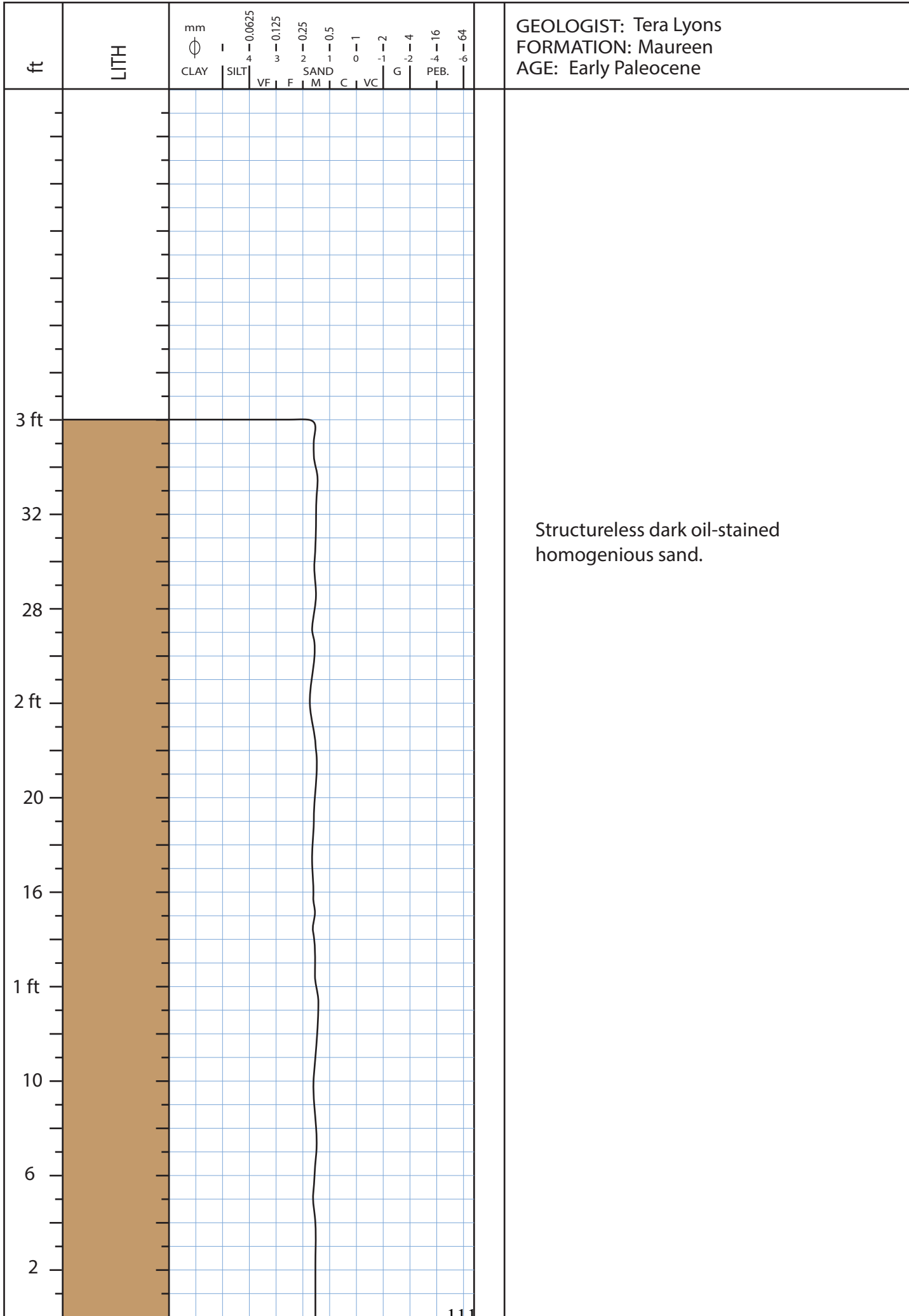
Legend

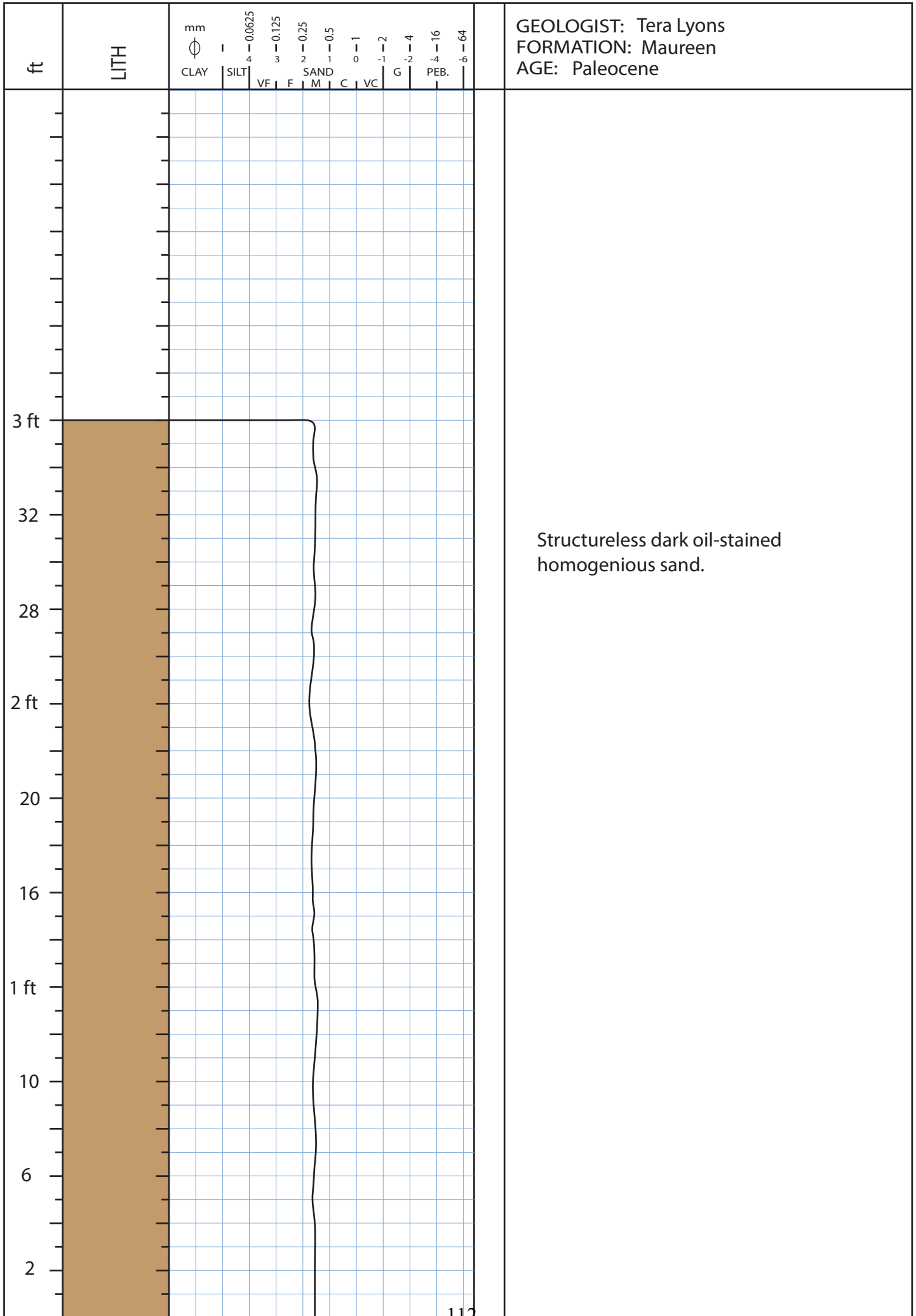
Lithology:	Sedimentary structures:
 Carbonate	 Weakly stained calcareous sand clasts with chalk clasts within
 Shale	 Chalk clasts
 Sandstone	 Rock fragments
 Heavy oil-stained sand	 Glauconite clasts
	 Clay veins
	 Chalk veins
	 Soft sediment deformation
	 Clay clast

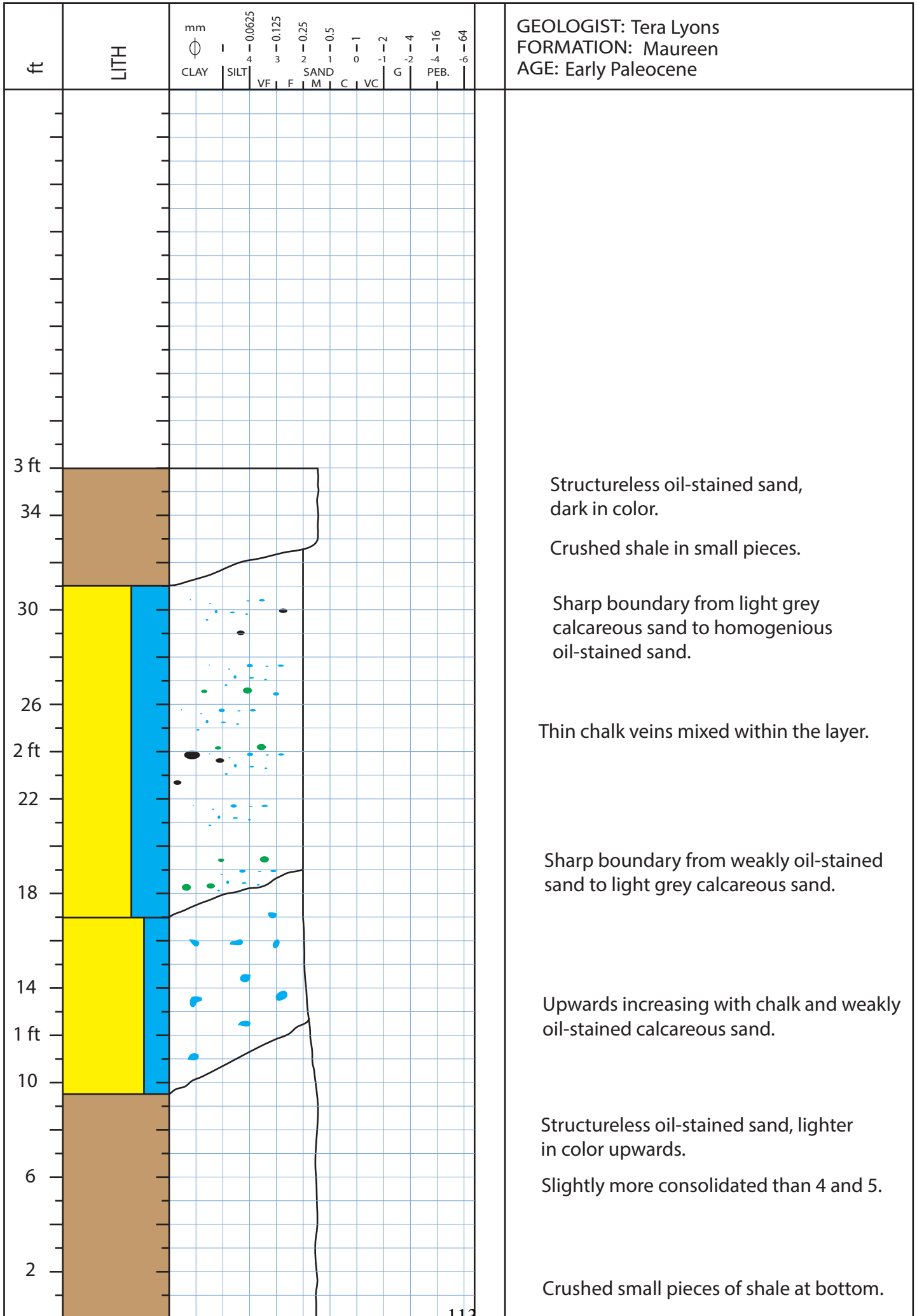


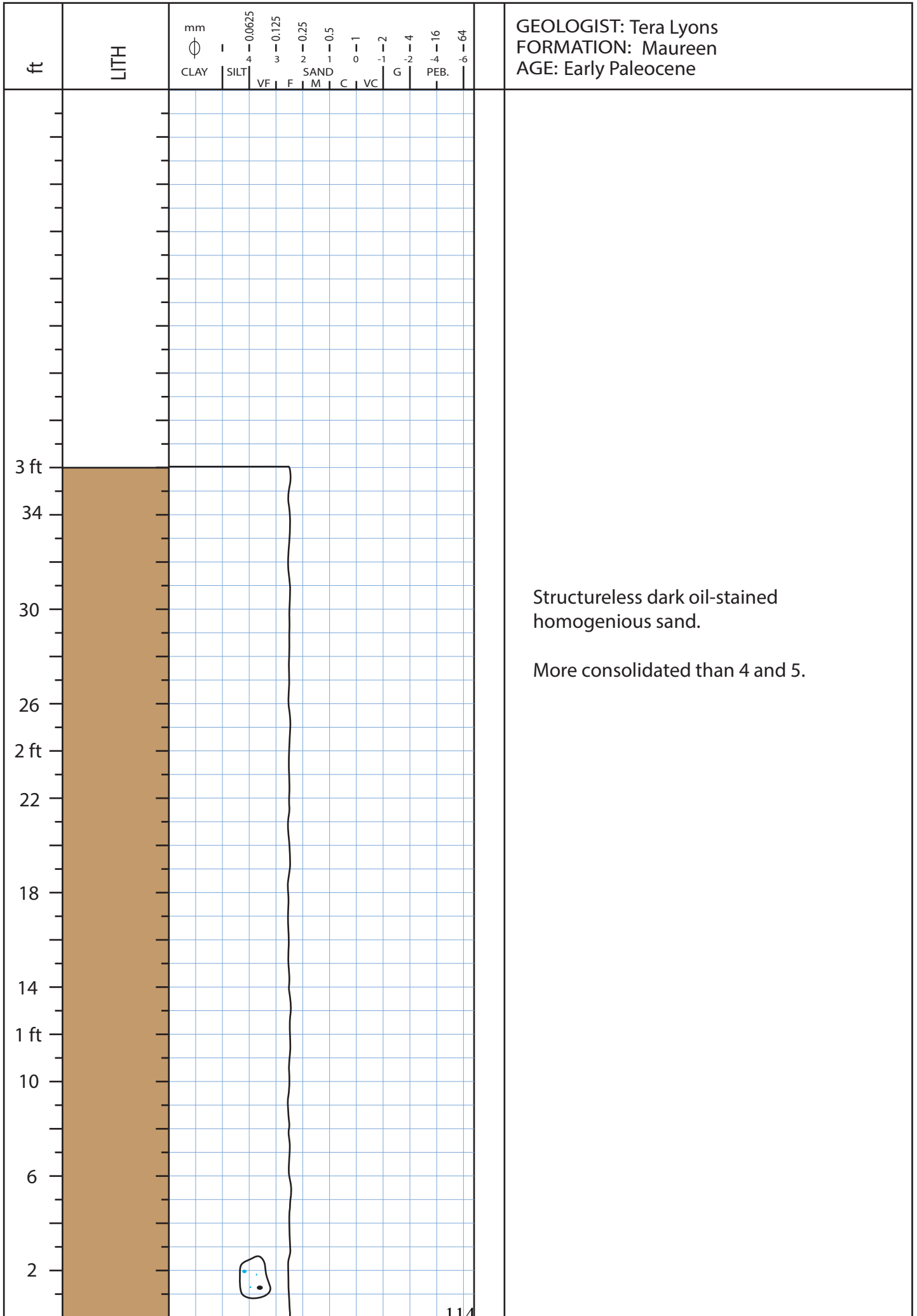






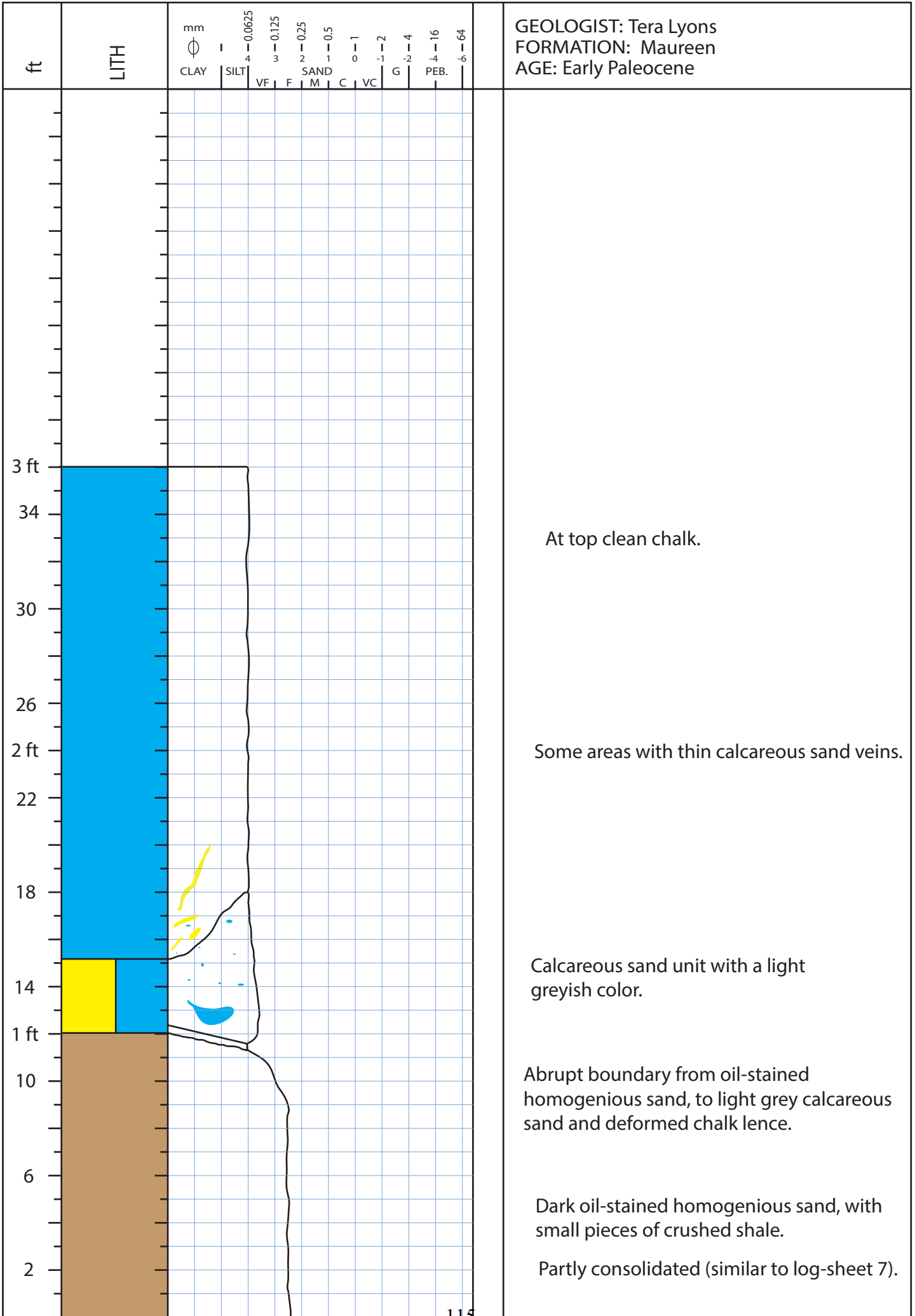


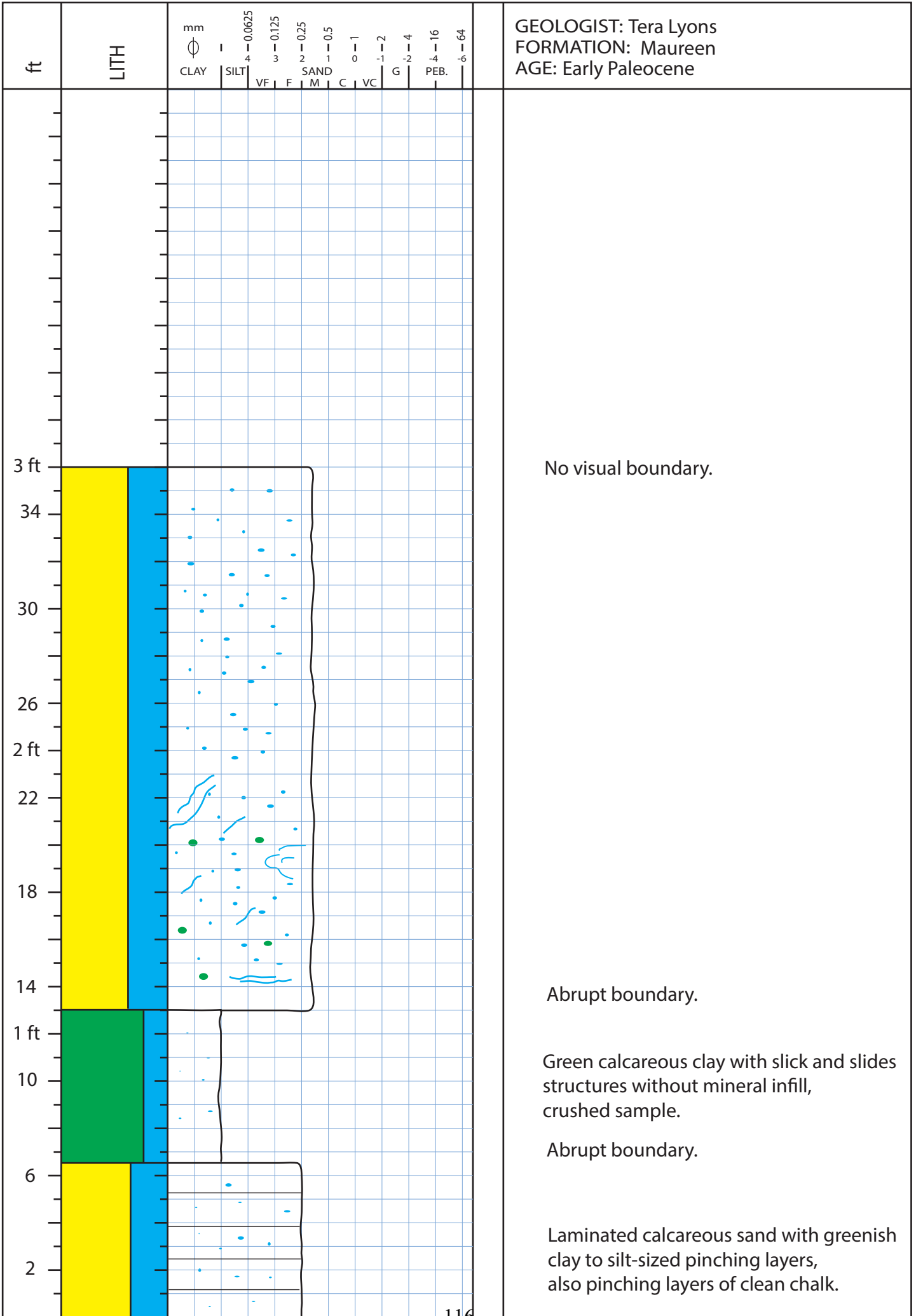


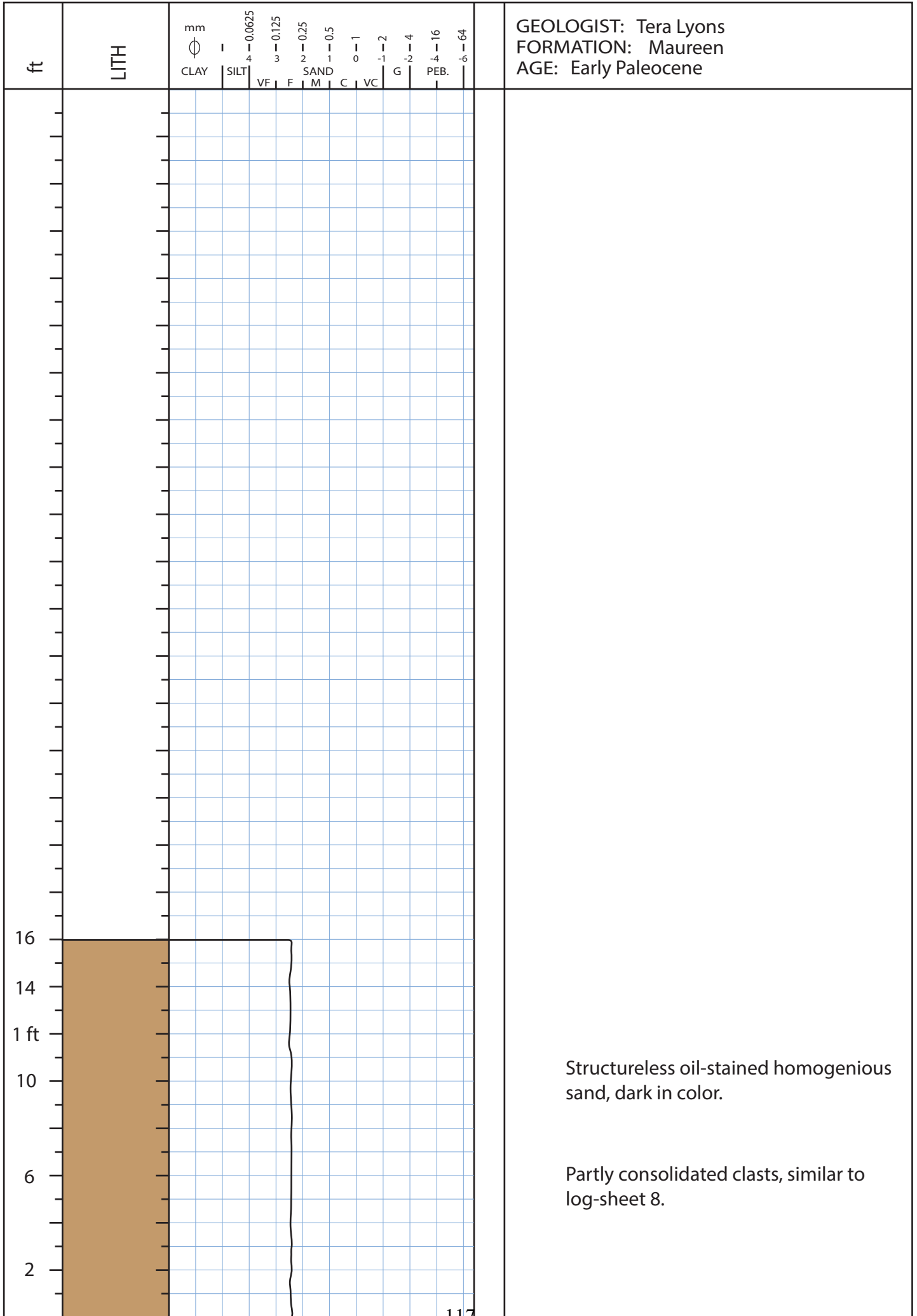


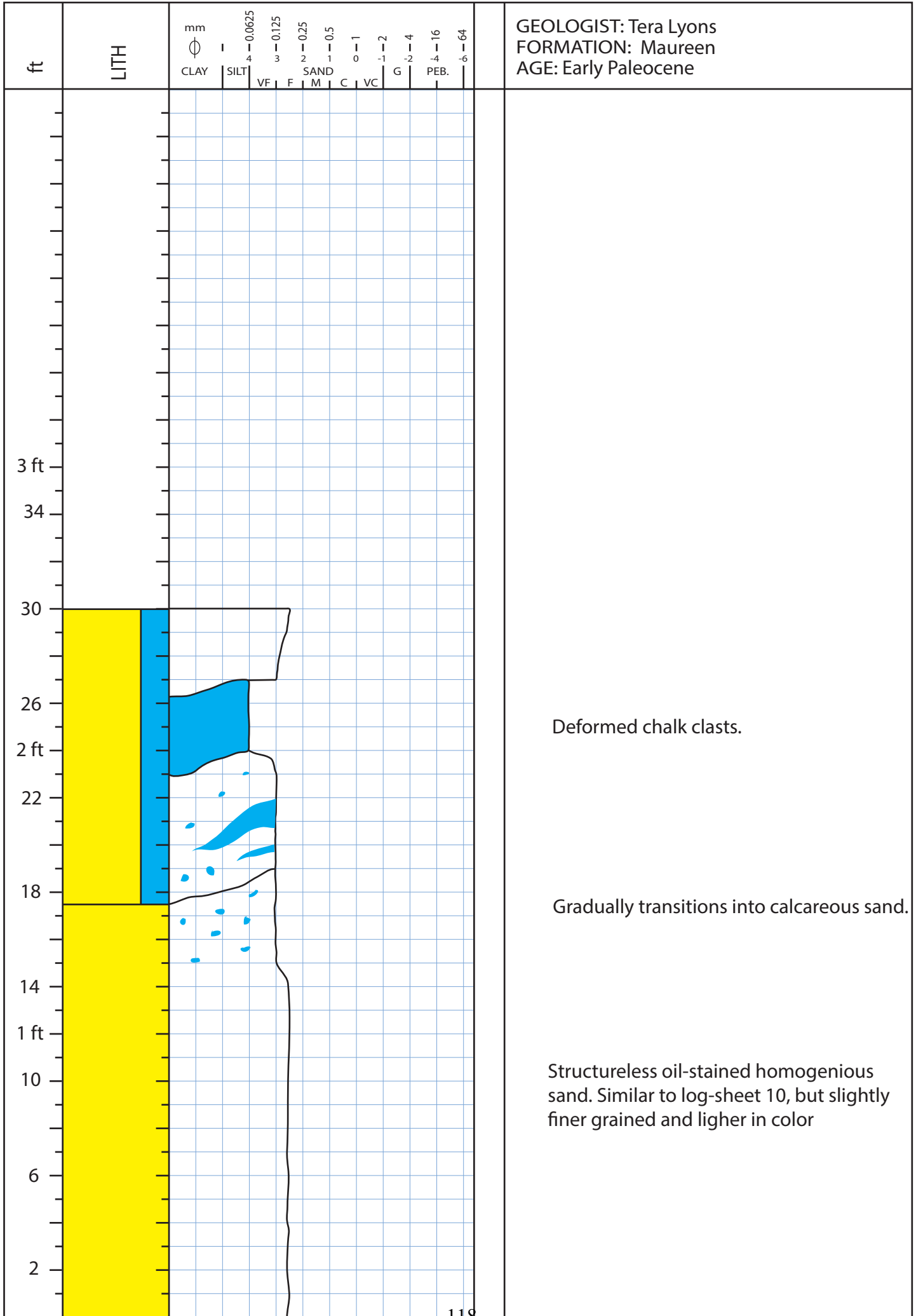
Structureless dark oil-stained homogenous sand.

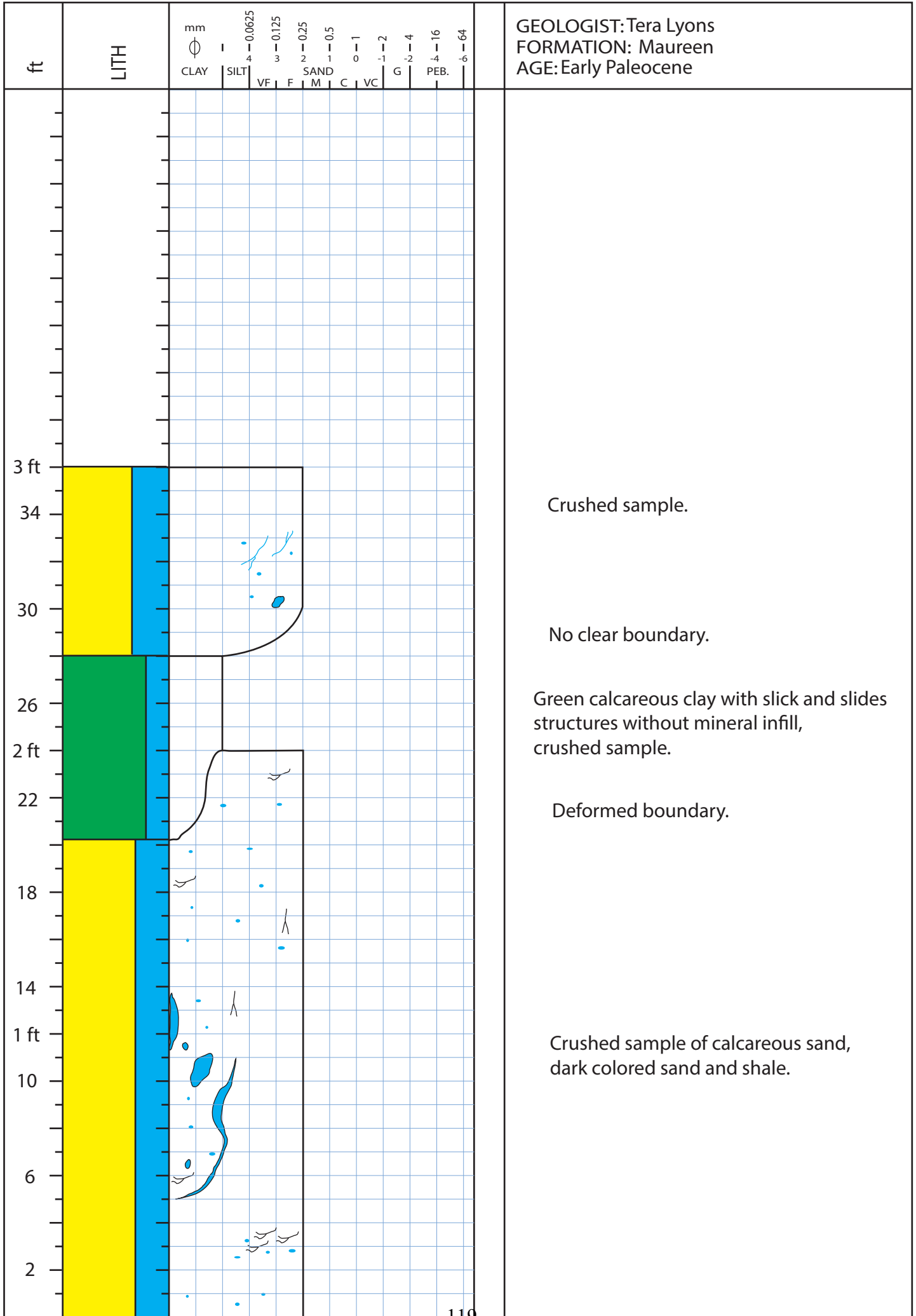
More consolidated than 4 and 5.

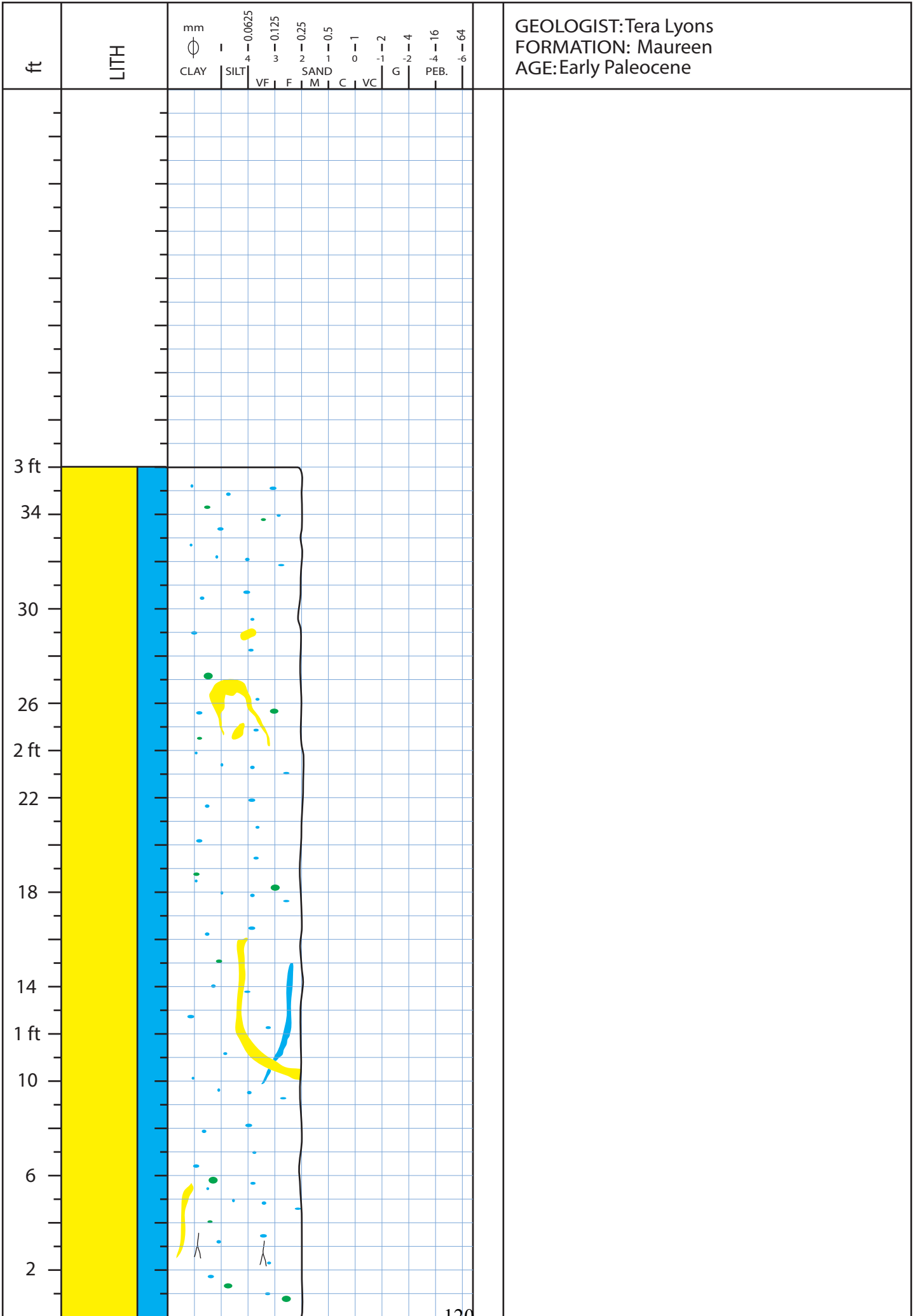




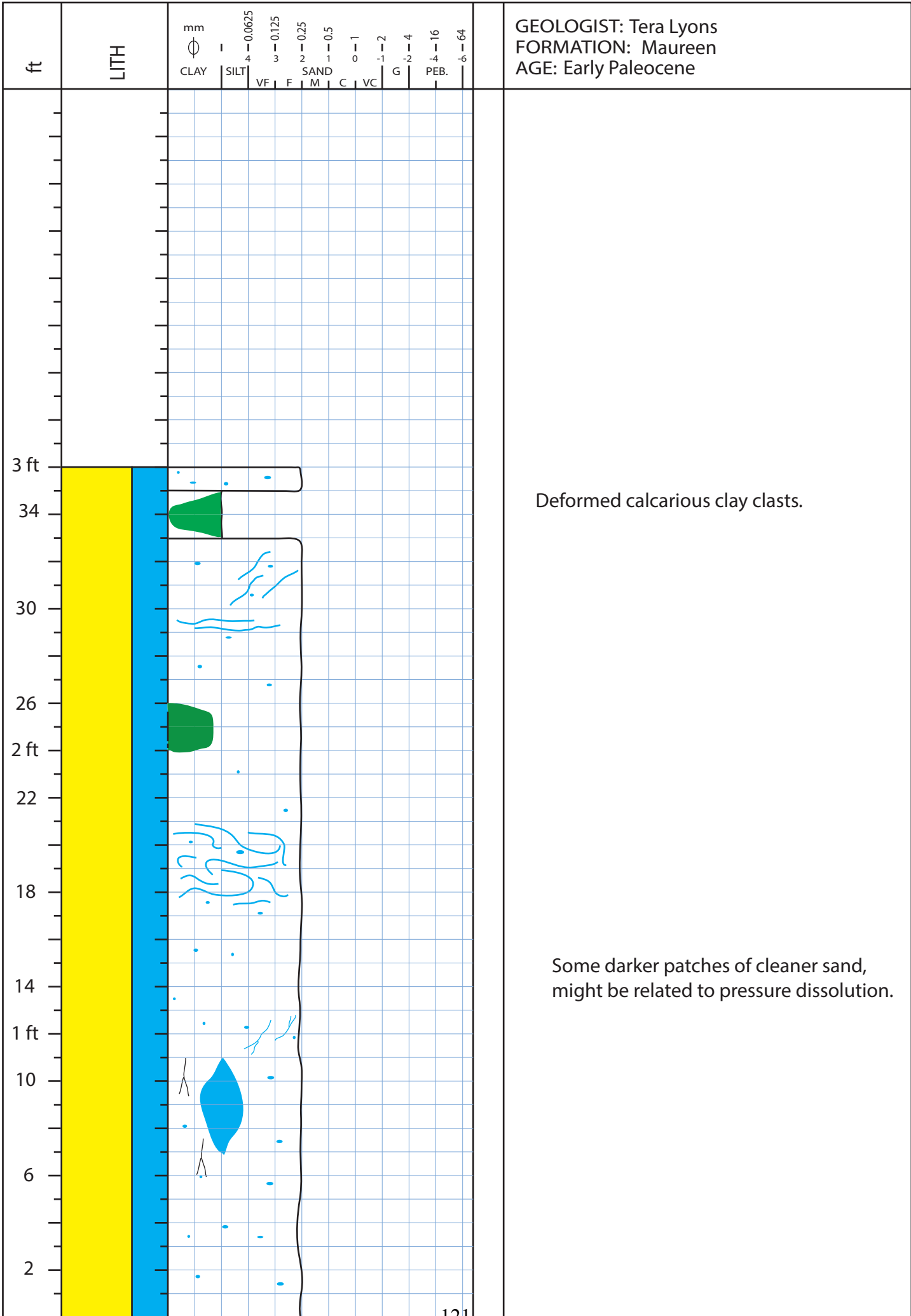


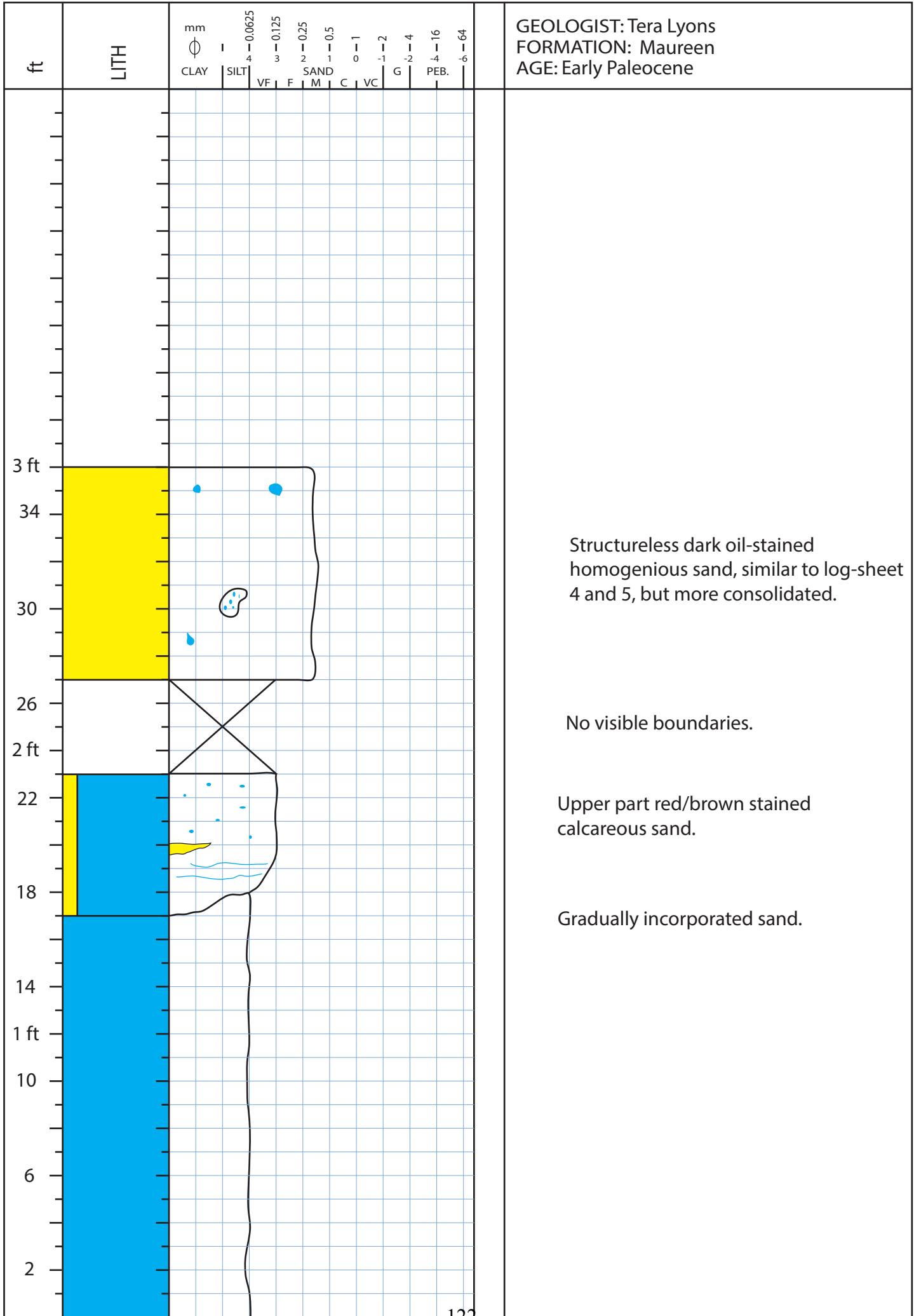


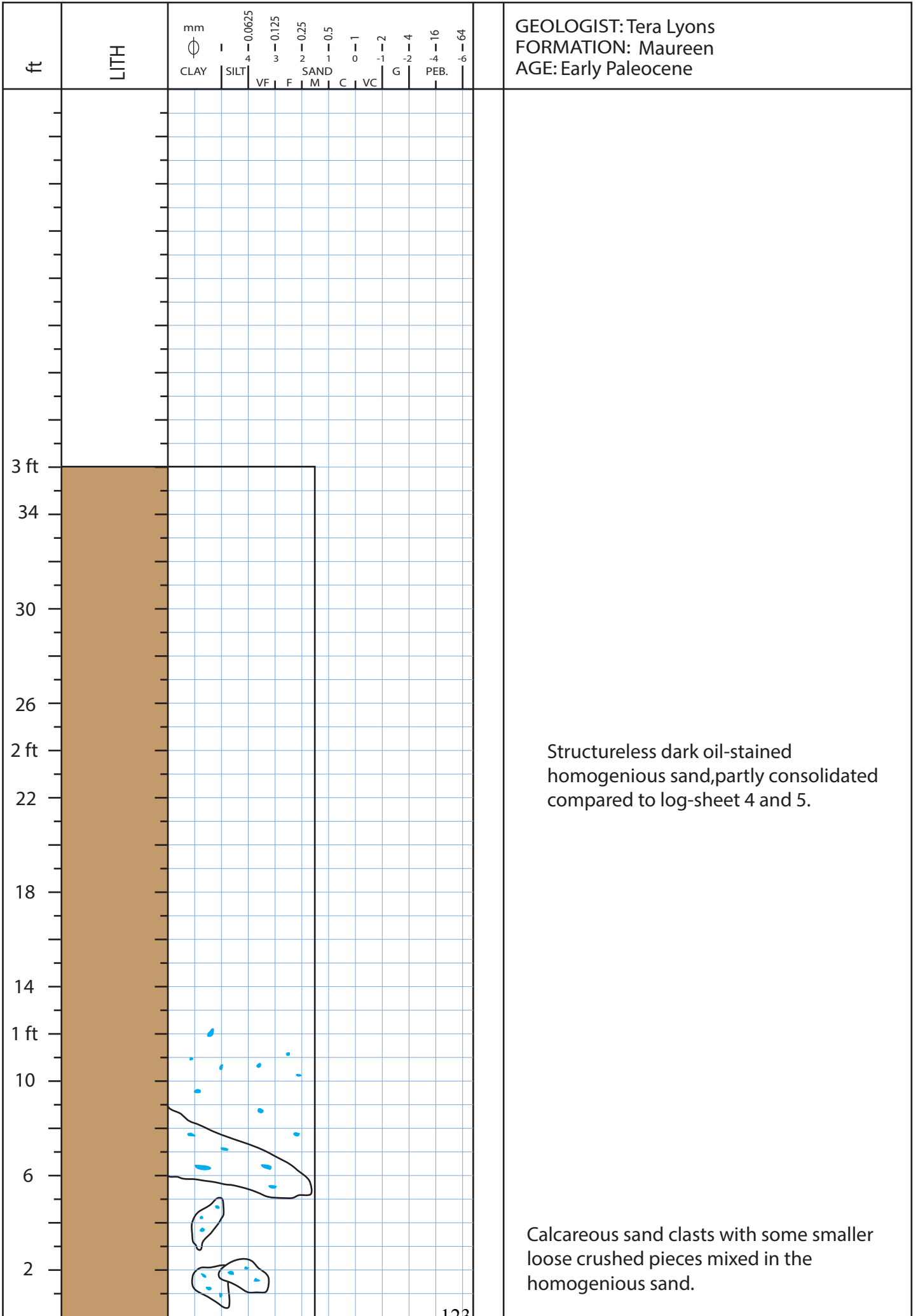




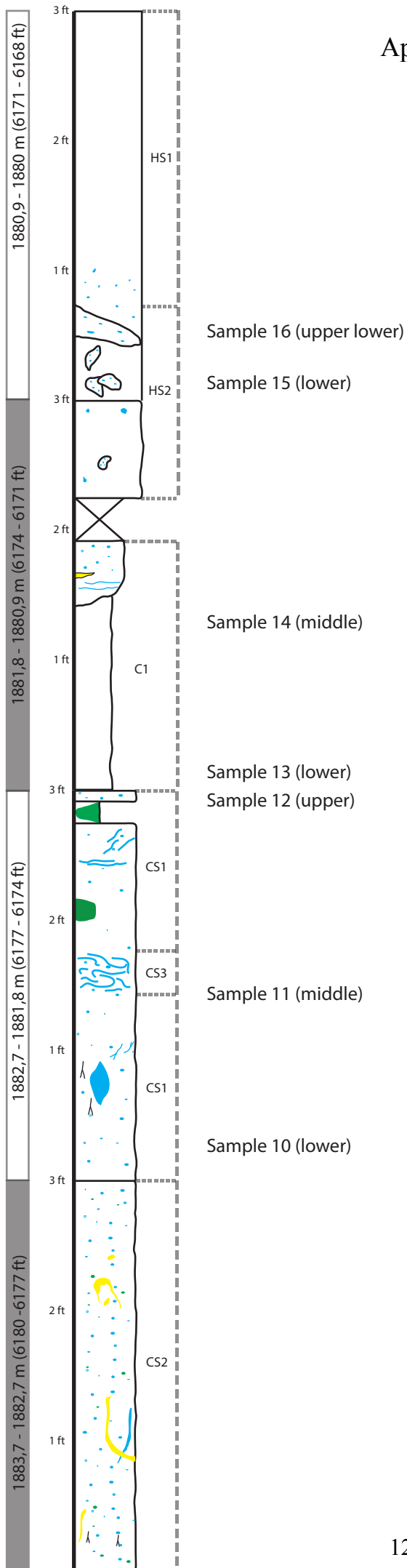
GEOLOGIST: Tera Lyons
 FORMATION: Maureen
 AGE: Early Paleocene

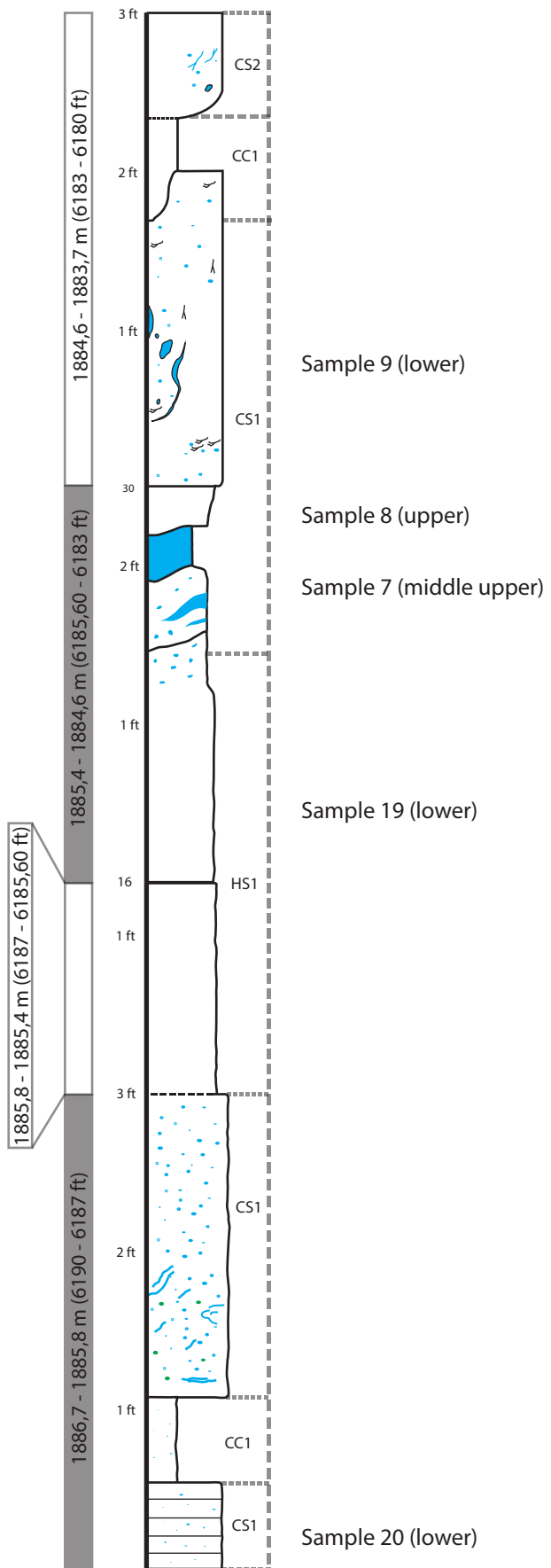


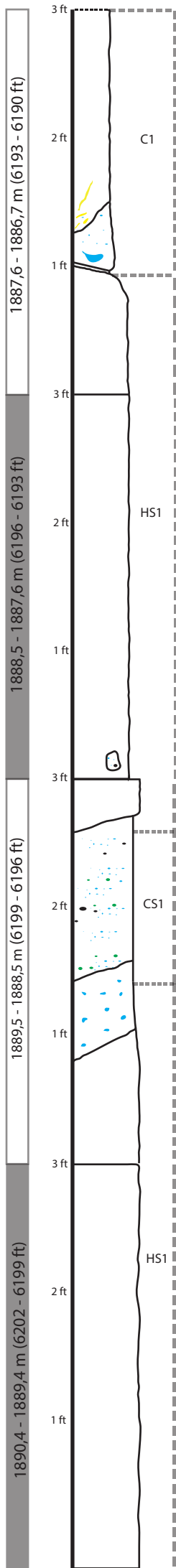




Appendix C - Stacked logs





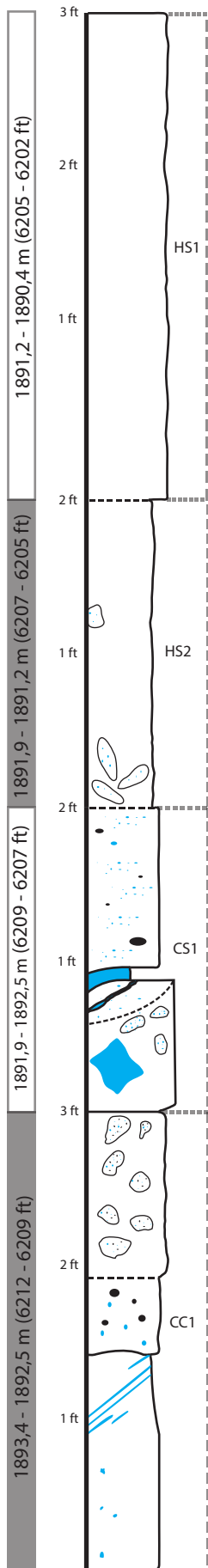


Sample 6: middle upper

Sample 5: middle lower

Sample 4: lower

Sample 3: middle



Sample 2: upper

Sample 1: middle

Appendix D – Thin sections

Modal analysis

Results from well 9/11b-11

Depth Below Sea Floor (feet)	Depth Below Sea Floor (meters)	Sample	Framework											Matrix Micritic Mud	Cement Pyrite	Porosity %	Avrage Grain Size µm	Sorting
			Monokrystaline Quartz	Polykrystaline Quartz	Feldspar	Mica	Glauconite	Heavy Minerals	Rock Fragments	Forams	Fossil Fragments							
6207 - 6209	1891,9 - 1892,5	1	39,8	2,8	2,0	0,5	1,5	0,5	4,5	1,5	3,3	41,0	1,5	1,3	275	Poorly Sorted		
6207 - 6209	1891,9 - 1892,5	2	36,0	3,3	0,3	1,0	1,0	0,5	3,5	4,5	2,3	43,8	2,3	1,8	237	Poorly Sorted		
6196 - 6199	1888,5 - 1889,5	3	39,5	3,5	1,3	0,5	1,0	0,3	4,0	2,8	2,8	42,8	0,3	1,5	225	Poorly Sorted		
6190 - 6193	1886,7 - 1887,6	4	42,8	4,8	3,0	1,5	1,5	0,3	2,3	1,8	4,3	16,8	0,0	21,3	175	Well Sorted / Poorly Sorted		
6190 - 6193	1886,7 - 1887,6	5	0,0	0,0	0,0	0,0	0,0	0,0	0,0	8,5	5,3	81,5	0,0	4,8	126	Moderately Well Sorted		
6190 - 6193	1886,7 - 1887,6	6	2,0	0,0	0,0	0,0	0,0	0,0	0,0	5,0	3,8	79,5	0,0	9,8	121	Moderately Well Sorted		
6183 - 6185,6	1884,6 - 1885,7	7	8,8	1,8	1,0	0,0	0,0	0,0	0,0	10,8	8,3	58,5	0,0	11,0	145	Moderately Sorted		
6183 - 6185,6	1884,6 - 1885,7	8	15,8	5,0	1,0	0,0	0,0	0,0	0,8	11,3	3,5	57,3	0,0	5,5	159	Poorly Sorted		
6180 - 61683	1883,7 - 1884,6	9	27,0	1,3	0,5	0,0	0,0	0,0	2,3	9,8	3,3	52,0	0,0	4,0	154	Moderately Sorted		
6174 - 6177	1881,8 - 1882,7	10	14,0	1,8	0,3	0,8	0,3	0,0	0,8	4,5	2,5	65,0	1,5	8,8	179	Poorly Sorted		
6174 - 6177	1881,8 - 1882,7	11	16,8	1,3	0,5	1,0	0,5	0,0	0,5	4,8	2,5	65,3	1,3	5,8	173	Poorly Sorted		
6174 - 6177	1881,8 - 1882,7	12	26,3	2,8	0,3	0,3	1,0	0,0	1,5	1,5	2,0	23,3	2,3	39,0	139	Moderately Well Sorted		
6171 - 6174	1880,9 - 1881,8	13	0,0	0,0	0,0	0,0	0,0	0,0	0,0	15,8	9,3	62,8	0,0	12,3	138	Moderately Well Sorted		
6171 - 6174	1880,9 - 1881,8	14	0,0	0,0	0,0	0,0	0,0	0,0	0,0	12,0	5,3	73,5	0,0	9,3	126	Moderately Well Sorted		
6168 - 6171	1880,0 - 1880,9	15	9,0	2,5	0,5	0,0	0,0	0,0	1,3	14,0	4,8	62,3	0,5	5,3	151	Moderately Sorted		
6168 - 6171	1880,0 - 1880,9	16	6,8	1,5	0,0	0,0	0,0	0,0	0,8	8,5	6,8	67,3	0,0	8,5	143	Moderately Sorted		
Unknown	Unknown	17	37,3	2,3	0,5	1,0	1,0	0,0	3,8	4,0	2,3	42,3	1,0	4,8	197	Poorly Sorted		
Unknown	Unknown	18	34,3	2,8	0,5	1,5	0,5	0,3	1,3	4,3	2,8	37,8	2,0	12,3	111	Moderately Well Sorted / Poorly Sorted		
Avregae			17,8	2,0	0,7	0,3	0,4	0,1	1,4	7,3	4,3	55,8	0,6	9,4	165,08			

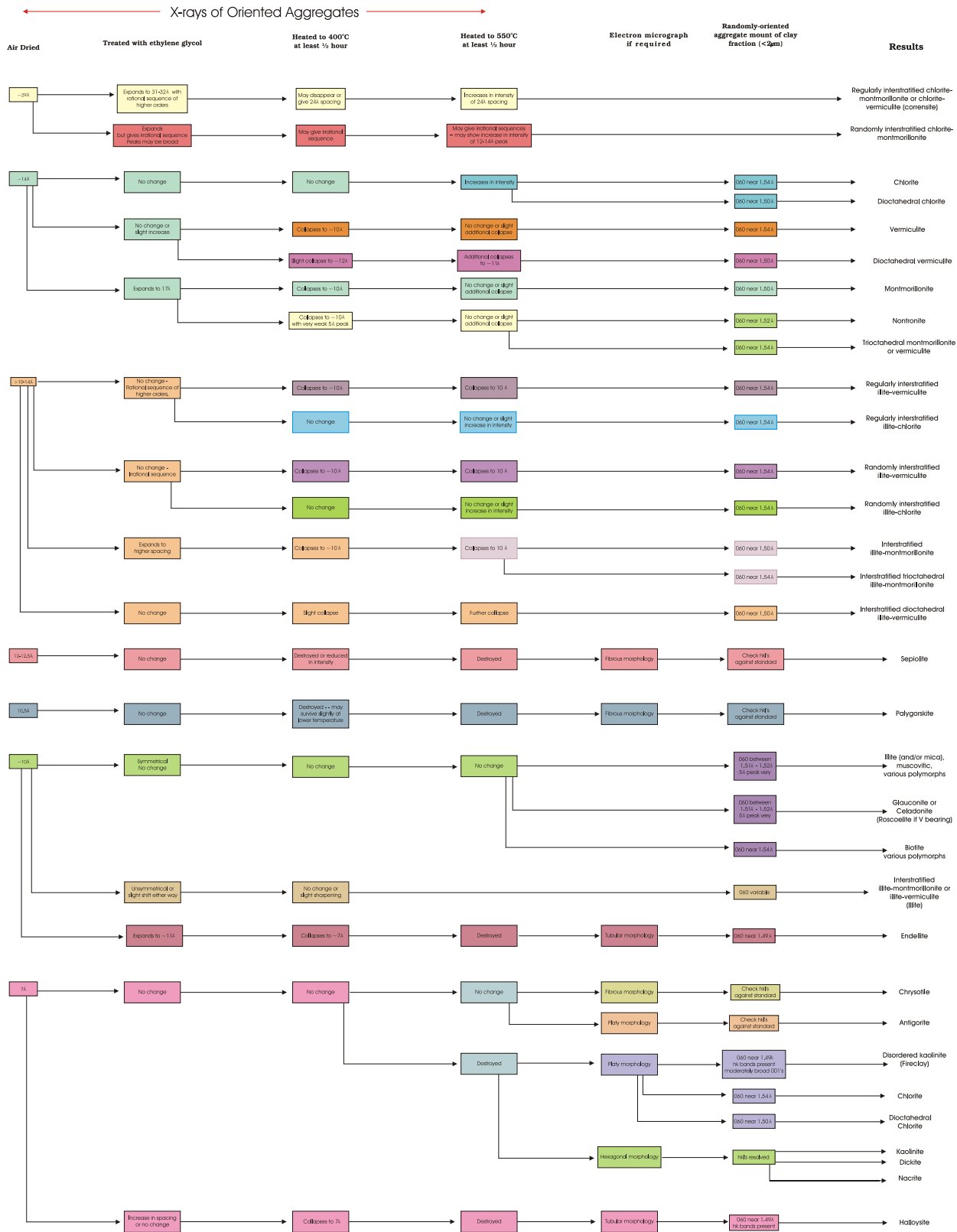
Appendix E – Quantification of XRD bulk samples

Results from well 9/11b-11

Sample Depth Below Sea Floor (feet)	Sample Depth Below Sea Floor (meters)	Samples	Quartz	Calcite	Albite	Microcline	Muscovite/Illite	Smectite/Illite	Kaolinite	Pyrite	Halite	Zircon	Anatase	SUM
6207 - 6209	1891,9 - 1892,5	Sample 1	52,5	28,0	7,0	6,1	2,7	1,1	1,4	1,1	0,0	0,0	0,0	99,9
6207 - 6209	1891,9 - 1892,5	Sample 2	43,4	36,5	6,1	5,9	2,9	2,0	1,6	1,7	0,0	0,0	0,0	100,1
6196 - 6199	1888,5 - 1889,5	Sample 3	59,0	22,9	6,8	6,2	2,9	0,4	1,2	0,7	0,0	0,0	0,0	100,1
6190 - 6193	1886,7 - 1887,6	Sample 4	60,7	8,4	11,3	9,5	4,2	1,9	2,1	2,0	0,0	0,0	0,0	100,1
6190 - 6193	1886,7 - 1887,6	Sample 6	7,6	91,5	0,0	0,0	0,6	0,0	0,0	0,0	0,3	0,0	0,0	100,0
6174 - 6177	1881,8 - 1882,7	Sample 10	18,8	69,9	4,8	1,2	1,5	0,0	0,0	3,5	0,0	0,2	0,0	99,9
6174 - 6177	1881,8 - 1882,7	Sample 11	26,4	60,1	4,2	3,0	1,9	0,8	0,9	2,8	0,0	0,0	0,0	100,1
Unknown	Unknown	Sample 17	53,3	27,0	7,0	5,9	2,6	1,0	1,5	1,3	0,3	0,0	0,0	99,9
Unknown	Unknown	Sample 18	50,5	14,7	7,8	13,2	5,6	1,7	4,1	2,3	0,0	0,0	0,0	99,9
6183 - 6185	1884,6 - 1885,2	Sample 19	51,4	1,5	18,7	15,5	5,7	1,7	2,8	2,6	0,0	0,0	0,0	99,9
6187 - 6190	1885,8 - 1886,7	Sample 20	10,5	14,1	11,8	7,0	29,2	18,4	0,0	3,2	2,9	0,0	2,8	99,9
		Avrage	39,5	34,1	7,8	6,7	5,4	2,6	1,4	1,9	0,3	0,0	0,3	

Appendix F – Flow Diagram for XRD clay fraction identification.

Clay Mineral Identification Flow Diagram



Appedix G- Well data and information for all corelated wells

Location: Mariner Filed, offshore Scotland

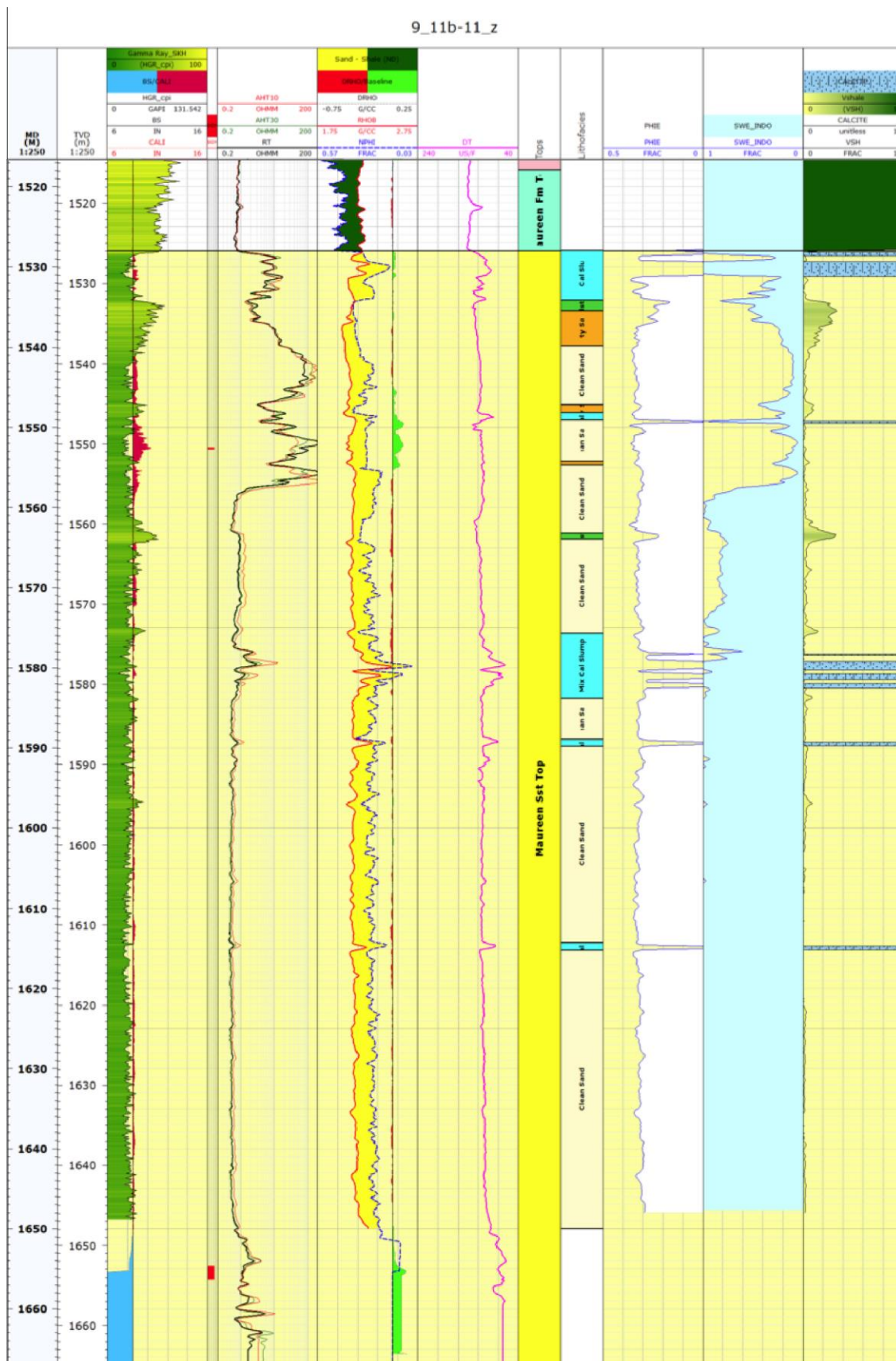
Formation name: Maureen Formation

Well name	MD Ref. RKB [m]	Horizontes	North [m]	East [m]
9/11a-10	1385.13	TopMaureenFm	6608421.28413143	389082.005025024
9/11a-10	1399.52	TopMaureenRes	6608421.06844989	389081.891652736
9/11a-10	1411.04	TopDirtySeq	6608420.86111117	389081.694457529
9/11a-10	1411.68	BaseDirtySeq	6608420.85037552	389081.683821339
9/11a-10	1424.63	BaseMaureenRes	6608420.66372854	389081.499425724
9/11a-10	1424.63	TopDevonian	6608420.66372854	389081.499425724
9/11a-10Z	2174.09	TopMaureenFm	6607807.51947708	390046.446131551
9/11a-10Z	2228.5	TopMaureenRes	6607781.3266173	390091.545219568
9/11a-10Z	2292.94	TopDirtySeq	6607750.5612569	390144.897206056
9/11a-10Z	2297.36	BaseDirtySeq	6607748.42971554	390148.536699192
9/11a-10Z	2365.5	BaseMaureenRes	6607715.19407351	390203.883336426
9/11a-10Z	2365.5	TopChalk	6607715.19407351	390203.883336426
9/11-3	1434.9	TopMaureenFm	6609938.731495881	393189.6380433887
9/11-3	1457.98	TopMaureenRes	6609938.586345892	393189.6373138856
9/11-3	1507.14	BaseMaureenRes	6609938.42787566	393189.5663093415
9/11-3	1507.14	TopChalk	6609938.42787566	393189.5663093415
9/11-3	1515.77	TopDevonian	6609938.458222919	393189.6358977875
9/11-4	1427.6	TopMaureenFm	6606146.82	389972.95
9/11-4	1434.69	TopMaureenRes	6606146.82	389972.95
9/11-4	1458.52	TopDirtySeq	6606146.82	389972.95
9/11-4	1459.74	BaseDirtySeq	6606146.82	389972.95
9/11-4	1487.05	BaseMaureenRes	6606146.82	389972.95
9/11-4	1487.05	TopChalk	6606146.82	389972.95
9/11-4	1499.95	TopDevonian	6606146.82	389972.95
9/11a-9	1438.89	TopMaureenFm	6606695.404011876	390674.5142433955
9/11a-9	1448.76	TopMaureenRes	6606695.521906747	390674.3279651143
9/11a-9	1471.09	TopDirtySeq	6606695.735114336	390673.9430601786
9/11a-9	1480.43	BaseDirtySeq	6606695.801844028	390673.7865971903
9/11a-9	1504.51	BaseMaureenRes	6606695.910139172	390673.5017760515
9/11a-9	1504.51	TopDevonian	6606695.910139172	390673.5017760515
9/11a-8	1434.03	TopMaureenFm	6607257.289524785	391430.1318251003
9/11a-8	1457	TopMaureenRes	6607257.531618807	391429.8122993889
9/11a-8	1475.34	TopDirtySeq	6607257.7249146	391429.5571796002
9/11a-8	1478.47	BaseDirtySeq	6607257.757903468	391429.5136395272
9/11a-8	1495.3	BaseMaureenRes	6607257.935284503	391429.2795246938
9/11a-8	1495.3	TopChalk	6607257.935284503	391429.2795246938
9/11a-8	1514.35	TopDevonian	6607258.136063394	391429.0145284028
9/11-2	1431.76	TopMaureenFm	6607025.65	392025.49
9/11-2	1449.69	TopMaureenRes	6607025.65	392025.49
9/11-2	1474.48	TopDirtySeq	6607025.65	392025.49
9/11-2	1480.92	BaseDirtySeq	6607025.65	392025.49
9/11-2	1530.4	BaseMaureenRes	6607025.65	392025.49
9/11-2	1530.4	TopDevonian	6607025.65	392025.49

9/11a-5	1441.01	TopMaureenFm	6606806.360784951	392253.6400111731
9/11a-5	1460	TopMaureenRes	6606806.65174996	392253.9580503178
9/11a-5	1484.93	TopDirtySeq	6606807.04627042	392254.3823071715
9/11a-5	1489.62	BaseDirtySeq	6606807.124098637	392254.4578758804
9/11a-5	1530.1	BaseMaureenRes	6606807.819560172	392255.0863926857
9/11a-5	1530.1	TopDevonian	6606807.819560172	392255.0863926857
9/11a-12	1437.37	TopMaureenFm	6607167.04620479	392727.796463842
9/11a-12	1451.48	TopMaureenRes	6607166.91644064	392727.533175933
9/11a-12	1478.27	TopDirtySeq	6607166.73957555	392727.072768287
9/11a-12	1483.21	BaseDirtySeq	6607166.72780444	392727.002629233
9/11a-12	1544.02	BaseMaureenRes	6607166.69837177	392725.796381612
9/11a-12	1544.02	TopDevonian	6607166.69837177	392725.796381612
9/11a-7	1438.98	TopMaureenFm	6606451.435169754	392882.7477974176
9/11a-7	1459.02	TopMaureenRes	6606451.860320119	392882.7773839337
9/11a-7	1502.88	TopDirtySeq	6606452.913535711	392882.7693674749
9/11a-7	1505.9	BaseDirtySeq	6606452.976008147	392882.7740603326
9/11a-7	1566.07	BaseMaureenRes	6606454.077679689	392883.2102693226
9/11a-7	1566.07	TopDevonian	6606454.077679689	392883.2102693226
9/11-1	1455.27	TopMaureenFm	6607366.38	393542.78
9/11-1	1478.49	TopMaureenRes	6607366.38	393542.78
9/11-1	1499.58	TopDirtySeq	6607366.38	393542.78
9/11-1	1501.65	BaseDirtySeq	6607366.38	393542.78
9/11-1	1539.8	BaseMaureenRes	6607366.38	393542.78
9/11-1	1539.8	TopChalk	6607366.38	393542.78
9/11-1	1552	TopDevonian	6607366.38	393542.78
9/11a-6	1489.57	TopMaureenFm	6606745.531212475	394724.4286474805
9/11a-6	1502.19	TopMaureenRes	6606746.208513653	394724.6526886275
9/11a-6	1556.82	TopDirtySeq	6606748.910628393	394725.4443505451
9/11a-6	1559.57	BaseDirtySeq	6606749.041169063	394725.4824660554
9/11a-6	1612.71	TopChalk	6606751.120681673	394726.2138415881
9/11a-6	1612.71	BaseMaureenRes	6606751.120681673	394726.2138415881
9/11a-6	1614.77	TopDevonian	6606751.191035643	394726.2513937618

Appexid H- Well sections from Mariner Easts

Well 9/11b-11z



Well 9/11b-11

